Diss. ETH No. 10243

# THE ATMOSPHERIC WATER VAPOUR BUDGET OVER GREENLAND

A dissertation submitted to the
SWISS FEDERAL INSTITUTE OF TECHNOLOGY ZURICH

for the degree of
Doctor of Natural Sciences

presented by
PIERLUIGI STEFANO CALANCA
Dipl. Natw. ETH
born June 14th 1963
citizen of Leontica, TI

accepted on the recommendation of
Prof. Dr. A. Ohmura, examiner
Prof. Dr. H.C. Davies, co-examiner
Prof. Dr. E.O. Holopainen (University of Helsinki), co-examiner

1993

Accepted for publication in Zürcher Geographische Schriften,
No. 55, 1994, Verlag Geographisches Institut ETH Zürich

## ACKNOWLEDGEMENTS

I am greatly indebted to many people who gave encouragement and support in the course of this work. Special thanks go first of all to my advisor, Prof. Atsumu Ohmura, who initiated the Greenland Project. His proverbial thirst for knowledge was crucial in addressing the pertinent questions that led to the completion of the thesis in the present form. The comments of my co-examiners, Prof. Huw Davies and Prof. Eero Holopainen, were extremely valuable. Thanks are also extended to Dr. Kooiti Masuda, of the Tokyo Metropolitan University, for his suggestions during the initial stages of my thesis. I am grateful to Susan Braun-Clarke, who carefully read and corrected the English. The responsibilty for the final form of the thesis of course remains my own. The European Centre for Medium-Range Weather Forecasts is acknowledged for providing the analyses. I am indebted to all my friends at the Geography Department for sharing with me the coffee breaks, the 'kondi' work-out sessions and the many kilometres covered around the 'Züriberg'. These moments were essentials as a source of mental refreshment. The work was supported by the Swiss National Foundation for Scientific Research (Grants No. 2-77-467-91 and No. 2-77-591-92). Finally, I would like to thank my parents for much love and support over the last 30 years.

## RIASSUNTO

Grazie all'impiego delle analisi meteorologiche prodotte dal Centro Europeo per le Previsioni del Tempo a Medio Termine (European Centre of Medium-Range Weather Forecasts, ECMWF), è stato possibile presentare in questo lavoro una descrizione consistente e completa del trasporto di vapore acqueo, della sua divergenza e delle condizioni meteorologiche in un'area comprendente la Groenlandia e delimitata a sud dal 50esimo parallelo, a est dal meridiano di Greenwich e a ovest dal 90esimo meridiano.

Benchè i risultati dei calcoli della divergenza del flusso di umidità siano affetti da diversi tipi di errore, dovuti in parte alla discretizzazione dei campi atmosferici nello spazio e nel tempo, è possibile, grazie all'applicazione di algoritmi di correzione appropriati e all'uso di un filtro spaziale, ricostruire una distribuzione geografica del campo di divergenza del trasporto di vapore acqueo molto realistica. Per alcune stazioni meteorologiche situate nell'area di studio, i valori mensili della divergenza del flusso di vapore sono paragonabili ai valori pluviometrici. Ciò offre concrete possibilità per il futuro di studiare i cicli annuali delle precipitazioni basandosi unicamente su dati del vento e dell'umidità e senza fare ricorso a particolari forme di parametrizzazione delle precipitazioni.

Durante le estati del 1990 e del 1991, l'Istituto di Geografia del Politecnico Federale di Zurigo ha organizzato due spedizioni climatologiche sulla costa ovest dell'Inlandsis. Il paragone tra la divergenza del flusso di vapore acqueo e le precipitazioni indica, per questa stazione, una stima delle precipitazioni estive leggermente in eccesso e una di quelle invernali sensibilmente in difetto. Per spiegare quest'ultima differenza bisogna tener presente che in inverno grandi quantità di neve vengono accumulati dai venti catabatici che soffiano costantemente in questa regione. Considerando la Groenlandia nel suo insieme, la divergenza del flusso di vapore acqueo ammonta annualmente a -380 mm, un valore che è prossimo, in termini assoluti, ai 340 mm delle precipitazioni.

La separazione del flusso di vapore acqueo in una componente legata alla circolazione media dell'atmosfera e in una rappresentante le perturbazioni atmosferiche ha mostrato chiaramente che meccanismi diversi operano sulla parte ovest e su quella est dell'Inlandsis. Sui pendii occidentali, l'incremento delle precipitazioni con l'aumento dell'altitudine si spiega con il sollevamento continuo di masse d'aria ad alto tenore di

umidità provenienti dall'Artico Canadese. L'alto contenuto in vapore acqueo è favorito in autunno dalle condizioni termiche nella Baia di Baffin. La costa est della Groenlandia, invece, è interessata dal passaggio frequente di perturbazioni provenienti dall'Atlantico. Il loro comportamento è spesso condizionato dalla presenza nell'Atlantico orientale di anticicloni stazionari, che ne bloccano il normale cammino verso nordest.

Il compito delle perturbazioni è quello di diminuire il gradiente sud-nord di umidità. Tale ruolo è svolto in parte tramite un trasporto di aria umida da meridione a settentrione ma anche, in modo sigificativo, tramite l'esportazione di aria secca dalle zone polari verso quelle subpolari e oltre. I due meccanismi non sono simmetrici. I flussi di aria secca verso sud sono più frequenti ma meno consistenti. I flussi di aria umida verso nord corrispondono a una più ampia varietà di eventi dove, a eventi normali e assai frequenti, si associano eventi esuberanti ma sporadici.

## ABSTRACT

Previous investigations of the moisture flux and moisture flux divergence in the Greenland area were based on rather incomplete data. In this study, the uninitialized analyses of the European Centre of Medium-Range Weather Forecasts (ECMWF) are used to produce a consistent picture of the moisture flux, the flux divergence and of the meteorological conditions in an area situated north of 50°N, and between 0° and 90°W.

The inaccuracies of the diagnosed divergence field due to deficiencies of the ECMWF analyses are discussed. A spatial filter is necessary to eliminate the small scale noise that affects in particular the moisture flux divergence field. The noise can be understood as the consequence of the discreteness of the analyses. The mass imbalance of the wind field can be also efficiently eliminated using a correction algorithm.

For Greenland, the calculated annual moisture flux divergence amounts to -380 mm $year^{-1}$. This value is in good agreement with the estimated annual precipitation of 340 mm $year^{-1}$. At the ETH Greenland Expedition site in West Greenland, the calculated convergence underestimates the winter accumulation but overestimates the summer precipitation. However, for most meteorological stations in the study area, the computations can reproduce the annual course of the monthly precipitation.

The breaking down of the total moisture flux into a component achieved by the mean circulation and an eddy component reveals the contrasting nature of the precipitation in western and eastern Greenland. In western Greenland, precipitation results mainly from the convergence of the water vapour flux achieved by the mean circulation. In southeastern Greenland, the mean circulation and the transient eddies contribute in equal parts to the total convergence. In northeastern Greenland, on the other hand, mean circulation and eddies act in opposite directions. The fact that, in all seasons, the convergence of the eddy flux can more than compensate for the divergence of the flux by the mean circulation is determinant for the precipitation regime in this area.

The transient eddies can be classified into two main categories: the synoptic disturbances, with periods of typically two to six days; and, low-frequency fluctuations, that are related, for example, to blocking episodes. The low-frequency fluctuations are supposed to modulate the behaviour of the synoptic disturbances. Thus, the northwestward shift of the cyclone path during blocking in the eastern North Atlantic

can explain why a significant convergence is observed in northeastern Greenland in association with the low-frequency fluctuations.

The transient eddies are slightly more efficient in transporting moist air northward than in exporting dry air from the Arctic towards lower latitudes. The two processes are not symmetric. The former is the sum of many small events, whereas large and sporadic wet spells are important for the latter.

## TABLE OF CONTENTS

Seite Leer /
Blank leaf

# 1 INTRODUCTION

Greenland is characterized by a large spectrum of precipitation regimes. These are caused, on the one hand, by the interplay between the atmospheric circulation and the orography and, on the other hand, by the frequent invasion of moist air masses in relation to travelling synoptic disturbances (Ohmura and Reeh, 1991). Climatologically, the variety of generating mechanisms is reflected in the average annual course of the monthly precipitation (Putnins, 1970). Thus, along the southeastern coast, the maximum precipitation is observed in winter, when the Icelandic Low is best developed, whereas, on the western coast, the precipitation maximum appears in summer and early autumn in relation to relatively warm and moist air masses from the west-southwest (Barry and Kiladis, 1982). The orographic forcing is probably best revealed by the spatial distribution of the annual precipitation (Ohmura and Reeh, 1991), which shows rather strong precipitation gradients on the steep southeastern slopes, a belt of increased precipitation on the middle western slopes and a region of low precipitation in northeastern Greenland.

The tropospheric circulation of the Arctic is dominated in all seasons by the circumpolar vortex (Wilson, 1967). The Greenland Ice Sheet is enbedded in the ring of strong westerlies around the vortex core, but the standing waves that are superimposed on the time-averaged, zonal symmetric flow result in a mid-tropospheric trough to the west of Greenland and, consequently, in a rather meridional time mean flow over the ice sheet (Namias, 1958; Hare, 1968). The stationary waves are forced by the topography and by the thermal characteristics of the Earth's surface (Wallace, 1983; Held, 1983; Broccoli and Manabe, 1992). Because of its meridional elongation and elevation, Greenland itself plays a significant role in the general circulation of the atmosphere of the Northern Hemisphere (Putnins, 1970).

The day-to-day variability of meteorological parameters in mid- and high latitudes is shaped by travelling synoptic disturbances that move along preferred paths, the so-called storm tracks (Whittacker and Horn, 1984; Hoskins and Valdes, 1990). The location of Greenland just to the north of one of the major storm tracks, the North Atlantic track, and the presence of a second, well-developed track crossing the Canadian Arctic during the summer (Reed and Kunkel, 1960) imply that transient disturbances play a primary role for the precipitation in Greenland, too. The signature of the synoptic eddy activity on the precipitation is apparent not only at the southeastern coast (evidently in relation to the Icelandic Low), but clearly also in the central part of

the ice sheet (Loewe, 1935), where precipitation events are often accompanied by a pressure fall and a rapid temperature increase typical of frontal passages. The possibility for low pressure centres and associated fronts to cross the ice sheet has been discussed by Dorsey (1945). In some cases, as a consequence of the shallowness of the systems, only the upper level trough moves over the ice sheet. When it reaches the east coast, secondary cyclogenesis may occur underneath, favoured by stretching of the atmospheric column (Rossby, 1940; Putnins, 1970) and by cold outbreaks of polar air.

In northeastern Greenland, the very low precipitation is the consequence of the shadowing effect of the ice sheet, either for southerly flow, in winter, or for southwesterly flow, in summer (Ohmura and Reeh, 1991). The bulk of the winter and summer precipitation falls when air masses of Atlantic origin are advected northwestward in connection with strong depressions in the Denmark Strait area (Hamilton, 1958a). In summer, in addition, appreciable precipitation may occur in southwesterly flows from the Davis Strait-Baffin Bay area (Hamilton, 1958b). These rather rare, but nonetheless important precipitation events may be explained by the considerably high moisture content of the air, which is a consequence of the thermal conditions in Baffin Bay (Barry and Kiladis, 1982).

The summer season is also characterized by an increased tendency for cyclogenesis along the southern rim of the Polar Basin (Namias, 1958; Reed and Kunkel, 1960). Cyclones that move around or across the Polar Basin are vital for providing precipitation to the northernmost islands of the Canadian Arctic Archipelago (Müller and Roskin-Sharlin, 1968). More generally, it seems that a substantial portion of the summer precipitation in the Canadian High Arctic falls under northerly flow conditions and originates therefore to a great extent within the Polar Basin (Bradley and Eischeid, 1985). This may well be true also for the northern slopes of Greenland.

The present knowledge of the precipitation regime of Greenland is limited by the difficulties encountered in gathering reliable information having sufficient accuracy and resolution. The network of rain gauges in Greenland (state of 1992, unpublished material of the Danish Meterological Institute) is made up of 11 stations distributed irregularly along the coast. Even without addressing the question of the quality and representativeness of such point measurements, it is clear that the meterological network is largely insufficient for a discussion of the spatial distribution of the precipitation. For the ice-covered part of the island, the annual accumulation for a time period spanning several years can be determined in snow pits or by isotopic analysis of ice cores. Such glaciological data can be used to reconstruct the distribution of both the average annual accumulation and, by considering of the mechanisms which lead from

the precipitation to the accumulation, of the average anuual precipitation (Ohmura and Reeh, 1991). However, they are not adequate for investigations of the precipitation variability on time scales shorter than one year.

Given these circumstances, the spatial and temporal distribution of the precipitation may be more easily determined indirectly through an evaluation of the atmospheric water budget, using the so-called aerological method (Palmén, 1967). The conservation of water for the atmosphere states that, neglecting the transport of water in the liquid or solid phase, the flux of water at the base of an atmospheric column fixed in space, i.e., the difference between evaporation and precipitation, is equal to the rate of change of the moisture content in the volume and the net flux of water vapour across the side walls of the column. The last two terms can be computed knowing the four-dimensional (space and time) distribution of the wind and moisture fields.

Earlier and successful applications of the aerological method on the regional to continental scale are the works of Hutchings (1957), Palmén (1966) and Rasmusson (1967 and 1968). All these studies were based on informations provided solely by the operational rawinsonde network. As discussed in Rasmusson (1977), the limitations of the network, as well as the accuracy of the basic data, restrict the choice of the time and space scales for which meaningful results can be obtained. The first attempt to compute the area averaged precipitation for Greenland by evaluating the atmospheric water balance (Wilson, summarized in Reed, 1959) also suffered from the paucity of aerological stations. The potentiality of the method was demonstrated, however, by the evident improvements obtained by the addition of subjectively analyzed wind and moisture data.

With the advent of numerical weather forecast products, subjective analyses of the basic meteorological fields have been replaced by objective analyses that are produced routinely at the major centres for weather forecast by the optimal combination of model results and observations. Among other products, the analyses of the European Centre for Medium-Range Weather Forecasts (ECMWF) have formed the basis for several investigations of the zonally averaged budgets of energy and moisture (Masuda, 1988; Michaud and Derome, 1991), of the horizontal distribution of diabatic heat sources (Fortelius and Holopainen, 1990), as well as for the assessment of the regional characteristics of the atmospheric hydrological cycle (Matsuyama, 1992, Schaack et al., 1993). The ECMWF analyses may therefore be well suited for the purpose of calculating the atmospheric water vapour budget in Greenland.

The present work seeks to provide quantitative estimates of the monthly and annual water vapour budget in Greenland and to elucidate the nature of the precipitation in the Greenland area. The water vapour flux and flux divergence are evaluated using analyses of the ECMWF for the years 1989 to 1991. In a first step, the quality of the analyses is examined. Subsequently, the distributions of the annual and monthly divergence are discussed and compared quantitatively to independent precipitation and evaporation estimates. Following, an updated description is given of the seasonal characteristics of the moisture flux and flux divergence in relation to the general atmospheric conditions. Finally, the attention is focused on the role played by the transient disturbances.

## 2 THE ATMOSPHERIC WATER VAPOUR BALANCE

For an atmospheric column of unit area of base, extending from the Earth's surface to the top of the atmosphere, the time-averaged water budget is usually written in the form (Peixoto, 1973):

$$\overline{E-P}=\overline{\frac{\partial}{\partial t}\left\{\frac{1}{g}\int_{p_t}^{p_s} q\,dp\right\}+\nabla_h\cdot\left\{\frac{1}{g}\int_{p_t}^{p_s} v_h q\,dp\right\}}, \qquad (2.1)$$

where $E$ is the evapotranspiration at the surface, $P$ is the precipitation at the surface, $p_s$ and $p_t$ are the pressure at the surface and at the top of the atmosphere, respectively, $g$ is the acceleration due to gravity, $q$ is the specific humidity, $v_h$ is the horizontal wind vector, $\partial/\partial t$ is the local time derivative ,$\nabla_h$ is the two-dimensional Nabla operator and an overbar indicates a time average. In studies of the moisture budget, the upper limit of integration is normally taken at an appropriate level, where the moisture content becomes negligibly small. The equation expresses the balance between the net flux of water at the surface, on the left hand side (lhs), and the sum of the change in the water vapour content plus the divergence of the horizontal water vapour flux, on the right hand side (rhs). It neglects the solid and liquid phase except in $P$. This latter approximation is discussed in Palmén (1967), Peixoto (1973) and Rasmusson (1977).

In (2.1), the surface pressure is itself a function of time, whereas the upper limit of integration can be set constant in time. For further rearrangement, the surface pressure is substituted with its time mean value. The effect of this approximation on the moisture budget is generally small. With the aid of the first mean value theorem of integration (Dutton, 1976) and scaling arguments, it is possible to demonstrate that the relative error involved in this approximation is in most cases of the order of 1% (see Appendix 1). The substitution makes it possible to reformulate (2.1) as follows:

$$\begin{aligned}\overline{E}-\overline{P}&=\left\{\frac{1}{g}\int_{p_t}^{\overline{p}_s}\frac{\partial\overline{q}}{\partial t}\,dp\right\}+\nabla_h\cdot\left\{\frac{1}{g}\int_{p_t}^{\overline{p}_s}\overline{v_h q}\,dp\right\} \\ &=\left\{\frac{1}{g}\int_{p_t}^{\overline{p}_s}\frac{\partial\overline{q}}{\partial t}\,dp\right\}+\nabla_h\cdot\left\{\frac{1}{g}\int_{p_t}^{\overline{p}_s}(\overline{v_h}\cdot\overline{q}+\overline{v_h'q'})\,dp\right\},\end{aligned} \qquad (2.2)$$

where a prime denotes a deviation from the time average. On the rhs of (2.2), $\overline{v_h} \cdot \overline{q}$ is the water vapour flux achieved by the mean circulation and $\overline{v_h' q'}$ the moisture flux achieved by the transient eddies, or the eddy moisture flux. The use of (2.2) instead of (2.1) has practical advantages, because only time averages appear on the rhs.

For the investigation of the eddy moisture flux, two approaches are chosen in the present work. In the first place, the characteristics of the transient eddy flux in the frequency space are investigated by spectral analysis (Panofsky and Dutton, 1984), which leads to the representation of the correlation $\overline{v_h' q}$ in terms of the cospectral density vector $C_{v_h q}(f) = \left(c_{uq}(f), c_{vq}(f)\right)$:

$$\overline{v_h' q'} = \int_{-\infty}^{\infty} C_{v_h q}(f)\, df = \int_0^{\infty} \left[ C_{v_h q}(+f) + C_{v_h q}(-f) \right] df = \int_0^{\infty} 2\, C_{v_h q}(+f)\, df \ , \qquad (2.3)$$

where

$$c_{uq}(f) = \int_{-\infty}^{\infty} r_{uq}(\ell) e^{-i2\pi f \ell}\, d\ell \quad \text{and} \quad c_{vq}(f) = \int_{-\infty}^{\infty} r_{vq}(\ell) e^{-i2\pi f \ell}\, d\ell \ . \qquad (2.4)$$

In (2.3) and (2.4), $f$ is the frequency, $\ell$ the time lag and $R_{v_h q}(\ell) = \left(r_{uq}(\ell), r_{vq}(\ell)\right)$ the correlation vector, which is assumed to depend only on the time lag. The second and third equalities in (2.3) follow from the fact that the cospectral density is, for real valued processes, an even function of $f$ (Preistley, 1981). Using (2.3), equation (2.2) becomes:

$$\overline{E} - \overline{P} = \frac{1}{g} \int_{p_t}^{\overline{p_s}} \frac{\partial \overline{q}}{\partial t}\, dp + \nabla_h \cdot \frac{1}{g} \int_{p_t}^{\overline{p_s}} \overline{v_h} \cdot \overline{q}\, dp + \int_0^{\infty} \left\{ \nabla_h \cdot \frac{1}{g} \int_{p_t}^{\overline{p_s}} 2 C_{v_h q}(f)\, dp \right\} df \ . \qquad (2.5)$$

The brackets in the last term of (2.5) represent the divergence of that contribution to the (vertically integrated) eddy moisture flux that falls in the frequency interval $[f, f+df]$. On the other hand, when the time-averaged surface pressure is not a function of the spatial coordinates (but the reasoning can be extended to the more general case by application of the Leibniz rule), this same term can be interpreted as the contribution by the frequency interval $[f, f+df]$ to the eddy moisture flux divergence. This is possible, since in this case the gradient operator $\nabla_h$ can be taken inside the Fourier representation (2.3).

In the second approach, the eddy flux is separated by conditional analysis in order to take the sign of $q'$ into account. The primary condition distinguishes between what may be called dry spells ($q' < 0$) and wet spells ($q' > 0$). An additional condition is defined

on the basis of the magnitude of the instantaneous eddy products $|v_h'q'|$ relative to the magnitude of the mean flux $|\overline{v_h'q'}|$. Mathematically:

$$WS_H = \langle v_h'q' \rangle_{WH} = \frac{1}{\tau}\int_0^{\tau} v_h'q' \cdot I_{WH}\, dt\ , \tag{2.6}$$

with

$$I_{WH} = \begin{cases} 1 & \text{if } q' > 0 \text{ and } |v_h'q'| \geq H \cdot |\overline{v_h'q'}| \\ 0 & \text{otherwise}\ , \end{cases} \tag{2.7}$$

and analogously,

$$DS_H = \langle v_h'q' \rangle_{DH} = \frac{1}{\tau}\int_0^{\tau} v_h'q' \cdot I_{DH}\, dt\ , \tag{2.8}$$

with

$$I_{DH} = \begin{cases} 1 & \text{if } q' < 0 \text{ and } |v_h'q'| \geq H \cdot |\overline{v_h'q'}| \\ 0 & \text{otherwise}\ . \end{cases} \tag{2.9}$$

Here, $WS_H$ are the wet events, $DS_H$ the dry events, $H$ the relative size and $\tau$ the averaging time. The eddy transport and transport divergence of the water vapour results from the addition of wet $WS_0$ and dry spells $DS_0$ at the relative size 0. This yields:

$$\overline{E} - \overline{P} = \left\{\frac{1}{g}\int_{P_t}^{\overline{p}_s} \frac{\partial \overline{q}}{\partial t}\, dp\right\} + \nabla_h \cdot \left\{\frac{1}{g}\int_{P_t}^{\overline{p}_s} \overline{v}_h \cdot \overline{q}\, dp\right\} + \nabla_h \cdot \left\{\frac{1}{g}\int_{P_t}^{\overline{p}_s} (WS_0 + DS_0)\, dp\right\}\ . \tag{2.10}$$

Seite Leer /
Blank leaf

# 3 DATA AND DATA PROCESSING

## 3.1 The data and the study area

Twice daily, uninitialized analyses at 00 and 12 UTC for the years 1989, 1990 and 1991 available from the ECMWF/TOGA Basic Level III Data Set at the European Centre for Medium-Range Weather Forecasts (ECMWF) are used to carry out the evaluation of the atmospheric water budget. At the ECMWF, the analyses are produced on model levels by intermittent assimilation of observations into the forecast cycle and by a statistically optimal combination of the observations with the 6 hour forecast fields (Bengtsson et al, 1982; ECMWF, 1992a). Subsequently, the analyzed fields are vertically interpolated to standard pressure levels and archived as spherical harmonic coefficients, with a horizontal resolution corresponding to the actual cycle of the forecast-analysis system. Since the forecast model as well as the analysis procedure are in permanent evolution, continuity in time of the assimilation products is not guaranteed. To be mentioned, for the three years examined in the present work, is the operational introduction on September 17, 1991, of the forecasting system with horizontal, triangular truncation at wavenumber 213 (i.e., resolving 213 waves around a great circle on the globe) and 31 vertical levels (T213L31), compared to the previous system with truncation at wavenumber 106 and 19 vertical levels (T106L19). This transition has evident effects on the analyzed surface fields and on upper air fields at low pressure levels. A full description of the ECMWF/WCRP archive and of the evolution of the analysis and forecasting systems since 1985 is given in ECMWF (1992b). A review of the major changes in the forecast-analysis system since 1979, as well as a critical discussion of their impact on atmospheric diagnostics, can be found also in Hoskins et al. (1989). Some aspects of the hydrological cycle in the forecast-analysis system are treated in Klinker (1993).

The analyzed fields consist of the so-called surface fields and upper air fields. The surface fields include: the mean sea-level pressure $mslp$, the surface pressure $p_s$, surface geopotential $\Phi_s$ and surface temperature $T_s$, the temperature $T$ and the dew-point $T_d$ at 2 m above ground and, finally, the horizontal wind components $u$ and $v$ at 10 m above ground. The upper air fields are the geopotential $\Phi$, the temperature $T$, the relative humidity $RH$ and the wind components $u$, $v$ and $\omega$ (the vertical velocity in isobaric coordinates). The surface fields are analyzed with respect to the model orography (Fig. 3.2b). The upper air fields are given on nine pressure levels, viz. 1000, 850, 700,

500, 400, 300, 200, 100 and 50 hPa. All values are gridpoint values on a spherical grid with an horizontal resolution of 2.5°.

The study area (Fig 3.1) is delimited by the 50°N and 87.5°N latitudinal circles and by the 90°W and 0°W meridians and it is resolved by 37 gridpoints in the zonal direction and 16 gridpoints in the meridional direction. Also shown in Fig 3.1 are meteorological stations for which monthly precipitation records for the three years 1989-1991 are available (cf. Chapter 5).

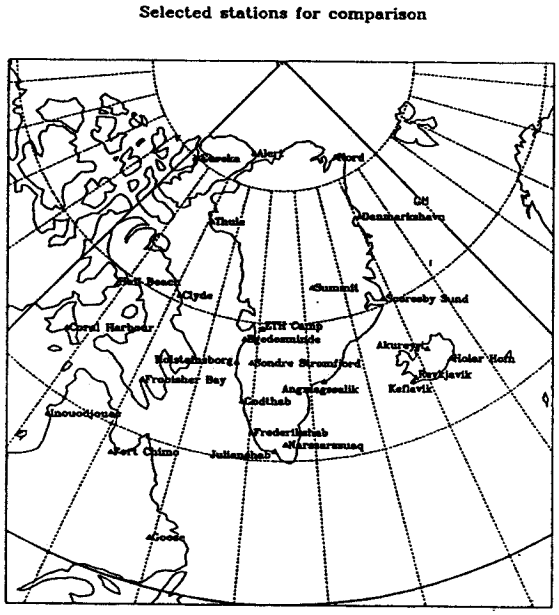


**Fig. 3.1**: Geographical map of the study region. The calculations are confined to the area delimited by the bold curve. Also shown are meteorological stations used for comparison.

The orography of the study area is displayed in Fig. 3.2a (more precisely, it is the ETOPO5 orography, kindly provided by the National Geophysical Data Center, Marine Geology and Geophysical Division, NOAA/NESDIS E/GC, Boulder, CO, U.S.A.). In Fig. 3.2b, in addition, the model orography for the T106 model version is shown for comparison. This latter is the so-called envelope orography, which is obtained by adding to the (grid-element-)area mean orography an increment proportional to the sub-grid-scale standard deviation (Wallace et al., 1983). The envelope orography was originally introduced to improve the medium-range forecasts (Tibaldi, 1986; Jarraud et al., 1988).

The departure of the model orography from the real one is best seen in cross sections. The latitudinal cross sections of Fig. 3.3 reveal that, for Greenland, the most conspicuous differences are encountered along the coast and are the consequence of the steepness of the orography there. In the marginal zones, the model orography is characterized by much weaker surface gradients. Although an examination of the

dynamical implications of this rather different situation will not be undertaken in the present study, it can safely be stated that, for the study area, large computational errors and large deviation of the results from the true fields are most likely to arise in the coastal sectors of the land masses.

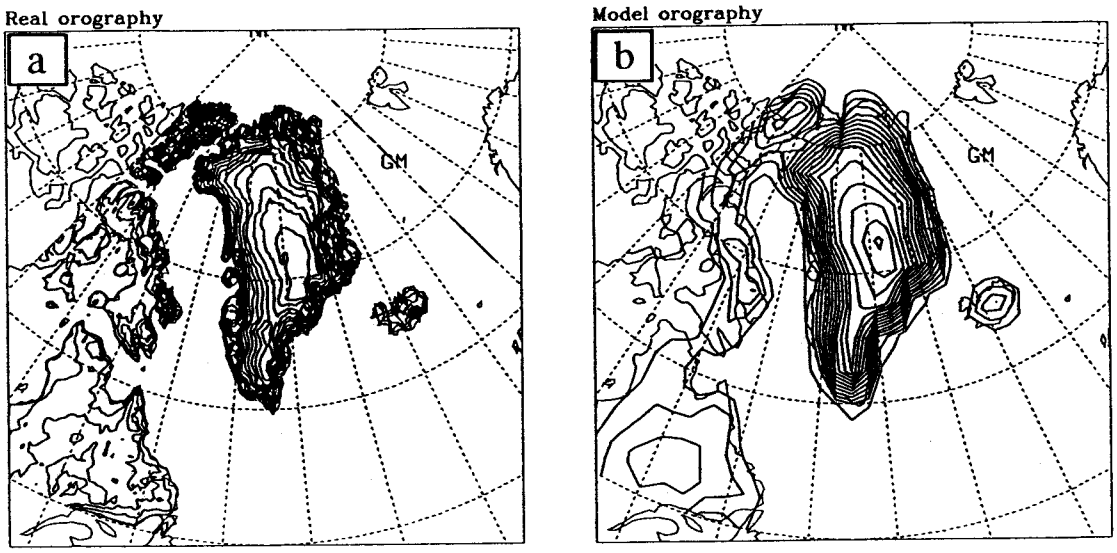


**Fig. 3.2** : Real (a) and model (b) orographies of the study area. Contour interval: 200 m.

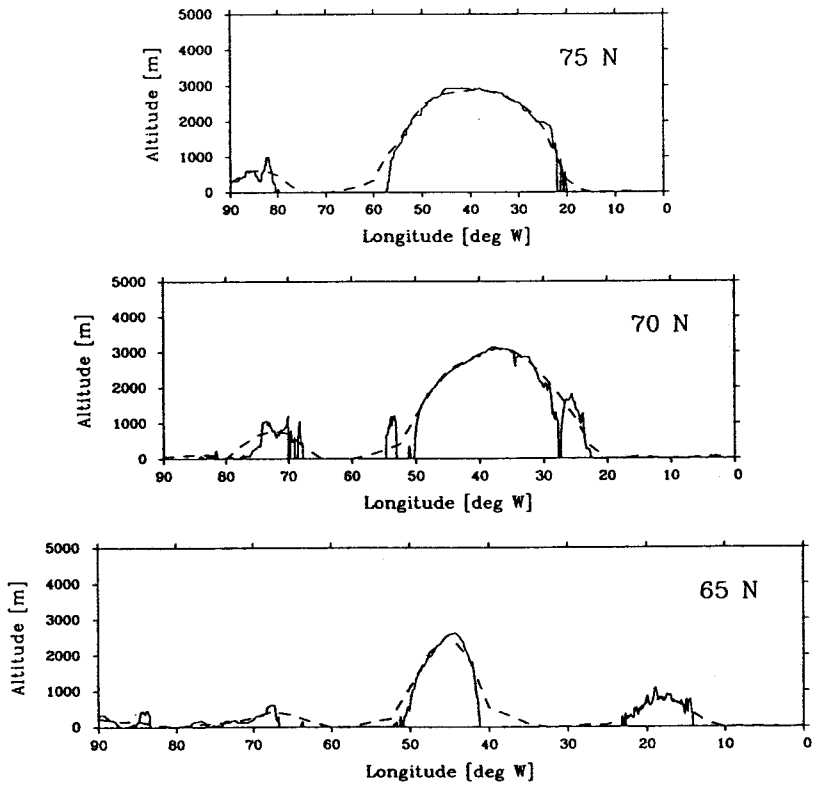


**Fig. 3.3** : Latitudinal cross-sections at 75°N (upper), 70°N (middle) and 65°N (lower panel). The ETOP topography (see text for explanation) is indicated by the full line, whereas the dashed line displays the model orography as used in the T106 cycle of the ECMWF forecast model.

## 3.2 Methods of evaluation

*Monthly and seasonal statistics*

As outlined in Alestalo and Holopainen (1980) and Oort (1983), the first step of the data processing is the computation of monthly averages, variances and covariances for each gridpoint from the twice daily analyses. The procedure is effective for the purpose of reducing the data storage requirements. In addition to the statistics for the basic fields, the calculated statistics include averages and variances of the specific humidity $q$, the potential temperature $\theta$, the pseudo-equivalent potential temperature $\theta_e$, the lifting condensation level $LCL$, the relative vorticity $\zeta$ and Ertel's potential vorticity $PV$, as well as the average fluxes $\overline{uq}$ and $\overline{vq}$, the covariances $\overline{u'q'}$ and $\overline{v'q'}$ and the local time derivative $\partial\overline{q}/\partial t$ (see Appendix 2 for a definition of the pseudo-equivalent potential temperature and a derivation of the lifting condensation level). The time integration is performed by the trapezoidal rule starting from 00 UTC of the first day of the month to 00 UTC of the first day of the next month. Consistent with this numeric formulation, the tendency $\partial\overline{q}/\partial t$ is simply calculated as the difference between the value at 00 UTC of the first day of the subsequent month and the value at 00 UTC of the first day of the month under consideration.

From the monthly statistics, seasonal statistics are derived through the relations (Oort, 1983):

$$\overline{\overline{A}} = \sum_{i=1}^{3} \frac{\tau_i}{\tau} \overline{A_i} \tag{3.1}$$

and

$$\overline{\overline{A''B''}} = \sum_{i=1}^{3} \frac{\tau_i}{\tau} \left\{ \left(\overline{A'B'}\right)_i + \left(\overline{A_i} - \overline{\overline{A}}\right)\left(\overline{B_i} - \overline{\overline{B}}\right) \right\}, \tag{3.2}$$

where a double over-bar indicates a seasonal average and a double prime the deviation from it, $\tau_i$ is the duration of month i and $\tau$ is the duration of the season. The seasons are defined as the successions; December-January-February (DJF) for the winter, March-April-May (MAM) for the spring, June-July-August (JJA) for the summer and September-October-November (SON) for the autumn.

*Vertical integrals and horizontal divergence*

Vertical integrals are calculated similarly to the time integrals by application of the trapezoidal rule. The first layer is taken as the layer between the surface and the first standard isobaric level above the surface. The formal expression is the same as given in Peixoto (1973, p. 74). The area averaged horizontal divergence of the vertically-integrated water vapour flux, $DQ_{i,j}$, and accordingly of the wind are calculated at the centre of each grid element by centred differences:

$$DQ_{i,j} = \frac{1}{S_{i,j}}\left[(UQ_{i+1,j} - UQ_{i,j}) + (VQ_{i,j+1} - VQ_{i,j})\right] \quad , \quad i = 1, I-1; j = 1, J-1 \, , \tag{3.3}$$

where (I-1) and (J-1) are the number of cells in the zonal and meridional direction, respectively, $S_{i,j}$ is the area ot the grid element (i,j) delimited by the latitudinal circles $\varphi_j$ and $\varphi_{j+1}$ and by the meridians $\lambda_i$ and $\lambda_{i+1}$, and $UQ_{i,j}$ and $VQ_{i,j}$ are the integrated fluxes normal to the side of the grid element. $S_{i,j}$, $UQ_{i,j}$, and $VQ_{i,j}$ are defined as through:

$$\begin{aligned} S_{i,j} &= \int_{\varphi_j}^{\varphi_{j+1}} \int_{\lambda_i}^{\lambda_{i+1}} a^2 \cos(\varphi)\, d\lambda\, d\varphi &&= a^2 \left[\sin(\varphi_{j+1}) - \sin(\varphi_j)\right] \Delta\lambda \\ UQ_{i,j} &= \int_{\varphi_j}^{\varphi_{j+1}} \langle uq(\lambda_i, \varphi) \rangle\, a\, d\varphi &&\cong \frac{1}{2}\left(\langle uq_{i,j} \rangle + \langle uq_{i,j+1} \rangle\right) a \Delta\varphi \\ VQ_{i,j} &= \int_{\lambda_i}^{\lambda_{i+1}} \langle vq(\lambda, \varphi_j) \rangle\, a \cos(\varphi_j)\, d\lambda &&\cong \frac{1}{2}\left(\langle vq_{i,j} \rangle + \langle vq_{i+1,j} \rangle\right) a \cos(\varphi_j) \Delta\lambda \quad , \end{aligned} \tag{3.4}$$

where $a$ is the Earth's radius, $\Delta\varphi = \varphi_{j+1} - \varphi_j$, $\Delta\lambda = \lambda_{i+1} - \lambda_i$ and $\langle ... \rangle = g^{-1} \int ... dp$ are the increments in the latitudinal and longitudinal direction and the vertical integrating operator, respectively. This formulation of the divergence is in fact an integral expression that makes implicit use of the Gauss' theorem. It is analogous to the one proposed by Ehrendorfer et al. (submitted) and is chosen explicitely to apply their correction algorithm to the wind field (see Chapter 4).

*Spectral analysis*

Spectra and cross spectra are estimated following Priestley (1981) and Newland (1984). The seasonal time series are linearly detrended and cosine tapered in the first and last 10% of the series. Fourier coefficients are computed by Fast-Fourier-Transform (FFT)

and spectral estimates are found by complex multiplication of the Fourier coefficients. The spectral estimates are slightly smoothed by application of a Bartlett-Priestley window. From the smoothed spectral densities, block sums (Kaimal, 1988) are constructed for the frequency intervals corresponding to: [32,128], [21,32], [16,21], [10,16], [9,10], [8,9], ..., [2,3], [1,2] days. The intervals are nearly equidistant in the log-frequency space, but a higher resolution is retained at high frequencies.

*Spatial smoothing*

In order to eliminate the overwhelming small scale structures from the wind divergence and water vapour flux divergence fields, a two-dimensional, isotropic filter is applied to these fields before graphical display. The filter is defined as follows:

$$w(\alpha) = \begin{cases} 1 - \left|\dfrac{\alpha}{\alpha_0}\right| & \text{if } \alpha \le \alpha_0 \\ 0 & \text{if } \alpha > \alpha_0 \end{cases}, \qquad (3.5)$$

where $w(\alpha)$ is the weight, $\alpha$ the great circle distance on the sphere and $\alpha_0$ defines the limit of the smoothing domain. Expressing $\alpha$ in degrees and choosing $\alpha_0 = 5°$ yields, for the given horizontal resolution of 2.5°, a filter that is similar to a 1-2-1 filter (Broccoli & Manabe, 1992). However, the definition (3.5) has the advantage of being independent on latitude. The filter yields comparable results to those obtained through bicubic spline smoothing, implemented for example in the subroutine E02DDF of the NAG library (NAG, 1990), but is computationally more efficient. It yields optically more balanced fields then the Tukey's median filter described in Oort (1983), since this latter creates isolines that are somewhat cornered and clustered.

# 4 PRELIMINARY INVESTIGATIONS

The first step in this investigation of the atmospheric water budget over Greenland is dedicated to an examination of possible sources of errors, specifically those related to, or arising directly from the discrete nature of the ECMWF analyses. The atmosphere is in fact a continuous medium that can be described numerically only in an approximative way. Concretely, the discussion will hinge on the vertical and horizontal discretization and the necessity for spatial smoothing, the time discretization and the mass imbalance of the wind field. The former two will be treated separately, because they are so in the forecast-analysis system (but the separation is justified by the shallowness of the atmosphere). The mass imbalance is, to a large degree, an artificial figure due to the practice of switching from model to pressure levels to meet the standard meteorological format of upper air data records.

## 4.1 Vertical discretization

In order to introduce the discussion about the vertical discretization of the atmosphere, vertical profiles of the specific humidity at two selected locations in Greenland are shown in Fig. 4.1 for June 20, 1991, 00 UTC. The data were extracted from the archive of the Greenland ETH Expedition 1991 (Ohmura et al., 1992). For comparison, specific humidity profiles as analyzed at the ECMWF are also plotted in this figure. The profiles are superimposed on a latitudinal cross section of the study area. The standard pressure levels are drawn to illustrate the vertical grid.

The outstanding feature in Fig. 4.1 is the concentration of the moisture in the lower half of the troposphere. In relation to this characteristic, and in view of the vertical grid structure, the failure of the standard pressure coordinates system to resolve adequately the lower troposphere becomes an obvious consequence. In principle, as proposed by Palmén (1967), a minimum resolution of 50 hPa should be prescribed below 400 hPa. The requirement could be even more stringent when the topography is considered, because not even a spatially homogeneous vertical resolution is guaranteed by vertical coordinates which do not follow the terrain (refer in Fig 4.1 to the relative altitude of the standard pressure levels with respect to the surface and at where they intersect the humidity profiles). For Greenland, furthermore, the standard pressure system is inadequate to describe the atmospheric boundary layer, which is characterized by stable

conditions and katabatic winds (Forrer, 1992; Niederbäumer, 1992). In the context of the atmospheric branch of the hydrological cycle it must be recognized that: the katabatic wind layer may affect considerably the mass flux (Parish and Waight III, 1987), and therefore the moisture flux; the evaporation rate at the surface is governed by the turbulence structure in the boundary layer.

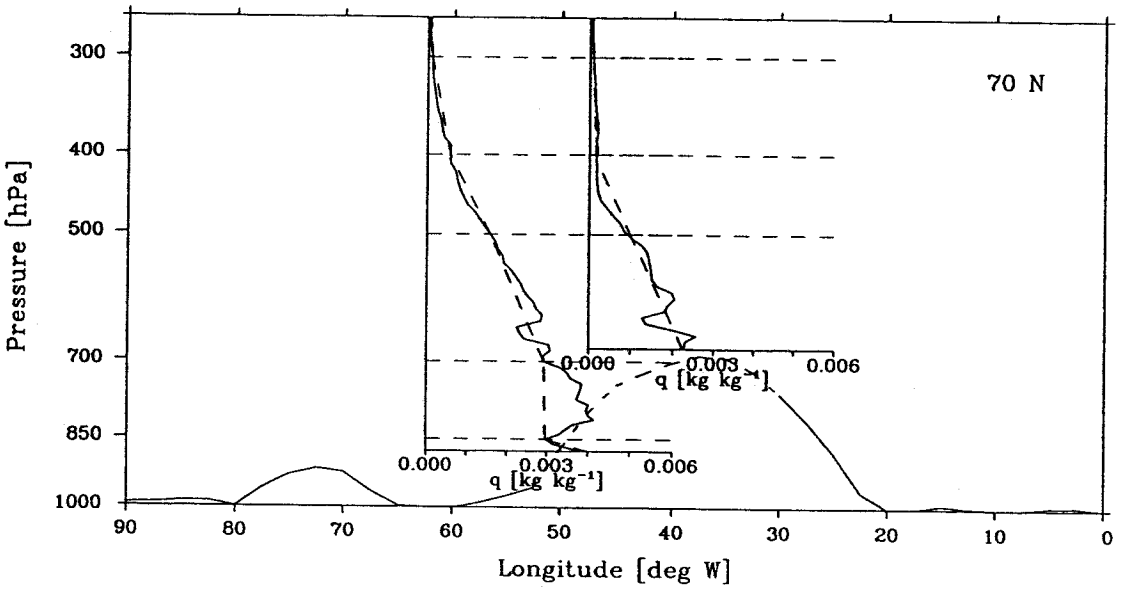


**Fig. 4.1** : Latitudinal cross sections of the study area at 70°N and specific humidity profiles at the ETH Camp (69°34'N, 49°18'W, 1155 m.a.s.l.) and at Summit (72°34'N, 37°37'W, 3230 m.a.s.l.), for June 20, 1991, 00 UTC. The broken line illustrates how the same profiles are approximated in the standard pressure system shown with thin horizontal lines.

Considering the whole troposphere, it is seen that the standard pressure grid is insufficient to account for the large variability that characterizes the vertical profiles of the specific humidity (Fig. 4.1) and of the wind (not shown). In theory, an exact numerical evaluation of vertical integrals would require a proper description of the subgrid-scale variability. In practice this latter is neglected, since a piecewise, linear functional dependence of the meteorological parameters on pressure is assumed. This approximation introduces an error, that potentially may be large. For the the ETH Greenland Expedition Camp (69°34' N, 49°18' W, 1155 m.a.s.l.; average surface pressure: 877 hPa) and for Summit (72°34' N, 37°37' W, 3230 m.a.s.l.; average surface pressure: 675 hPa), the inaccuracy of vertical integrated quantities due to the use of the standard pressure system can be estimated on the basis of humidity and wind profiles from the ETH Greenland Expedition Data Archive (Ohmura et al., 1992).

From June 13 to July 18, 1991, radiosondes were launched simultaneously once a day (00 UTC) at the ETH Camp and at Summit. In addition, on June 15, July 1 and July 9,

radiosondes were also started at intermediate hours (see Ohmura et al., 1992, for details). On June 29 and 30, and July 10 to 12, problems with the OMEGA finding system caused incomplete wind profiles at Summit. These days are neglected in the analysis. In summary, a total of 39 soundings with complete wind and humidity profiles can be used to calculate vertical integrals. The data preparation is as follows. In a first step, vertical profiles of $u$, $v$, and $q$ with a resolution of 10 hPa are derived for each sounding through cubic spline interpolation from the original profiles. Profiles of the zonal and meridional moisture flux, $uq$ and $vq$, are computed at each time and with the same vertical resolution. Profiles of $\overline{q}$, $\overline{uq}$, $\overline{vq}$, $\overline{u'q'}$ and $\overline{v'q'}$ are then approximately derived by computing, on each pressure level, the arithmetic mean of the appropriate quantity over the 39 realizations. Finally, vertical integrals of the averaged variables are calculated taking all levels into account, on the one hand, and on the basis of the standard pressure levels only, on the other hand. The departure of the standard levels computations from the integrals obtained with all levels, which are considered as the exact values, yields a quantitative estimate of the accuracy of vertical integrals in the standard pressure system.

The comparison shows, for all variables, relative departures in the order of 5% for the ETH Camp site, whereas the deviations amount to more than 10% for Summit. Absolute differences are comparable for both locations, although they tend to be slightly larger for Summit. Considering the profiles in Fig. 4.1, the magnitude of the relative departures is at first surprising. However, it must be recognized that the processing scheme, in which time averaging is performed prior to vertical integration, yields relatively smooth profiles that do not suffer to much from the lack of vertical resolution. This is clearly seen in Fig. 4.2, which shows profiles of $\overline{q}$, $\overline{uq}$, $\overline{vq}$ at the ETH Camp site. For comparison, individual profiles for $q$, $uq$, $vq$ on June 20, 1991, 00 UTC, are also depicted.

A larger departure is obtained when the order of computation is reversed, that is, when vertical integration is performed before time averaging. In fact, the error arising from the use of standard pressure levels only increases to about 20% for Summit, whereas it is in the order of 5% to 10% for the ETH Camp.

The issue of the vertical resolution can not be left without mentioning its implications for the moisture flux divergence field. Numerically, the divergence is the difference of two numbers. Often it is the small difference between two large values and, in some circumstances, it may be as small as the error in one of the two original values. This means that relative errors as large as 100% may occur. Consider for instance a purely zonal flow in the x-direction and a humidity distribution such that the vertically-

integrated zonal moisture flux at two locations $x_1$ and $x_2$ is given by $UQ_1$ and $UQ_2=UQ_1+\Delta UQ$. Typically, $\Delta UQ= 0.1*UQ_1$ for $\Delta x=x_2-x_1 \sim 10^2$ to $10^3$ km (consider e.g. Fig. 5 in Peixoto and Oort, 1983). For the sake of simplicity, assume that the vertically-integrated moisture flux could be determined exactly at $x_1$ but only with an accuracy of approximately 5% at $x_2$, the error being due to the vertical coordinate system. In full terms, $UQ_2=UQ_1+\Delta UQ\pm\delta UQ$, where $\delta UQ \sim 0.05*UQ_1$. Since the flow is zonal, the water vapour flux divergence is simply $\nabla UQ=(UQ_1-UQ_2)/\Delta x$ or $\nabla UQ=\Delta UQ/\Delta x\pm\delta UQ/\Delta x$ . Finally, the ratio of the error to the true value is $\delta UQ/\Delta UQ$ and, based on the previous assumptions, it is equal to 0.05/0.10=0.5 or 50%. Clearly, there exists an intrinsic potential for large errors when the divergence is evaluated numerically from slightly inexact values of the moisture flux.

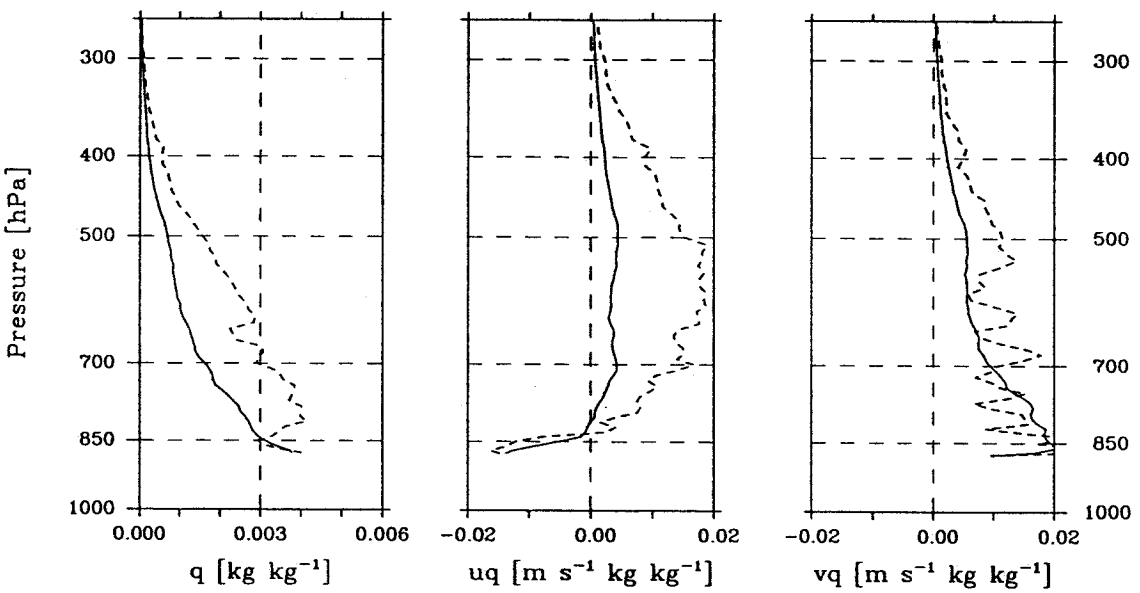


**Fig. 4.2** : Profiles of $\overline{q}$, $\overline{uq}$ and $\overline{vq}$ (full line), as well as individual profiles of $q$, $uq$ and $vq$ for June 20, 1991, 00 UTC (broken line) at the ETH Camp site (69°34'N, 49°18'W, 1155 m.a.s.l.).

## 4.2 Spatial smoothing

Very recently, Trenberth and Solomon (1993) have drawn attention to a computational problem that has its origins in the way the horizontal dimension is handled in the forecast model of the ECMWF. Consistent with the model formulation, the analyses are routinely stored as spherical harmonic coefficients with a spectral resolution corresponding to the actual state of the forecast model (viz. a triangular truncation at total number 106 for the period January 1, 1989 to September 16, 1991, and a triangular truncation at total wavenumber 213 for September 17 to December 31, 1991). If required, gridpoint values with a specified resolution are retrieved directly from the spherical harmonic coefficients. An additional truncation in the wavenumber space to match the desired resolution in the physical space is omitted and, as a consequence, high wavenumber information is aliased back into resolvable scales. This consideration applies both to the archived fields as well as to the (wind and) moisture flux divergence field. For most of the archived fields (except perhaps the omega field, which is however retrieved in a second step), the natural predominance of large scale features dim the effects of the aliasing. In the geopotential field, for instance, wavy patterns with large wavenumber can be unequivocally discerned only at sea level over the oceans, i.e. only in the absence of an orographic signature. Physically impossible values of the relative humidity are also easily detected, but even so it is impossible to work out a general criterion to separate the error from the signal. In the case of the (wind and) moisture flux divergence, on the other hand, the distortion is expected to be large. Furthermore, it is superimposed on and not distinguishable from the error due to the vertical discretization, and the general impression (Fig. 4.3a) is that they dominate the overall appearance. In such circumstances, it may be more efficient to filter out all information in a defined interval of spatial scales instead of trying to model the error and eliminate it formally.

The effect of the filter (3.5) on the spatial distribution of the annual total divergence is shown in Fig. 4.3 for several choices of the parameter $\alpha_0$. The unsmoothed distribution is completely dominated by the small-scale noise. Clusters of isolines are seen overall, but especially along the coast of Greenland, where the calculations are particularly sensitive to horizontal gradients of the topography. As pointed out in Section 3.1 (Fig 3.3), the coastal regions are also those where the deviation of the model from the real topography is greatest and where, therefore, the departure of the computed divergence form the true value becomes possibly extreme. For $\alpha_0$=2.5° the noise still determines the overall appearance of the picture, although some natural patterns can

already be discerned, for instance, the area of low convergence, resp. divergence, in northeastern Greenland. As for the unsmoothed distribution, sharp, unrealistic peaks are still observed along the steep coastal escarpments of southeastern Greenland, which is indicative of the computational origins of these patterns. It may be noted that, for the given grid spacing of 2.5°, this choice of $\alpha_0$ implies smoothing only in the zonal direction. For $\alpha_0$=5.0°, the distribution over Greenland bears a much better resemblance to the annual distribution of precipitation as determined by Ohmura and Reeh (1991) (their Fig. 2, which appears in the present work as Fig. 5.2). Moreover, meridional gradients in the right magnitude appear over the North Atlantic, if they are compared to the difference of the evaporation from Isemer and Hasse (1987) minus the precipitation of Willmott and Legates (1990). For $\alpha_0$=7.5°, the major features remain in place, but the distribution seems subjectively too smooth. More and more information is lost when $\alpha_0$ is further increased, and for $\alpha_0 \geq 10.0°$ (not shown) only the area of strong convergence between Greenland and Iceland is still resolved.

A statistical measure of the effect of the filter can be obtained by comparing monthly values of the moisture flux divergence, derived at selected locations by bivariate interpolation from the smoothed distribution (Akima, 1978), with monthly precipitation data extracted from the monthly annexes to the 'Berliner Wetterkarten' (Institut für Meteorologie der Freien Universität Berlin) . The diagrams are presented in Fig. 5.4. The total root-mean-square (rms) difference, i.e., the averaged squared departure of the computed convergence (neg. divergence) from the measured precipitation for all stations and months, decreases from 55 mm month$^{-1}$ for the unsmoothed distribution to a minimum of 33 mm month$^{-1}$ for $\alpha_0$=5.0° and $\alpha_0$=7.5°, to increase again to 37 mm month$^{-1}$ for $\alpha_0$=15.0°. Although certainly not conclusive, the statistics support the impression that a choice of $\alpha_0$ between 5.0° and 7.5° yields an optimum distribution.

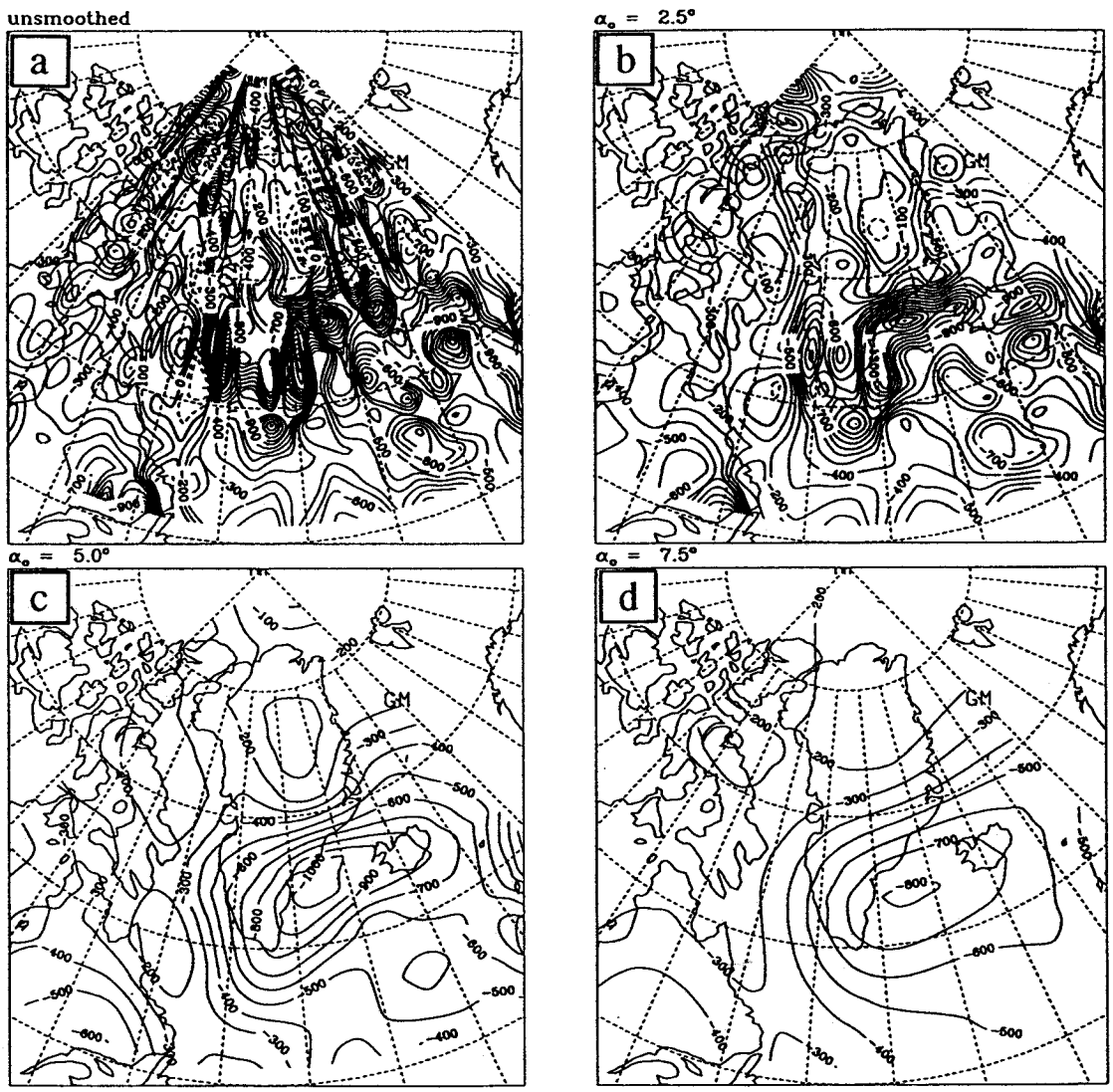


**Fig. 4.3** : Annual total divergence of the vertically-integrated water vapour transport [mm year$^{-1}$] smoothed according to eq. (3.5) for different choices of the parameter $\alpha_0$: a) unsmoothed ($\alpha_0$=0°) (upper left panel); b) $\alpha_0$=2.5° (upper right panel); c) $\alpha_0$=5.0° (lower left panel); d) $\alpha_0$=7.5° (lower right panel).

## 4.3 Sampling interval

During the warm season (in high latitudes) and under fair weather conditions, the atmospheric boundary layer is characterized by important diurnal fluctuations of the meteorological parameters. This is so even over the Greenland Ice Sheet (Ohmura et al., 1991. For the Canadian High Arctic see also Müller and Roskin-Sharlin, 1967). At the ETH Greenland Expedition site during the summer of 1990, the amplitude of the diurnal cycle of the water vapour pressure was as large 1 mb or 100 Pa. Diurnal cycles in the boundary layer are forced by the incoming solar radiation. On the meso- to continental scale, diurnal variations of the free atmospheric wind are capable of inducing corresponding diurnal fluctuations of the total moisture transport and transport divergence (Rasmusson, 1967 and 1968). These observations raise the question of whether a sampling rate of two times a day is sufficient to properly account for diurnal cycles.

A well-known limitation of discrete sampling is the fact that critical sampling of a sine wave of given frequency is two sample point per cycle (Press et al., 1986, p. 386). This is a necessary requirement but not a sufficient one, since it is also necessary for the sampling procedures to sample at the positive and negative peaks. In the extreme case when sampling leads or backs the peaks by a quarter of a period, sampling at a rate of twice per cycle results in a constant valued series. Thus, even in the most simple situation, sampling twice a day may not be sufficient to account properly for diurnal cycles. One could object that, at the critical sampling frequency of twice the wave frequency, the mean value of the resulting discrete time series is not dependent on the phase between wave and sampling. This is true for perfect sine waves, but not for wave-like functions which have, for example, a time dependent amplitude. Moreover, the standard deviation of the sampled series do depend on the phase, even for perfect sine waves.

Real processes can seldom be described in terms of a single sine wave. Rather, they can be expressed as the sum of several waves with different amplitude and frequency. For the same property of discrete sampling discussed in the previous paragraph, fixing the sampling rate determines unequivocally the maximum frequency that can still be resolved. Frequencies higher than this critical frequency becomes aliased back into lower frequencies.

Working with meteorological analyses adds another complication. Whereas diurnal cycles are related (by an appropriate phase) to the true solar time, the meteorological

conventions prescribe fixed (simultaneous) sampling times for the Earth as a whole. This may introduce a latitudinal dependence of the error.

To try to infer the adequacy of the 12-hour sampling interval for the evaluation of the moisture budget in the present study area, additional analyses at 06 and 18 UTC for June, July and August 1990 were included in the calculations. The analyses are retrieved from the so-called ECMWF/TOGA Advanced Operational Data Sets. Although basically produced with the same algorithm, the analyses at 06 and 18 UTC are more deepely shaped by the forecast than those at 00 and 12 UTC, since upper air observations are often carried out only at 00 and 12 UTC (Fortelius and Holopainen, 1990). The results presented in this section must therefore be interpreted with some caution.

The moisture flux divergence for July 1990 calculated on the basis of the standard set of analyses at 00 and 12 UTC is shown in Fig. 4.4. Its departure from the reference field computed on the basis of all four available analyses is displayed in Fig. 4.5. The corresponding fields for June and August 1990 (not presented) show the same large-scale features. In both figures, the total field is divided into a component by the mean circulation and one by the transient eddies. As seen in Fig. 4.5, the transient eddy contribution seems slightly less sensitive to the choice of the sampling rate than the contribution by the mean circulation. For the transient eddy contribution, the largest residual (in this context, residual is used as a synonym of departure) of the standard calculations from the reference computations is observed over the Labrador Peninsula and the eastern North Atlantic. Over Greenland, the residual of the eddy flux divergence is negligibly small. This is not so for the contribution by the mean circulation, which indicates an overestimation of the moisture flux divergence (underestimation of the convergence) over central western Greenland and an understimation of the divergence (over-estimation of the convergence) along the southeastern coast of Greenland. The water vapour flux divergence is also largely overestimated in the western North Atlantic, just off the coast of Labrador.

A quantitative measure of the importance of the residual moisture flux divergence field can be inferred by comparing it to the moisture flux divergence field itself. The ratio of the former to the latter is spatially averaged for four major subareas of Greenland, that is: northwestern (NW), northeastern (NE), southwestern (SW) and southeastern (SE) Greenland. These subregions are obtained by separating northern from southern Greenland at 70°N, and western and eastern Greenland along the major longitudinal ridge. For July 90, the areally averaged, relative residual of the moisture flux divergence by the transient eddies is only in the order of 5%, whereby the standard

calculations overestimate the divergence everywhere but in NE Greenland. For the water vapour flux divergence by the mean circulation, the range of values is much larger, going from an underestimation of the flux convergence by 50% in SW Greenland, to an almost unaccectable overestimation of the flux convergence by 100% in SE Greenland. Of course, large relative residual arise as a consequence of very small absolute values. The situation is in fact much less dramatic if the geographical distribution of the moisture flux divergence is considered. Adding daily two additional analyses at 06 and 18 UTC does not modify severely the large scale features of the flux divergence distribution shown in Fig 4.4.

The distribution of the residual moisture flux divergence can be better understood by also displaying the residual flux that generates it (Fig. 4.6). In the North Atlantic, the residual moisture flow by the mean circulation has a predominant easterly component. This means that the standard calculations based on only two analyses per day understimate systematically the westerly component of the moisture flux. The same holds for the southerly component of the water vapour flux by the mean circulation, which is understimated everywhere in the study area, except in the Denmark Strait. This additional on-shore component at the eastern coast of Greenland is clearly responsible for the excess of convergence seen in Fig 4.5. In the Baffin Bay the standard calculations based on the 00 and 12 UTC analyses yield a too-large export of moisture by the mean circulation and, as a consequence, a positive residual divergence. Comparing the magnitude of the residual moisture fluxes (Fig. 4.6) and the residual moisture flux divergence it is seen that, although the residual moisture flux achieved by the transients is much smaller than that achieved by the mean circulation, the same holds only to a lesser extent for the residual divergence. As pointed out by Salstein et. al. (1980), the moisture flow by the mean circulation is essentially a rotational flow as opposed to the merely divergent eddy moisture flow. This property seems also to apply, at least partly, to the residual fields presented here.

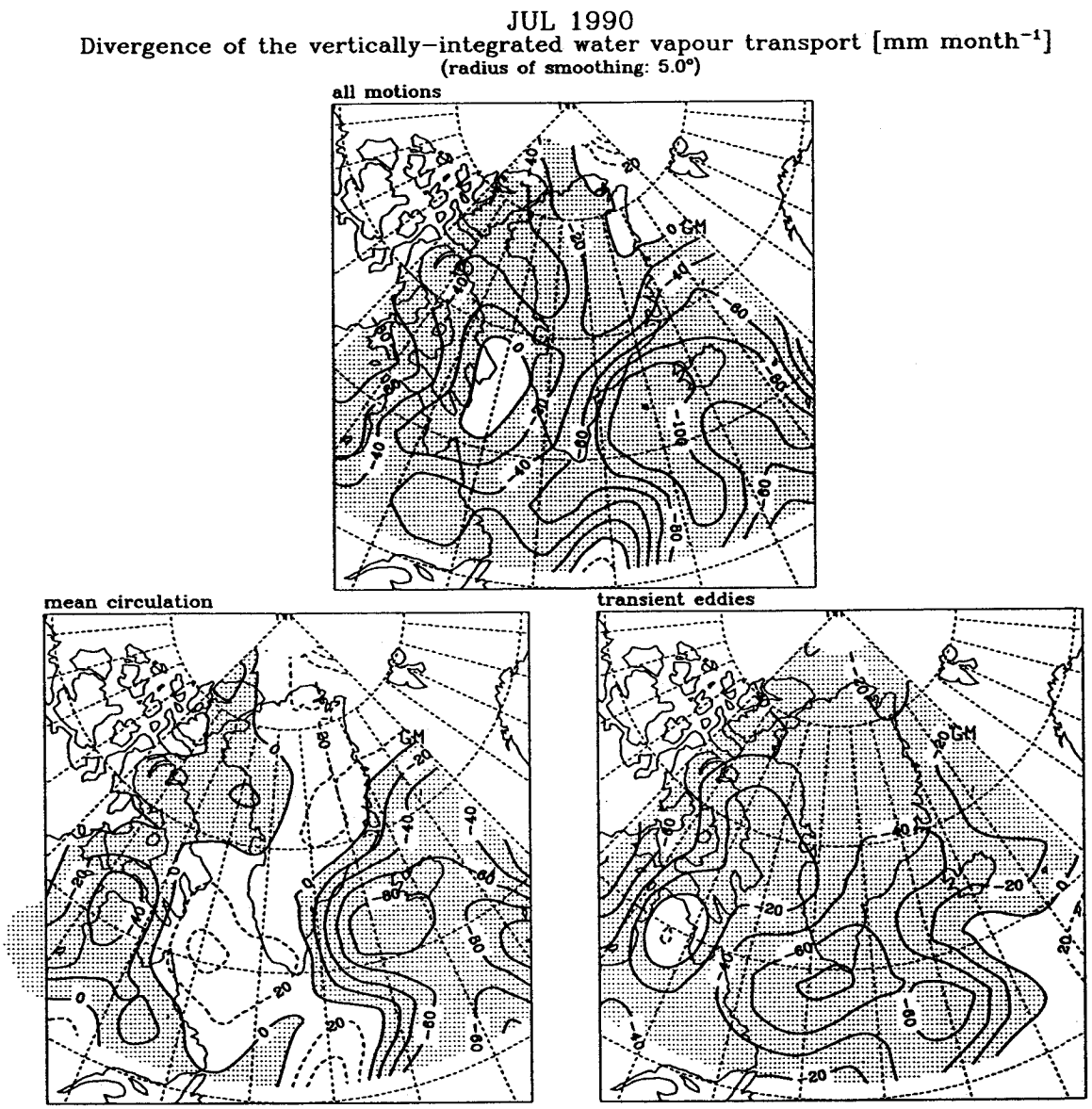


**Fig. 4.4** : Monthly total divergence of the vertically-integrated water vapour transport [mm month$^{-1}$] for July 1990 , calculated using the 00 and 12 UTC analyses [mm month$^{-1}$]. Shading indicates negative divergence or positive convergence, i.e., precipitation exceeding evaporation.

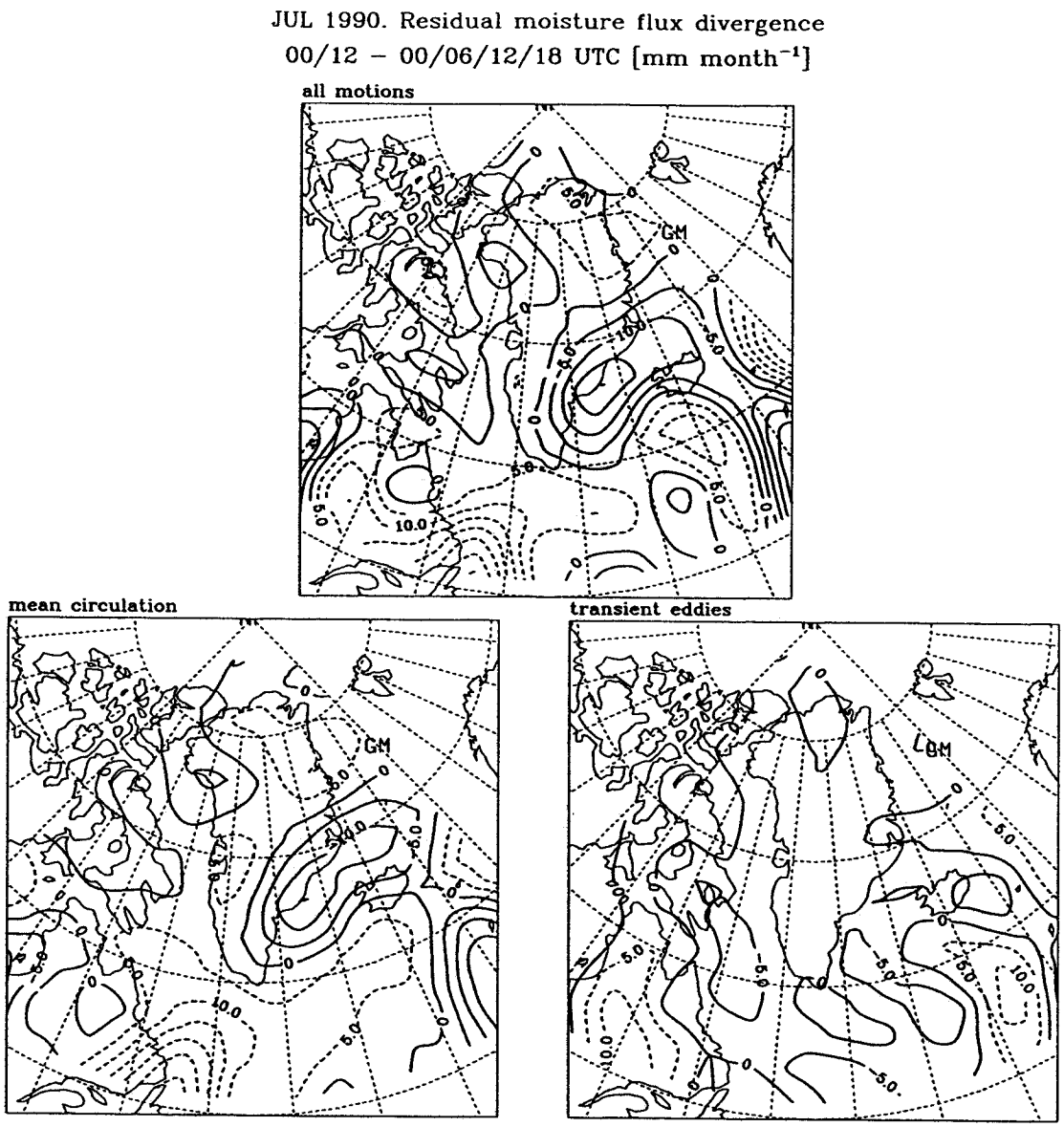


**Fig. 4.5** : July 1990. Deviation of the moisture flux divergence calculated on the basis of the standard 00 and 12 UTC analyses from the reference computed using all available analyses, i.e., at 00, 06, 12 and 18 UTC, [mm month$^{-1}$]. Negative departures indicating an underestimation of the divergence by the standard computations (or an overestimation of the convergence) are shown with dashed lines.

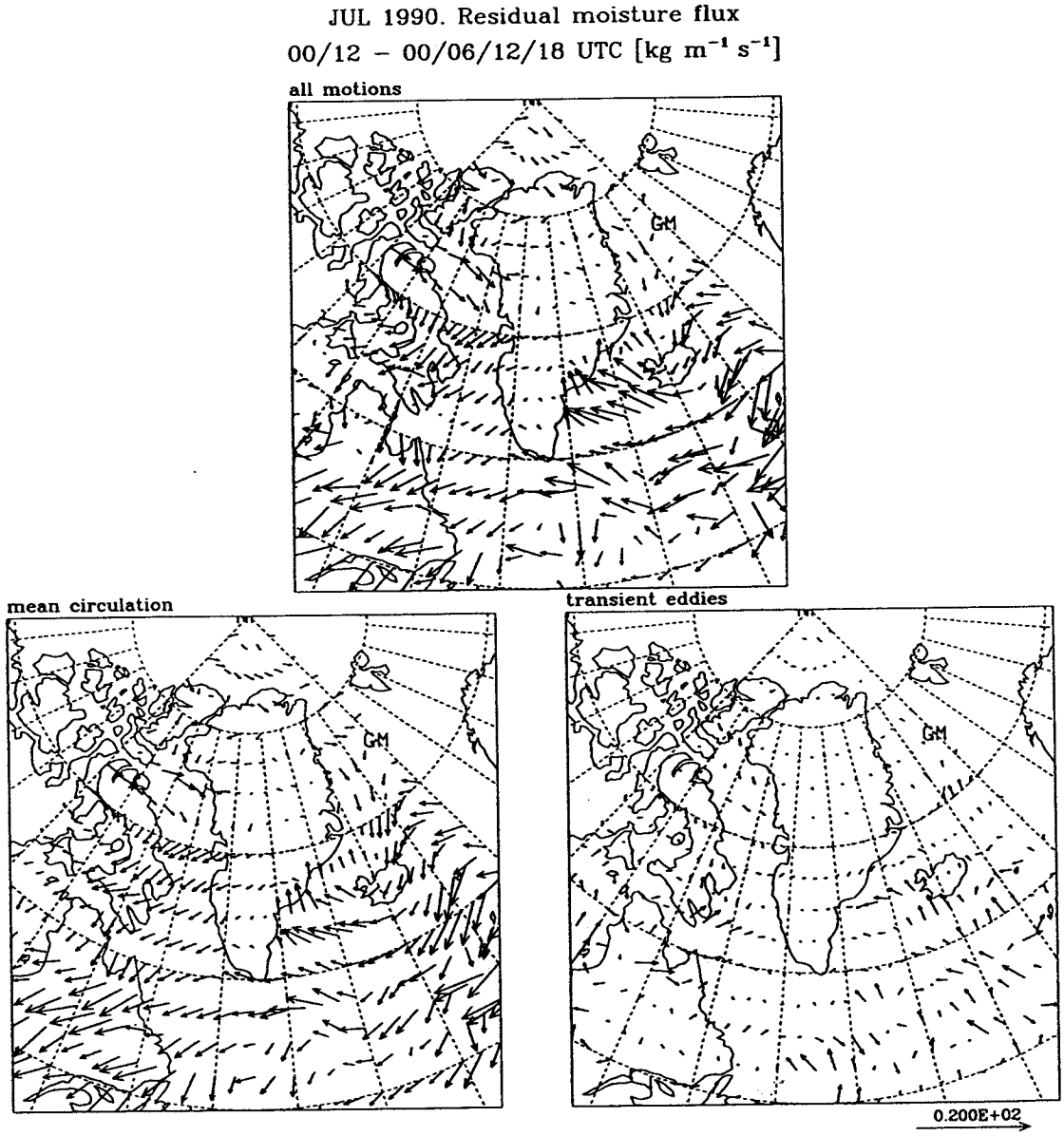


**Fig. 4.6** : July 1990. Deviation of the moisture flux calculated on the basis of the standard 00 and 12 UTC analyses from the reference computed using all available analyses, i.e., at 00, 06, 12 and 18 UTC, [kg $m^{-1}$ $s^{-1}$]. The scale is given in the lower right corner.

## 4.4 Mass balance

The vertical interpolation of the analyses, from the terrain-following model coordinates to the conventional pressure coordinates, during the post-processing phase introduces an inconsistency between the mass field and the wind field (Masuda, 1988; Trenberth, 1991). This is valid for uninitialized analyses as well as for initialized analyses (K. Masuda, pers. comm.), although the initialization is thought to restore the balance. The effect of the mass imbalance on calculations of the enthalpy budget is quite dramatic but previous studies (Alestalo, 1981; Trenberth, 1991) have clearly indicated that the moisture budget remains largely unaffected. An explanation can be given in terms of scaling considerations. For the sake of simplicity, a barotropic wind error (or, conversely, a barotropic wind correction, Trenberth, 1991) is assumed to affect only the two horizontal components . This is an acceptable assumption because the present investigation deals only with vertically integrated moisture fluxes and flux divergences.

The analyzed, horizontal wind field $v_h^a$ may be written as the sum of the true wind $v_h$ and a wind error equal to minus the barotropic wind modification $v_h^m$ required to restore the true wind. In full terms:

$$v_h^a(p) = v_h(p) + (-v_h^m) \ , \tag{4.1}$$

whereby only the dependence on pressure has been formally retained. Inserting (4.1) into the expression for the divergence of the vertically-integrated moisture flux yields:

$$\begin{aligned} \nabla \cdot \left\{ \frac{1}{g} \int_{p_t}^{p_s} v_h^a q \, dp \right\} &= \frac{p_s}{g} \nabla \cdot \langle v_h^a q \rangle \\ &= \frac{p_s}{g} \left\{ \nabla \cdot \langle v_h q \rangle - v_h^m \cdot \nabla \langle q \rangle - \langle q \rangle \nabla \cdot v_h^m \right\} \ . \end{aligned} \tag{4.2}$$

Here, $\langle ... \rangle$ denotes a vertical average, the lower limit of integration $p_t$ has been assumed to be negligibly small compared to $p_s$, the surface pressure has been taken as approximately independent on the horizontal position and the barotropy of the wind correction has been invoked to separate the divergence of the vertically averaged moisture flux correction. An equivalent expression can be derived for the divergence of the temperature flux (the enthalphy flux is obtained by multiplying throughout by $C_p$, the specific heat at constant pressure):

$$\nabla\cdot\left\{\frac{1}{g}\int_{p_t}^{p_s} v_h^a T\,dp\right\}=\frac{p_s}{g}\nabla\cdot\langle v_h^a T\rangle$$
$$=\frac{p_s}{g}\left\{\nabla\cdot\langle v_h T\rangle - v_h^m\cdot\nabla\langle T\rangle - \langle T\rangle\nabla\cdot v_h^m\right\}\ , \qquad (4.3)$$

where $T$ is the temperature. To show the influence of the wind error, typical values for the quantities appearing on the rhs of (4.2) and (4.3) are proposed as follows:

$$\begin{aligned}
\frac{p_s}{g}\nabla\cdot\langle v_h q\rangle &\approx 10^{-5}\ \text{kg m}^{-2}\ \text{s}^{-1} \qquad (\equiv 30\ \text{mm month}^{-1})\\
\frac{p_s}{g}\nabla\cdot\langle v_h T\rangle &\approx 10^{-1}\ \text{kg m}^{-2}\ \text{s}^{-1}\ \text{K}^{-1} \quad (\equiv 100\ \text{W mm}^{-2})\\
v_h &\approx 10^{-1}\ \text{m s}^{-1}\\
\nabla\cdot v_h &\approx 10^{-7}\ \text{s}^{-1}\\
\frac{p_s}{g}\langle q\rangle &\approx 10^{+1}\ \text{kg m}^{-2}\\
\frac{p_s}{g}\nabla\cdot\langle q\rangle &\approx 10^{-6}\ \text{kg m}^{-3}\\
\frac{p_s}{g}\langle T\rangle &\approx 10^{+6}\ \text{kg m}^{-2}\ \text{K}\\
\frac{p_s}{g}\nabla\cdot\langle T\rangle &\approx 10^{-1}\text{-}10^{0}\ \text{kg m}^{-3}\ .
\end{aligned} \qquad (4.4)$$

These values were derived from the statistics presented in Oort (1983) explicitely for the study area so as to strengthen the results of this simple scale analysis. Insertion of (4.4) into (4.2) and (4.3) gives:

$$\nabla\cdot\left\{\frac{1}{g}\int_{p_t}^{p_s} v_h^a q\,dp\right\}=\frac{p_s}{g}\nabla\cdot\langle v_h q\rangle - v_h^m\cdot\frac{p_s}{g}\nabla\langle q\rangle - \frac{p_s}{g}\langle q\rangle\nabla\cdot v_h^m$$
$$\approx \quad 10^{-5} \qquad 10^{-7} \qquad 10^{-6} \qquad \text{kg m}^{-2}\ \text{s}^{-1}\ , \qquad (4.5)$$

and

$$\nabla\cdot\left\{\frac{1}{g}\int_{p_t}^{p_s} v_h^a T\,dp\right\}=\frac{p_s}{g}\nabla\cdot\langle v_h T\rangle - v_h^m\cdot\frac{p_s}{g}\nabla\langle T\rangle - \frac{p_s}{g}\langle T\rangle\nabla\cdot v_h^m$$
$$\approx \quad 10^{-1} \qquad 10^{-2}\text{-}10^{-1} \qquad 10^{-1} \qquad \text{kg m}^{-2}\ \text{s}^{-1}\ \text{K}^{-1}\ . \qquad (4.6)$$

In both cases, the error due to the wind divergence is an order of magnitude larger than the error in the advection term (the second on the rhs). However, in the case of the temperature flux divergence, the signal itself (the first term on the rhs) is only of the same order as the dominant error. On the other hand, by the values given in (4.5), the moisture flux divergence may be assumed to be rather insensitive to a possible wind error resulting from a mass imbalance.

To proceed in the discussion, the analytical formulation for the barotropic wind modification is derived again following Trenberth (1991) closely. The conservation equation for the mass of dry air states that:

$$\left\{\frac{1}{g}\frac{\partial p_s}{\partial t}-\frac{\partial W}{\partial t}\right\}+\nabla_h\left\{\frac{1}{g}\int_{p_t}^{p_s}(1-q)\cdot v_h\,dp\right\}=0\,, \tag{4.7}$$

where $W$ is the precipitable water. When (4.7) is evaluated with the analyzed wind $v_h^a = v_h - v_h^m$, where again $v_h^m$ is the barotropic correction, an imbalance $RES$ arises that is given by:

$$RES=\nabla_h\left\{\frac{1}{g}\int_{p_t}^{p_s}(1-q)\cdot v_h^a\,dp\right\}\,. \tag{4.8}$$

The residual can be eliminated by adjusting the wind field according to:

$$v_h = v_h^a + v_h^m\,. \tag{4.9}$$

The barotropic correction $v_h^m$ is then given by:

$$v_h^m=\frac{\nabla\chi}{\frac{p_t-p_s}{g}+W}\,, \tag{4.10}$$

where $\chi$ is the velocity potential defined through:

$$\nabla^2\chi = RES\,. \tag{4.11}$$

An outstanding characteristic of the proposed adjustment procedure is revealed by the fact that the elimination of the mass imbalance does not at all require a complete elimination of the wind divergence, as would be the case if the moisture were not included in the conservation equation. Rather, the wind is altered in such a way that the divergence of the vertically-integrated, modified wind becomes numerically identical to the divergence of the vertically-integrated water vapour flux (this is verified by the

calculations). This means a reduction of the wind divergence by about 3 orders of magnitude (the relative magnitude of $q$ compared to 1). Therefore, the following symmetry can be observed: the divergence of the modifying wind controls the modification of the moisture flux divergence, whereas the divergence of the modified wind is constrained by the divergence of the moisture flux.

In order to make a concrete investigation of the repercussions of the barotropic wind modification (4.10) on the moisture flux divergence, the correction procedure (4.7) through (4.11) is implemented using a two-dimensional version of the numerical algorithm of Ehrendorfer et al. (accepted). The peculiarity of the algorithm is the integral expression of the divergence, eq. (3.3) multiplied by $S_{i,j}$, which involves the integrated normal fluxes in (3.4). The algorithm can be sketched as follows: Firstly, the boundary values are adjusted so that eq. (4.7) is fullfilled when spatially integrated over the whole domain. In this step use is made of Gauss's divergence theorem. Secondly, for the interior gridpoints, the velocity potential is calculated from (4.11) by solving a tridiagonal system of equations (either directly or by relaxation). The modifying, integrated normal fluxes on the sides of the grid are derived as the gradient of the potential. This is the final step in Ehrendorfer et al. Thirdly, the modifying flux at the gridpoints is recovered from the normal flux by inverting the second and third equations (3.4). This requires an additional specification of the normal components on the West and South boundaries. Finally, the modifying wind at the gridpoints is computed by dividing the gridpoint modifying flux by the term appearing in the denominator of (4.10).

The algorithm yields staggered variables and a set of simultaneous equations for the velocity potential that are formally independent of the type of horizontal coordinates. The former characteristic was found by Lynch (1988) to be necessary for the accurate reconstruction of the wind field from the divergence and the vorticity, a problem that is analogous to the present one. Analytically, the correction procedure preserves the vorticity by (4.10). Numerically, the vorticity is conserved in the sense that the gradient of the velocity potential yields normal flux components, whereas the tangential flux components enter the integral formulation of the vorticity. However, the conservation of the vorticity is only partially fulfilled after the backward interpolation of the modifying flux to the gridpoints, with relative departures of about 10%.

The adjustment procedure was tested on the data of the 3 summer months of June, July, and August 1990. The wind field is modified according to (4.9) at each nominal time and the time averages $\overline{q}$, $\overline{u}$, $\overline{v}$, $\overline{uq}$ and $\overline{vq}$ as well as the covariances $\overline{u'q'}$ and $\overline{v'q'}$ are subsequently recalculated. The results for July 1990 are presented in Figs. 4.7 and 4.8,

which show the geographical distribution of the residual moisture flux divergence and the residual moisture flux. The residual fields are obtained as the difference between the fields based on the unmodified wind and those derived using the modified wind. The distributions in Figs. 4.7 and 4.8 can be compared directly to those in Figs. 4.5 and 4.6. Considering first Fig. 4.8, the striking difference to Fig. 4.6 is the much weaker systematicity of the mass imbalance residual flux field. This is particularly true for the moisture flux by the mean circulation (the very large wind modifications at the northern border of the study area are a consequence of the way the wind is adjusted, i.e., first on the borders and then in the interior of the domain). There are of course regions that are characterized by a higher degree of a certain order, as for instance the Baffin Bay area, where the wind error by the mass imbalance results in a too strong southerly component of the vertically-integrated water vapour flux. At least in the North Atlantic, there is an alternation between southerly and northerly residual flux component along a parallel circle, and between easterly and westerly residual flux component along a meridian. This alternation is caused by the fact that, in the numerical algorithm of Ehrendorfer et al. (accepted), the variables are staggered. Fig. 4.6 also reveals that the water vapour flux by the transient eddies is even less affected by the mass imbalance than by a reduction of the sampling interval from 6 to 12 hours.

The distribution of the residual moisture flux divergence in Fig. 4.7 shows a residual comparable to those of the distribution in Fig. 4.5, except for the transient eddy contribution, which is negligible over the entire domain. It is interesting to express the residual moisture flux divergence again in relative terms of the moisture flux divergence shown in Fig. 4.4 for the same four sectors of Greenland discussed in the previous section. For all sectors, the areally averaged relative residual is in the order of 10%. It increases to 15% when only the contribution achieved by the mean circulation is considered, whereas it is in the order of merely 1% for the transient eddy contribution. The reason is that large positive or negative values of the residual appear in conjuction with large positive or negative values of the moisture flux divergence itself. This because the divergence of the modified wind is constrained by the divergence of the water vapour flux.

The technical reason for the mass imbalance is the interpolation from model to pressure coordinates. However, for vertically-integrated budgets, Trenberth (1991) found a dominant wavenumber 2 signal related to the failure of the twice daily analyses to resolve semidiurnal tides. Semidiurnal tides are decaying very rapidly toward the Poles, with a first order functional dependence on latitude of the form $\cos^3(\varphi)$ (Lindzen, 1991). In the presence of a topographic barrier, the pressure difference across the mountain also displays semidiurnal fluctuations (H.C. Davies, pers. comm). Such a

mechanism, which is evident in the Alps, would probably be weaker in Greenland (H.C. Davies, pers. comm).

In a more recent publication, Trenberth and Solomon (1993) present evidence for the aliasing of high wavenumber contributions into larger scales during the derivation of gridpoint values. The noise dims completely the physically realistic semidiurnal signature. In order to verify the presence or absence of semidiurnal fluctuations in the present analyses, the mass correction algorithm was applied subsequently to twice-daily analyses at 00 and 12 UTC, to twice-daily analyses at 06 and 18 UTC and to the complete set of analyses, i.e. 00, 06, 12 and 18 UTC. For a clear semidiurnal signal, a reversal of the polarity in the wind divergence field should be observed when switching from computations based on the 00 and 12 UTC analyses to calculations based on the 06 and 18 UTC fields, whereas a cancellation should occur by combining the two sets. None of these responses can be observed concretely. The distribution looks very much the same in all three cases. It can therefore be concluded that, if a semidiurnal signal exists in the mass imbalance, it is darkened by aliasing effects due to the choice of the horizontal mesh size.


**Fig. 4.7** : July 1990. Residual of the moisture flux divergence after application of the correction procedure (4.10) [mm month$^{-1}$]. Negative departures indicating an underestimation of the divergence by the standard computations (or an overestimation of the convergence) are indicated with dashed lines.

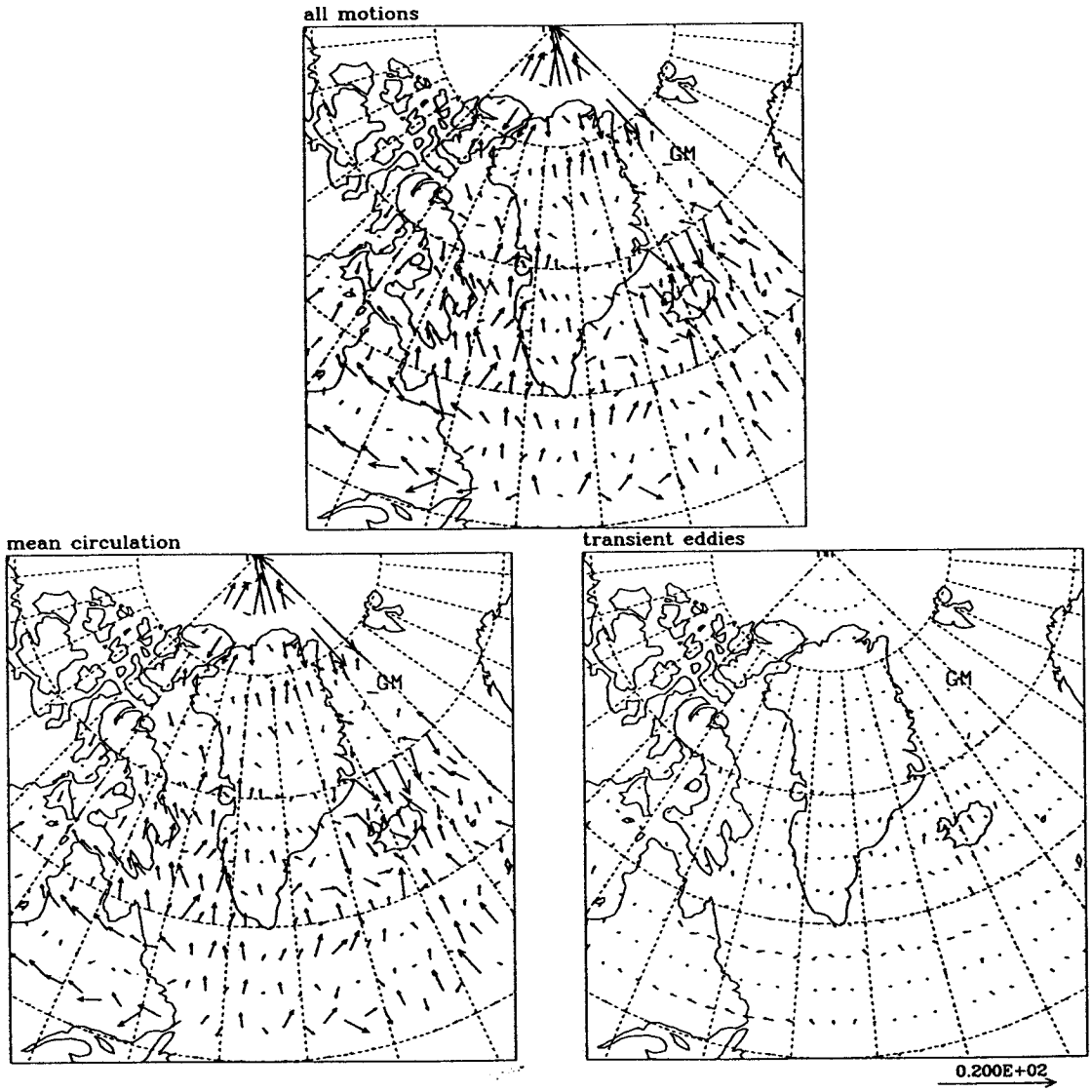


**Fig. 4.6** : July 1990. Residual of moisture flux obtained by application of the correction procedure (4.10) [kg m$^{-1}$ s$^{-1}$]. The scale is given in the lower right corner.

Seite Leer /
Blank leaf

# 5. THE ANNUAL AND MONTHLY MOISTURE FLUX DIVERGENCE

## 5.1 Annual moisture flux divergence, evaporation and precipitation

On an annual basis, the water vapour flux divergence completely determines the difference between evaporation and precipitation but, of course, independent estimates of the evaporation and precipitation are required to further separate the net moisture flux at the surface. In addition, such estimates are necessary to verify, at least in terms of orders of magnitude, the computed moisture flux divergence.

Data from several sources were gathered and projected onto the ECMWF grid for preparing maps of the annual total evaporation and of the annual total precipitation . For the evaporation, the compilation of Isemer and Hasse (1987) for the North Atlantic area south of 60°N was combined with the estimates of Walmsey (1966) for the Davis Strait and Baffin Bay area and Baumgartner and Reichel (1975) for latitudes between 60° and 70°N. Over Greenland, evaporation measurements are too occasional to allow a realistic depiction of the spatial distribution and no attempt was made to fill the spatial gap. Concerning the precipitation, the map of the annual total precipitation by Ohmura and Reeh (1991) for Greenland was graphically inserted into the map by Legates and Willmott (1990) for the whole study area. Although the Legates and Willmott map does portray the annual precipitation over Greenland, preference was given to the map by Ohmura and Reeh as it is based on additional accumulation data at more than 200 locations on the ice sheet.

The annual total moisture flux divergence, the annual total precipitation and the annual total evaporation are displayed in Figs. 5.1a, 5.1b and 5.1c, respectively. The precipitation distribution is a smoothed version suitable for comparison with the moisture flux divergence and the evaporation distribution. It was obtained through application of the spatial filter (3.5) with $\alpha_0 = 5°$ from the original distribution, shown for the sake of completness in Fig. 5.2.

The distribution of the annual total moisture flux divergence for Greenland shows at least two important characteristics of the precipitation map, namely: the convergence zone of less than 100 mm year$^{-1}$ over northeastern Greenland, and, the zonal gradient between southwestern and southeastern Greenland. There is also an allusion to the belt of higher precipitation (convergence) on the western slope, around 70°N.

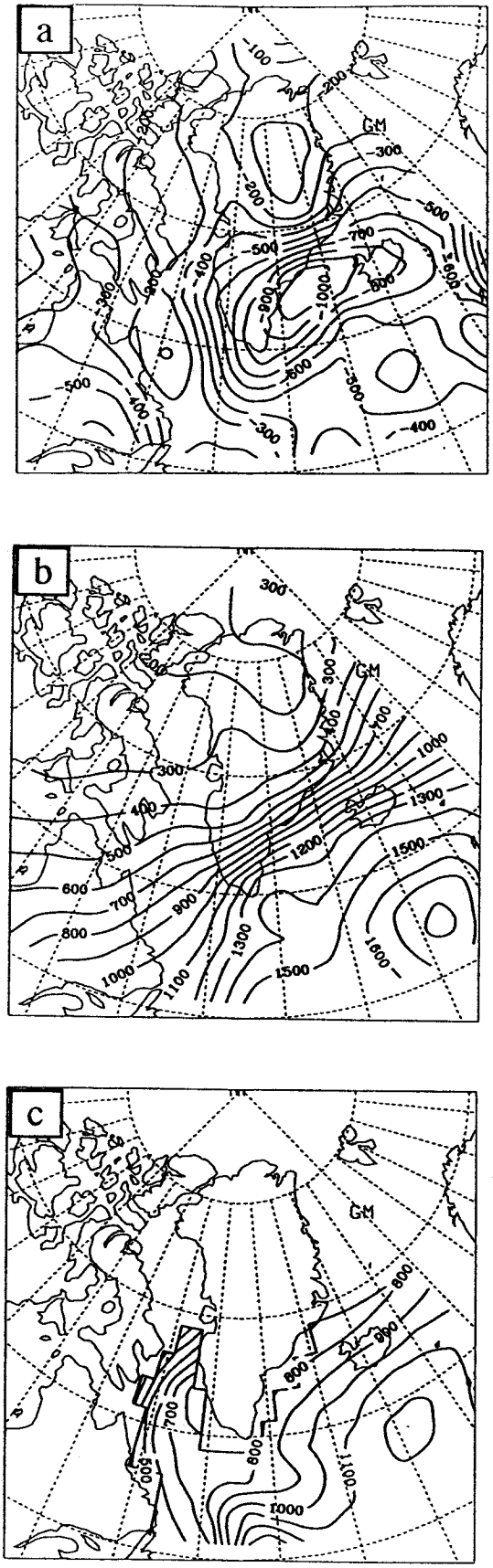


**Fig. 5.1** : From top to bottom, average spatial distributions of: (a) the smoothed annual total moisture flux divergence derived from the ECMWF analyses; (b) the smoothed annual total precipitation (from Legates and Willmott, 1990, and Ohmura and Reeh, 1991); and (c) the annual total evaporation (from Walmsley, 1966; Baumgartner and Reichel, 1975, and Isemer and Hasse, 1987). All fields in [mm year$^{-1}$]. The contour interval is 100 mm year$^{-1}$.

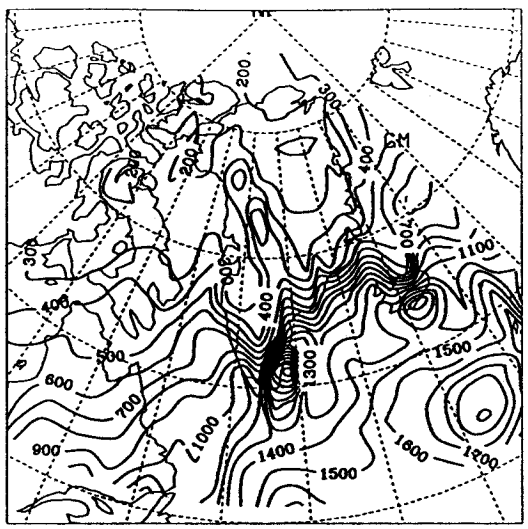


**Fig. 5.2** : Unsmoothed distribution of the annual total precipitation (Legates and Willmott, 1990, and Ohmura and Reeh, 1991). Isolines in [mm year$^{-1}$]. Contour intervall: 100 mm year$^{-1}$.

The largest difference between the moisture flux divergence and the precipitation is found in southeastern Greenland, where the difference amounts to about 300 mm year$^{-1}$, a value which ,however, compares well with the evaporation estimate of Baumgartner and Reichel (1975). Evaporation may also be important along the southwestern coast and on the ice sheet at elevations below the mean equilibrium line altitude. During the EGIG field campaign, careful micrometeorological investigations were carried out at about 70°N and an altitude of approximately 1000 m.a.s.l. (Ambach, 1963). During the suumer season 1959, it was determined that the evaporation averaged up to to 35 cal cm$^{-2}$ day$^{-1}$, or 18 mm month$^{-1}$. Calculations by Greuell (1992) for the same site yielded an evaporation figure of 25 mm month$^{-1}$ for the 1990 summer season. During the University of Michigan Expedition in the Søndrestrømfjord area, Church (1941) estimated the monthly total evaporation from the tundra to be 0.57 inches month$^{-1}$, or 15 mm month$^{-1}$. For a snow and ice surface, Church's estimations yield 1.00 inches month$^{-1}$, or 25 mm month$^{-1}$. In the same area, Rott and Obleitner (1992) measured a daily total evaporation of 1.7 mm day$^{-1}$ for the measurement period running from May 21 to June 12. Integrated over one month, this daily rate gives an evaporation of 50 mm month$^{-1}$. Over the tundra, evaporation amounts as much as 40 to 50 mm month$^{-1}$ are not uncommon during the summer season, even at higher latitudes. For his measurements site on Axel Heiberg, Canadian Arctic Archipelago, Ohmura (1982) found that the evaporation is negligibly small from October to March, amounts to a total of about 20 mm during the snow period (April, May and June), reaches a maximum of about 100 mm in summer, during the snow free season (July and August), and is still in the order of 20 mm in September, during the transition from summer to

winter. Thus, the annual total evaporation amounts to 140 mm, of which 70% is accounted for by the summer evaporation alone.

If the evaporation is significant at the coast, over the interior of the Greenland Ice Sheet it may be of less importance compared to the precipitation and to the moisture flux divergence. It must also be recognized that the annual total precipitation of Ohmura and Reeh (1991) is, except at the coast, numerically equal to the annual total accumulation. Since the accumulation is, with other processes, the product of the difference between the precipitation and the evaporation, the precipitation distribution over Greenland shown in Fig 5.1b or 5.2 is fully representative of the moisture flux divergence distribution. In this sense, the overall agreement of the distribution of the moisture flux divergence and of the precipitation distribution (Figs. 5.1a and 5.1b, respectively) may be viewed as a confirmation of the validity of the computed moisture flux divergence. Quantitatively, the areally averaged annual total divergence for the three years 1989 to 1991 amounting to -380 mm (-340 mm for 1989, -390 mm for 1990, and -410 mm for 1991) is also very close to the 340 mm figure given by Ohmura and Reeh (1991) for the areally averaged annual total precipitation.

Over the seas, the evaporation is more conspicuous and, in addition, it is greatest during the winter season. The spatial patterns of the evaporation distribution, like the sharp gradients in Davis Strait or the tongue of lower evaporation protruding from the southern tip of Greenland southeastward into the North Atlantic, reflect the thermal conditions over the sea surface and the oceanic currents. Thus, it is well known that the eastern portion of Davis Strait, which is affected by the West Greenland Current, is normally free of sea ice even during the winter months (Parkinson et al., 1987). The opposite is observed in the western part of Davis Strait and in the Labrador Sea, where sea ice is transported southward by the Labrador current. These settings create very strong, zonal gradients of evaporation in Davis Strait and the Labrador Sea. On the other hand, the greater evaporation in the eastern North Atlantic is certainly favoured in winter by the thermal contrast between the warm waters of the Atlantic Current and the cold air. The same holds true for Denmark Strait, where relatively warm water is carried by the Irmiger Current.

The spatially smoothed difference between the annual total evaporation and the annual total precipitation over the North Atlantic is depicted in Fig. 5.3. The difference is negative everywhere, implying that precipitation exceeds evaporation everywhere in the North Atlantic. The largest absolute values are observed at the southeastern coast of Greenland and in the eastern North Atlantic. Owing to the rapid northward depletion of the precipitation, the difference decreases in absolute terms as one moves into Davis

Strait. The gradient of the difference is very small in an oceanic sector starting south of Greenland and extending northeastward toward Iceland.

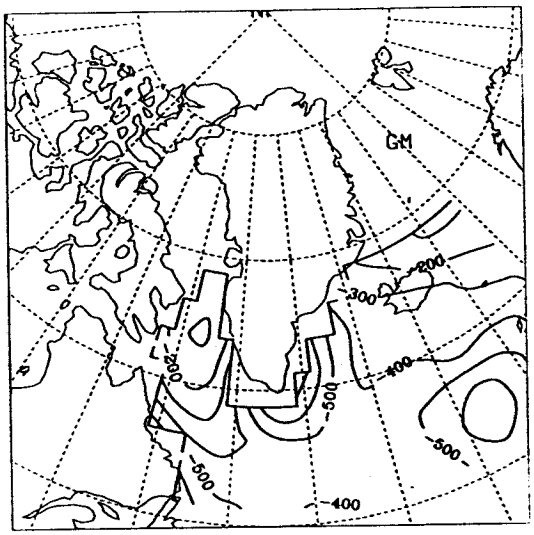


**Fig. 5.3** : Distribution of the difference between the annual total evaporation of Fig. 5.1c and the annual total precipitation of Fig. 5.1b. Values are given in [mm year$^{-1}$]. The contour intervall is 100 mm year$^{-1}$.

Qualitatively similar patterns are found also in the map of the moisture flux divergence (Fig. 5.1a). The large departures around Iceland may be due to an underestimation of the evaporation following Baumgartner and Reichel (1975). The agreement is better in the North Atlantic and in the Davis Strait area, where the evaporation estimates are more definite, and demonstrate again the validity of the present moisture flux divergence computations.

## 5.2 The monthly moisture flux divergence

In this section, the monthly total flux divergence will be discussed in relation to the measured monthly precipitation for the meterological stations shown in Fig. 3.1. To avoid complications involving the sign, negative values of the moisture flux divergence have been commutated to positive values of the moisture flux convergence. Point values of the moisture flux convergence were derived via bivariate interpolation (Akima, 1978) from the smoothed spatial divergence distribution depicted in Fig. 5.1a. The precipitation values were extracted from the monthly annexes to the 'Berliner Wetterkarten' (Institut für Meteorologie der Freien Universität Berlin) and supplemented with unpublished data provided by the Danish Meteorological Institute. The 1989 to 1991 average monthly values of the moisture flux convergence and of the precipitation are displayed in Fig. 5.4.

For most of the stations, the two curves are surprisingly similar. The calculations are able to reproduce not only the annual precipitation (see also previous section), but even the annual progression of the monthly precipitation. The agreement between the computed moisture flux divergence and the measured precipitation is not restricted to stations in a particular climatic zone: it is as good for stations in the Canadian Arctic as for stations in Iceland The largest departures are observed for stations where the precipitation regime is believed to be shaped by local influences. One must in fact realize that the calculated moisture flux convergence is representative only of large scale atmospheric processes. A typical example is Søndrestrømfjord. The station is situated at the head of the Kangerlussuaq fjord. The coastal mountains (Church, 1941; Rott and Obleitner, 1992), but also the orographic ridge at the ice sheet surface southeast of the station and its prolongation into the Sukkertoppoen Ice Cap (Ohmura and Reeh, 1991), interact locally with the large-scale moisture flow and are responsible for the relative dryness of the Søndrestrømfjord area. The peculiarity of Søndrestrøm-fjord is even more apparent if the station is compared to Egedesminde, Holsteinsborg and Godthåb, all located more or less directly at the west coast of Greenland, at comparable latitudes. Concretely, the annual course of the calculated moisture flux convergence bears but little resemblance to that of the measured precipitation. On the other hand, the moisture flux convergence at Søndrestrømfjord is practically identical to that at Holsteinsborg, located at a distance corresponding approximately to twice the grid size at this latitude.

As far as the Greenland stations are concerned, the annual course of the average monthly convergence for the three years 1989 to 1991 follows closely the annual course of the long-term average monthly precipitation (Putnins, 1970). For the stations on the western coast, the maximum convergence is observed in late summer and autumn, whereas the minimum appears in midwinter. Moving toward the south and around the southern tip of Greenland, there is an increase in the autumn precipitation first, and in the winter precipitation, afterwards. Along the southeastern coast, the maximum is recorded in winter, while the minimum appears in late spring and summer. The influence of the Icelandic Low extends quite far north, and a winter maximum still characterizes the precipitation regime at Danmarkshavn. However, the winter maximum is accompanied by a second maximum in summer, which is the only one at Nord. As will be shown later, transient disturbances moving in summer within the Polar Basin set up a northerly water vapour flux that contributes significantly to the moisture flux convergence at the northern coast of Greenland and in the Canadian high Arctic (Müller and Roskin-Sharlin, 1967).

1989–1991 . Comparison between
the convergence of the vertically–integrated water vapour transport (ECMWF) and
the measured precipitation at selected locations (Berl. Wetterkarten) [mm month$^{-1}$]

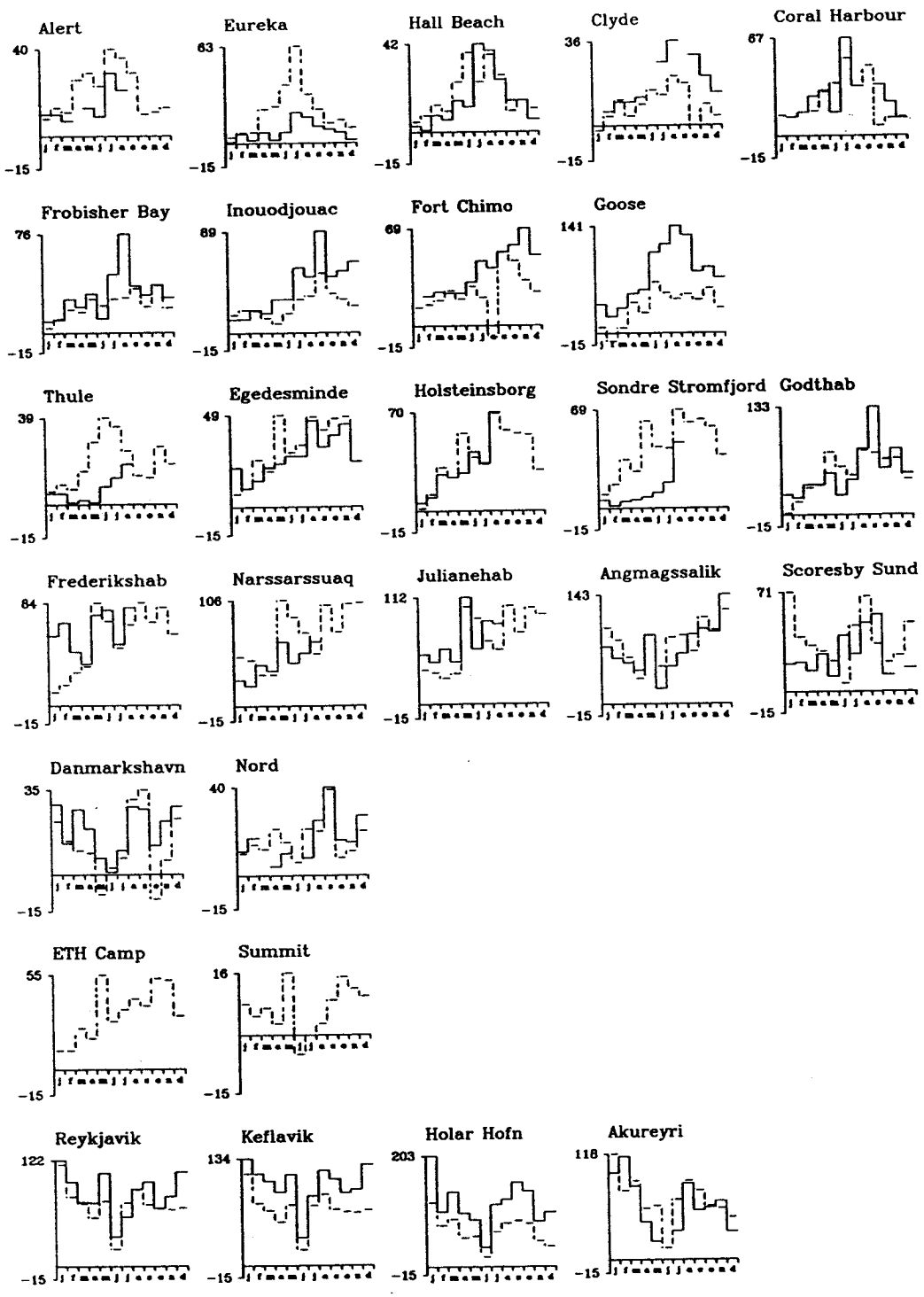


**Fig. 5.4** : Comparison between the convergence of the vertically-integrated water vapour transport (broken line) and the measured precipitation (continuous line) for the locations shown in Fig. 3.1. The values are average monthly total amounts for the three years 1989 to 1991. Units are [mm month$^{-1}$]. Note the different scale on the axis of the ordinates. The labels on the axis of the abscissa indicate the months.

During the summers of 1990 and 1991, the Geography Department of the Swiss Federal Institute of Technology (ETH) carried out two intensive field campaigns in West Greenland (Ohmura et al, 1991 and 1992). Additional field investigations were undertaken at the GRIP drilling site on Summit in June and July 1991 (Ohmura et al., 1992). The position of the ETH camp (69°34' N, 49°18' W, 1155 m.a.s.l.) was chosen as close as possible to the altitude of the long-term equilibrium line. The annual precipitation is about 300 mm at this location (Ohmura and Reeh, 1991). From here, the precipitation increases gradually upslope and eastward, reaching the maximum at an altitude between 2000 and 2500 m.a.s.l. The same trend is observed also in the mass balance (a compilation of recent measurements is found in Ohmura, 1993).

At the ETH camp, in summer, the precipitation was measured directly with a Canadian Standard snow gauge four times a day. The winter mass balance (for definition, see Paterson, 1980, p. 44) for the two balance years 1989/1990 and 1990/1991 was determined at the beginning of the following summer season. Neglecting melting and evaporative losses, which are small in winter, and assuming that losses and gains through snow drift are roughly in balance, the winter mass balance can be taken as a representative value for the cumulative precipitation.

The measured precipitation and the calculated convergence for the summer seasons 1990 and 1991 are presented in Table 5.1. In the first four columns, the monthly and seasonal totals are presented as they are. In the last column, corrected values of the summer total are tabulated. The precipitation was adjusted for the wind-induced error of the measurements. For this type of snow gauge and for typical wind speeds in the range of 5 to 10 m $s^{-1}$, the measured precipitation underestimates the real precipitation typically by 30% (Sevruk, 1982). The convergence was modified in order to account for the evaporation, which was set at a total of 60 mm for both summers (see discussion in the previous section).

| | | June | July | August | Summer | corr. |
|---|---|---|---|---|---|---|
| 1990 | prec | 0 | 33 | 42 | 75 | 100 |
| | conv | -4 | 21 | 42 | 59 | 120 |
| 1991 | prec | 42 | 11 | 57 | 110 | 140 |
| | conv | 83 | 47 | 65 | 195 | 250 |

**Table 5.1** : Measured precipitation (uncorrected) and calculated convergence, both in [mm $month^{-1}$] and [mm $season^{-1}$], respectively, at the ETH Greenland Expedition Camp. The values in the last column are obtained by adding 30% to the measured precipitation and 60 mm $month^{-1}$ to the convergence.

The total summer precipitation is well reproduced in 1990, but overestimated in 1991 by the calculations, the largest differences being observed for June and July 1991. It is possible that the measured precipitation was more strongly underestimated during the 1991 summer season. At least during June 1991, a large amount of precipitation fell as snow (T. Konzelmann, pers. comm.) and losses produced by the deformation of the wind field around the gauge, therefore, may have been particularly large. On the other hand, a deviation of approximatively 30 mm month$^{-1}$ may also reflect the inaccuracy of the computations and in the worst case accumulate to the observed 100 mm for the whole season.

According to Ohmura et al. (1982), the cumulative precipitation for the winter 1989/1990 is 480 mm Water Equivalent (W.E.), whereas the total convergence is a mere 270 mm. For the following winter, the cumulative precipitation is 670 mm W.E., almost double as much as the calculated convergence of 340 mm. An extremely large winter balance for the winter season 1990/1991 was observed also along the mass balance line of the Geological Survey of Greenland (H.H. Thomsen, pers. comm.). For the highest pole, located about 10 km west of the ETH Camp and at an altitude of 1050 m.a.s.l., the winter cumulative precipitation for the winter 90/91 was measured as 490 mm. This is by about 200 mm lower than the value measured at the ETH Camp, but still 150 mm larger than the calculated convergence. The question arises, why there is such a large underestimation in winter, whereas the convergence overestimaties the precipitation in both summers. A possible reason is the failure of the computational algorithm to catch extreme events, so as to fail to reproduce the medium-scale feature of the spatial distribution. In addition, snow drift may become important in the marginal parts of the Ice Sheet. For the Qamanârssûp Sermia (West Greenland, 64°28' N, 49°30' W), the annual meteorological precipitation is 270 mm lower than the glaciological winter balance plus the meteorological summer precipitation (Ohmura et. al., 1992), which can be only partly explained by the underestimation of the precipitation when this is measured with snow gauges.

For Summit, the average annual total accumulation was determined from ice cores to be 210 mm W.E. (J. Schwander, pers. comm.; Ohmura and Reeh, 1991). The annual course is believed to be rather smooth, with the maximum occurring probably in summer (J. Schwander, pers. comm.). For the three years 1989 to 1991, the computed average annual total convergence is 84 mm, i.e., about 100 mm less than the observed accumulation. The monthly convergence (Fig. 5.4) ranges from -5 mm month$^{-1}$ to 15 mm month$^{-1}$, with a minimum in May and a maximum in October. The winter maximum is plausible since the moisture flux is from the southeast in this season (Ohmura and Reeh, 1991). In summer, the evaporation may be significant even at this

altitude (A. Abe-Ouchi, pers. comm.). It is, however, interesting to try to find out why the calculations yield a negative convergence in summer, since this may also explain the difference between moisture flux convergence and the precipitation in the annual total. As will be demonstrated in the next chapter (see, for example, Fig 6.3), the very small (in absolute) values of the convergence in central Greenland result from a delicate interplay between the mean circulation and the transient eddy circulation. In the other seasons, the positive eddy moisture flux convergence overcompensates for the negative convergence achieved by the mean circulation. In summer, a slight westward expansion of the core of negative moisture flux convergence in the distribution for the mean circulation is not accompanied by a comparable intensification of the positive eddy flux convergence. Given the moisture flux distribution shown in Fig 6.2, it seems that in the ECMWF analyses, both the mean circulation as well as the eddy circulation are not able to carry enough moisture toward central Greenland.

# 6 WATER VAPOUR FLUX, FLUX DIVERGENCE AND ATMOSPHERIC CONDITIONS

In this chapter, the moisture flux and flux divergence are discussed in relation to the atmospheric conditions on the basis of ensemble averaged 1989 to 1991 seasonal statistics. For the interpretation, the following variables are chosen: the mean sea-level pressure (mslp) and the 700 hPa geopotential height $Z$, 700 hPa being the level of average moisture conditions, to show the dynamic conditions; the precipitable water (W), to illustrate the availability of moisture and its geographical distribution; the vertical velocity $\omega$ [Pa $s^{-1}$] in pressure coordinates, from which the usual vertical velocity $w$ [m $s^{-1}$] is obtained by dividing by 10 and by changing the sign, to show rising motion and subsidence; a bulk measure $\sigma_e$ for the conditional stability defined as:

$$\sigma_e = \frac{\theta_e(p_{k+1}) - \theta_e(p_k)}{Z(p_{k+1}) - Z(p_k)} \cong \frac{d\theta_e}{dz}; \text{ k such that } Z(p_k) = \min(Z(p)) > Z_s , \qquad (6.1)$$

where $\theta_e$ is the equivalent potential temperature, $Z$ is the geopotential height (in geopotential meters), a subscript $k$ indicates the $k^{th}$ standard level and a subscript $s$ refers to the surface. This formulation attempts to estimate the stability of the first layer outside the boundary layer in an easy manner. Thus $p_k$ and $p_{k+1}$ are the first two standard pressure levels above the surface. A more stringent assumption, e.g., $k$ such that $Z(p_k)$-$Z_s$ > 400 m, would have required more refined calculations. The bulk stability parameter is chosen to illustrate the tendency of a given air mass to rise or not.

Further, a bulk measure of undersaturation $\delta LCL$ [Pa] is defined as the (negative) difference between the lifting condensation level (LCL, expressed in [Pa], see Appendix 2) and the pressure level to which it refers, or the relative lifting condensation level, viz.:

$$\delta LCL = p_k - LCL(p_k), \text{ k such that } p_k \geq 850 \text{ hPa and } (Z(p_k) - Z_s) \geq 400 \text{ m} . \qquad (6.2)$$

The relative condensation level is preferred to the relative humidity, since it expresses undersaturation in terms of the altitude of the lifting condensation level. In fact, this latter is roughly equal to the value of $\delta LCL$ [Pa] divided by 10 and added to the altitude of the pressure level $p_k$. Here, too, an effort is made to avoid the boundary layer. The 1000 hPa level is not considered at all. Thus over the ocean the representative level is

the 850 hPa level. In the presence of the topography, a minimum altitude relative to the surface of 400 m is assumed. The limit is defined in relation to expected boundary layer height over Greenland. For the radiosonde profiles of the ETH Greenland Expedition, both the inversion height and the height of the wind speed maximum are usually found below 400 m above ground (Niederbäumer, 1992).

Seasonal maps of the previously mentioned variables, of the vertically-integrated water vapour flux, of its streamlines and of the water vapour flux divergence are shown in Figs. 6.1 to 6.4 (a: winter; b: spring; c: summer; and d: autumn).

The circulation characteristics displayed by the mean sea-level pressure and the 700 hPa geopotential are well established (Namias, 1958; Wilson, 1967). The Icelandic low is best developed in winter, but low pressure in the Denmark Strait is a distinctive feature throughout the year. The same can be said for the Baffin Bay trough that appears here in the 700 hPa geopotential maps (Barry and Kiladis, 1982). The northward retreat and the simultaneous weakening of the trough observed in the warm season follow the shrinking of the circumpolar vortex (Wilson, 1967), but also reflect the thermal conditions in the Baffin Bay. The surface conditions are marked by the evolution of the sea ice (Parkinson et al, 1987) and by the oceanic currents. The bulk stability parameter (Figs. 6.1a-d) displays a relative maximum in summer, when the air temperature is maximum but the surface temperature still relatively low, and a minimum in autumn, when the sea ice has retreated to its northernmost limit and the temperature contrast between the sea surface and the air is minimal.

The 700 hPa is approximately the level of vertical mean moisture conditions. The geopotentail distribution at this level largely determines the direction of the vertically-integrated water vapour flux by the mean circulation and of the total flux, since the former is generally much larger than the transient eddy flux (cf. Figs. 6.1a-d with Figs. 6.2a-d). In winter, the flow is westerly south of 60°N but backs over the Foxe Basin, in the Davis Strait and in Denmark Strait to become southerly or southeasterly in Baffin Bay, over southern and northwestern Greenland. Over eastern Greenland, at about 70°N, the southeasterly flow veers and points toward northeast. Spring and autumn are symmetric with respect to the mean circulation. The flow is mainly southwesterly over the whole Greenland Ice Sheet. In summer, the westerly-, northwesterly flow from the Canadian Arctic backs toward the north only when it reaches the western coast of Greenland. An even more extreme backing is observed in the Denmark Strait, where a cyclonic structure develops, together with a smaller anticyclonic counterpart to the north.

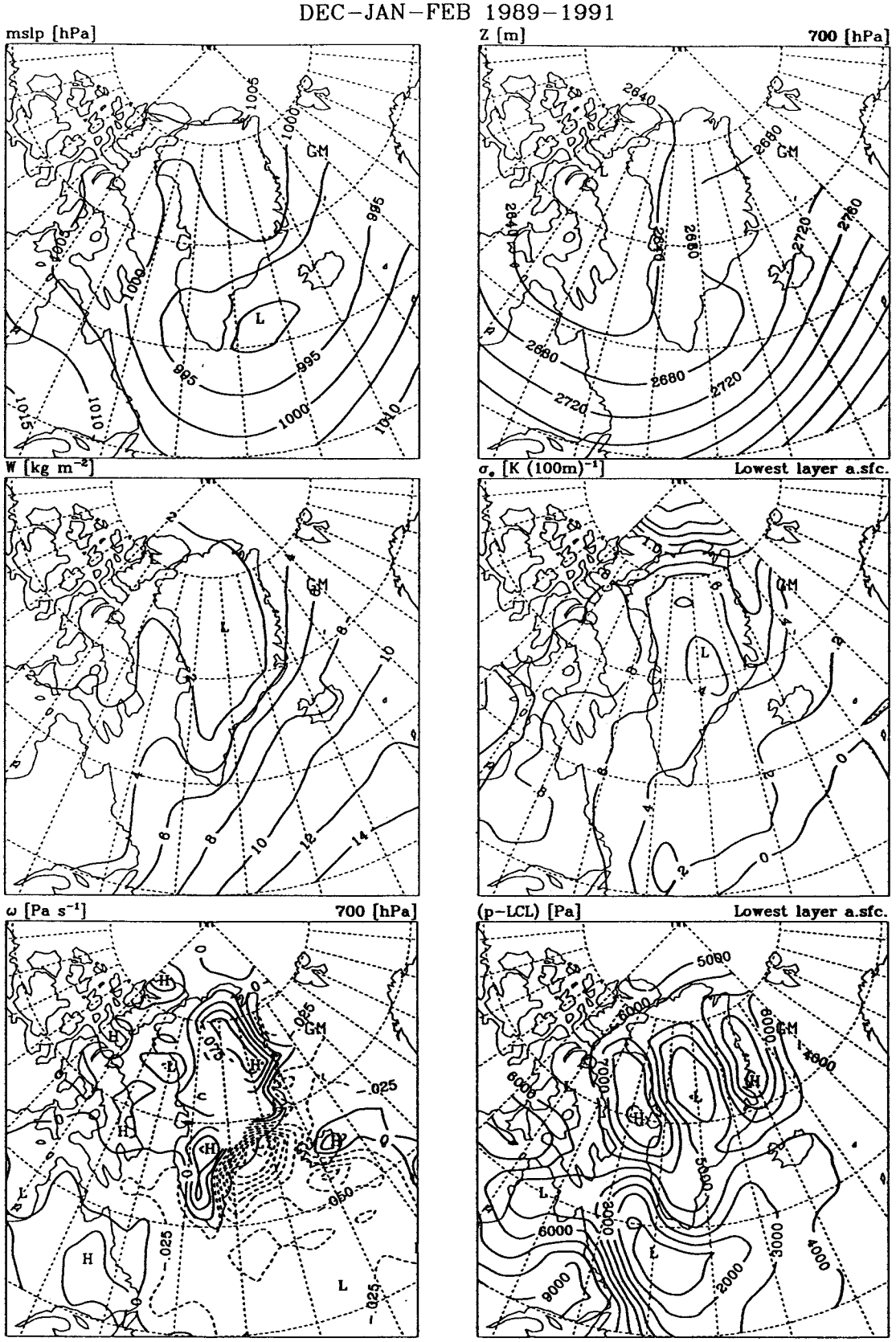


**Fig. 6.1a**: Geographical distribution of the mean sea-level pressure *mslp* (upper left panel), of the 700 hPa geopotential height *Z* (upper right panel), of the precipitable water *W* (middle left panel), of the bulk stability parameter $\sigma_e$ (middle right panel), of the vertical velocity $\omega$ (lower left panel), and of the relative lifting condensation *δLCL* (lower right panel). The units are given in the caption above each panel. Winter.

MAR–APR–MAY 1989–1991

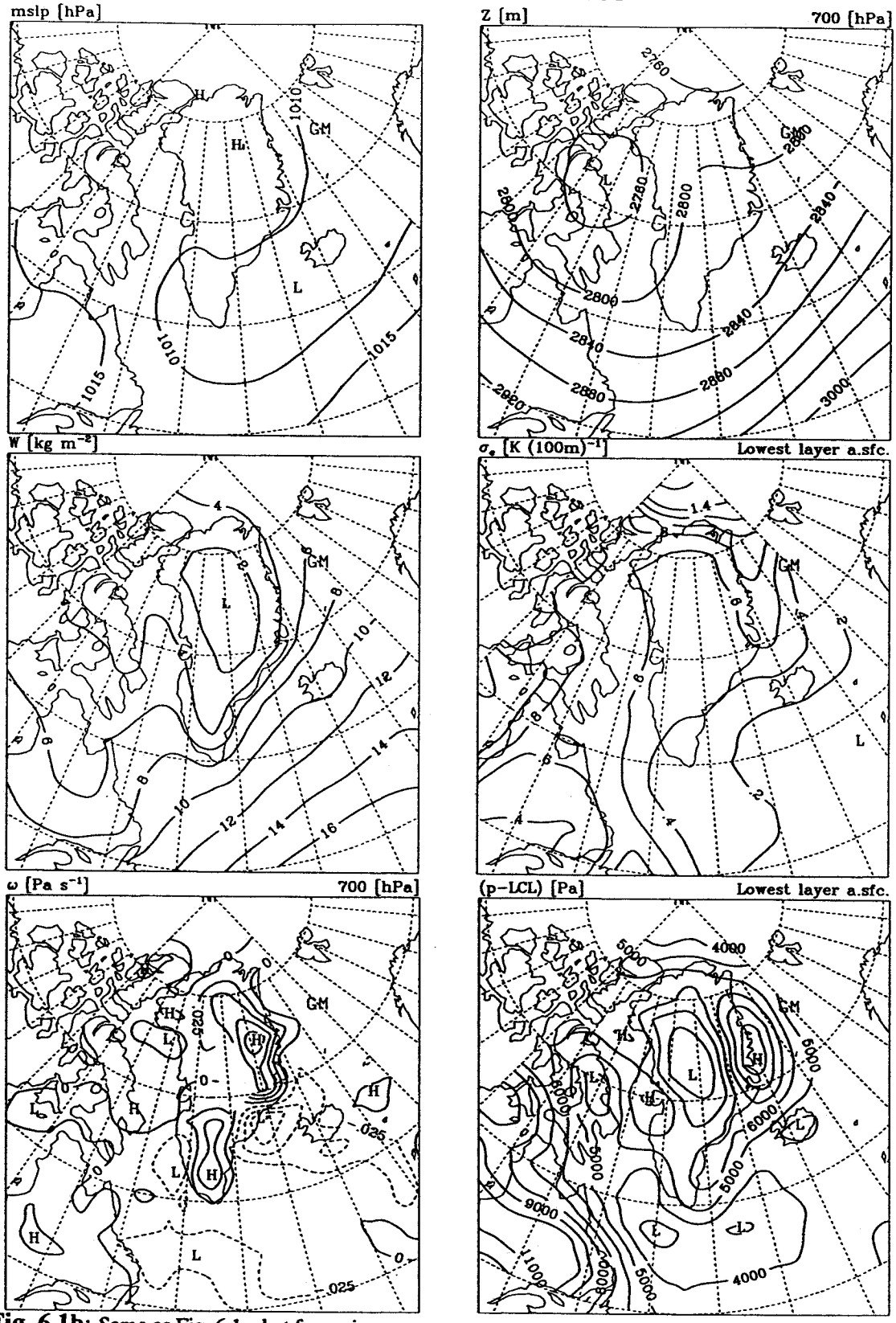


**Fig. 6.1b**: Same as Fig. 6.1a, but for spring.

JUN–JUL–AUG 1989–1991

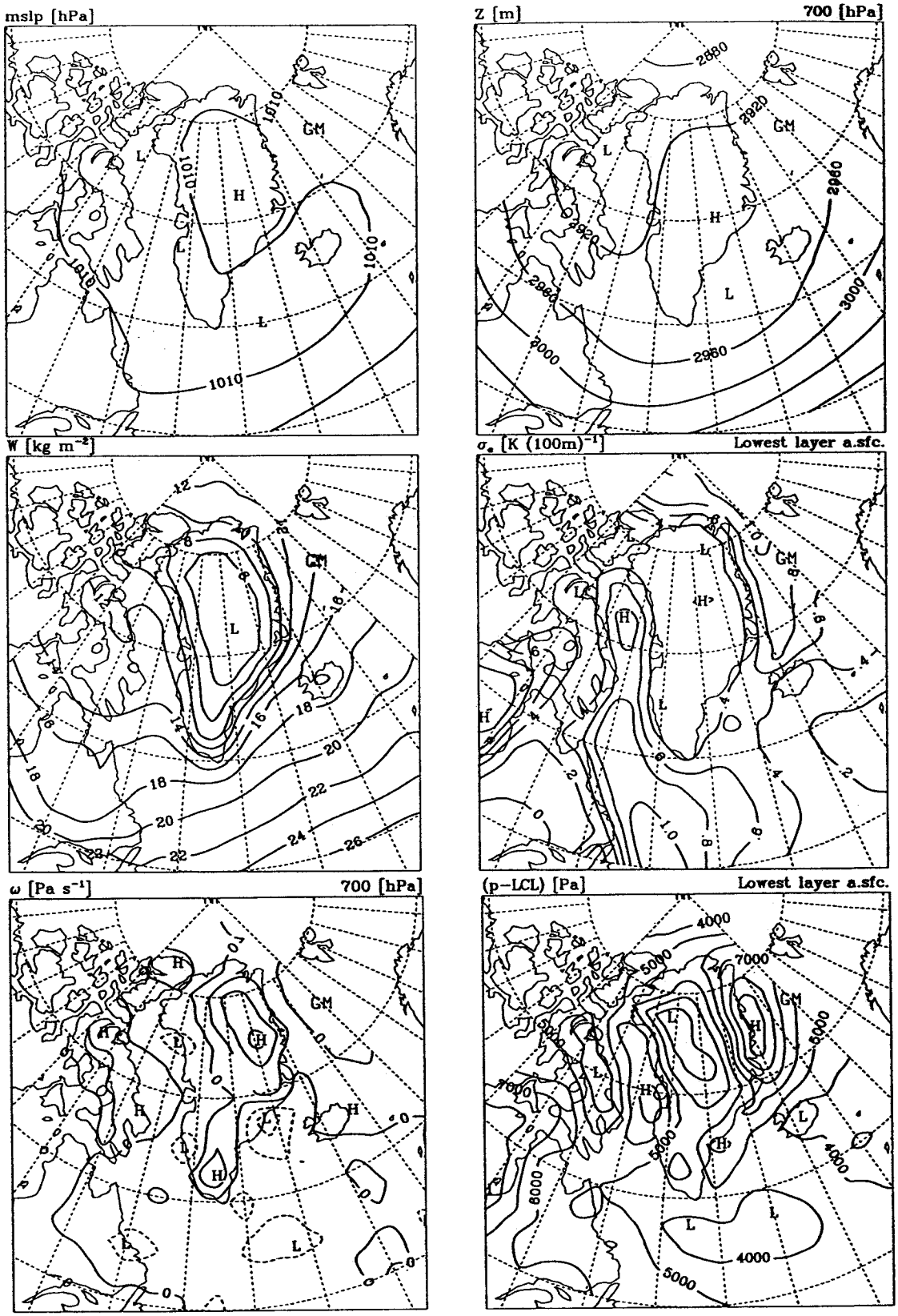


**Fig. 6.1c**: Same as Fig. 6.1a, but for summer.

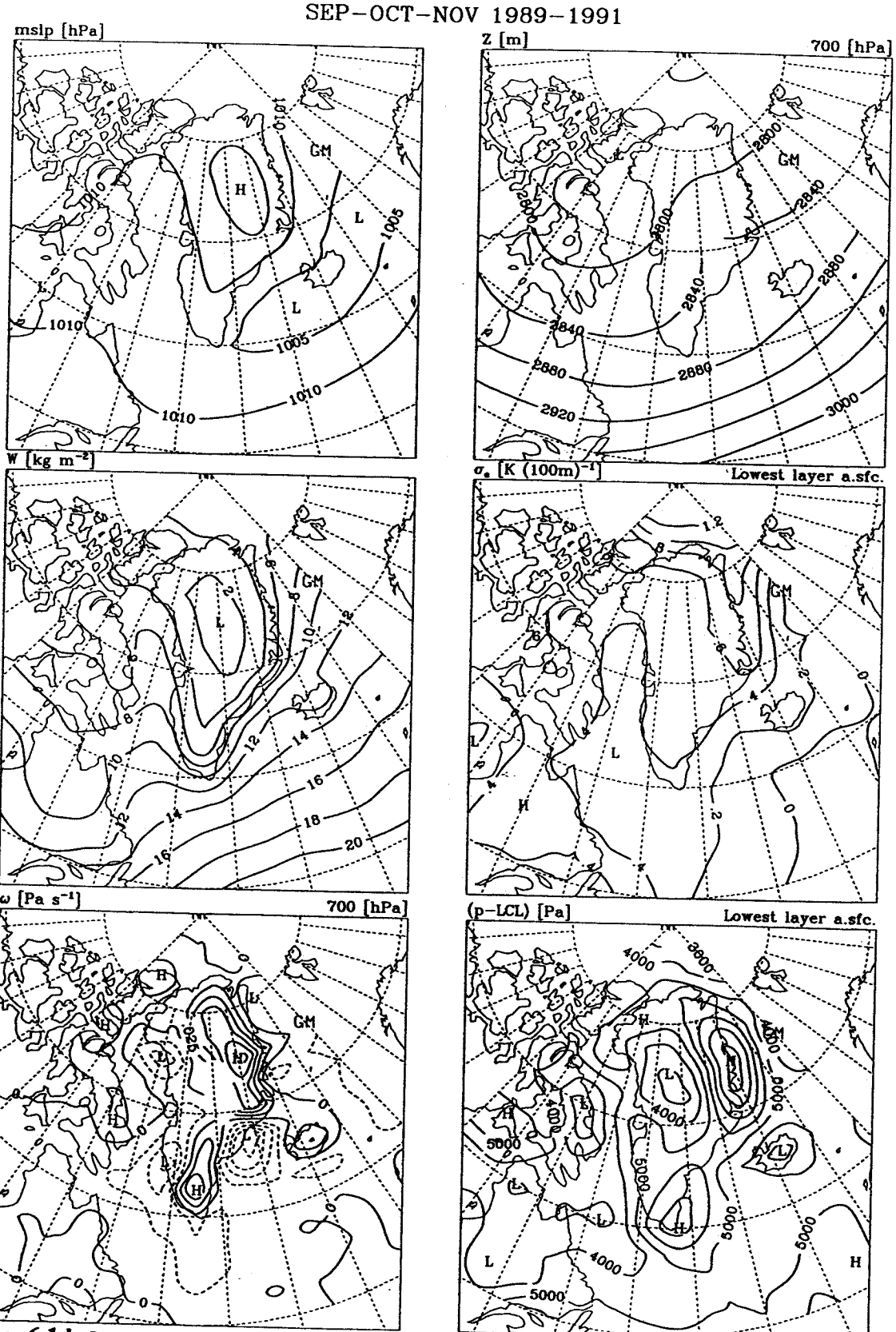


**Fig. 6.1d**: Same as Fig. 6.1a, but for autumn.

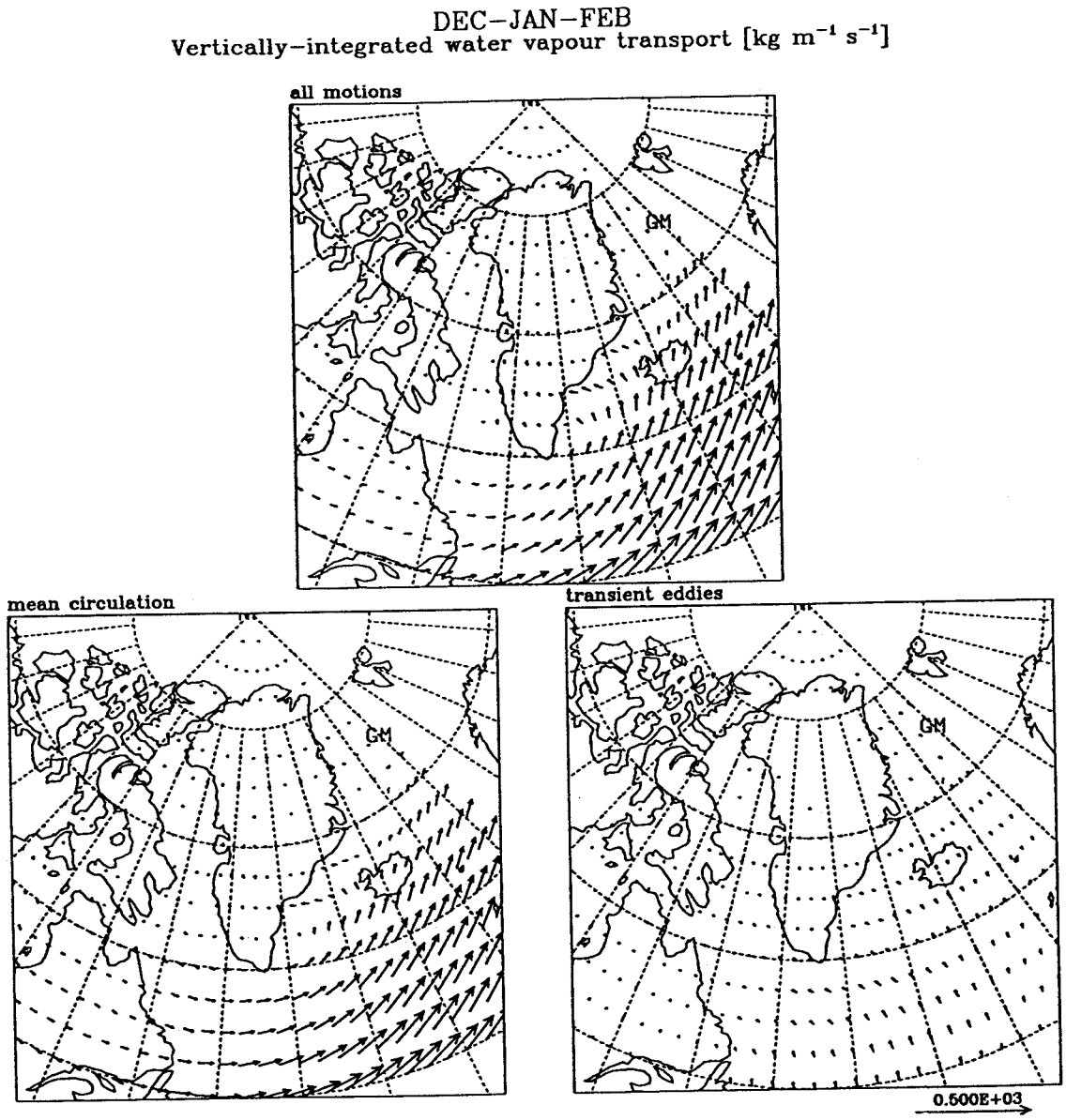


**Fig. 6.2a**: Vertically-averaged water vapour flux in winter. Units are [kg $m^{-1}$ $s^{-1}$]. The scale is shown in the lower right corner.

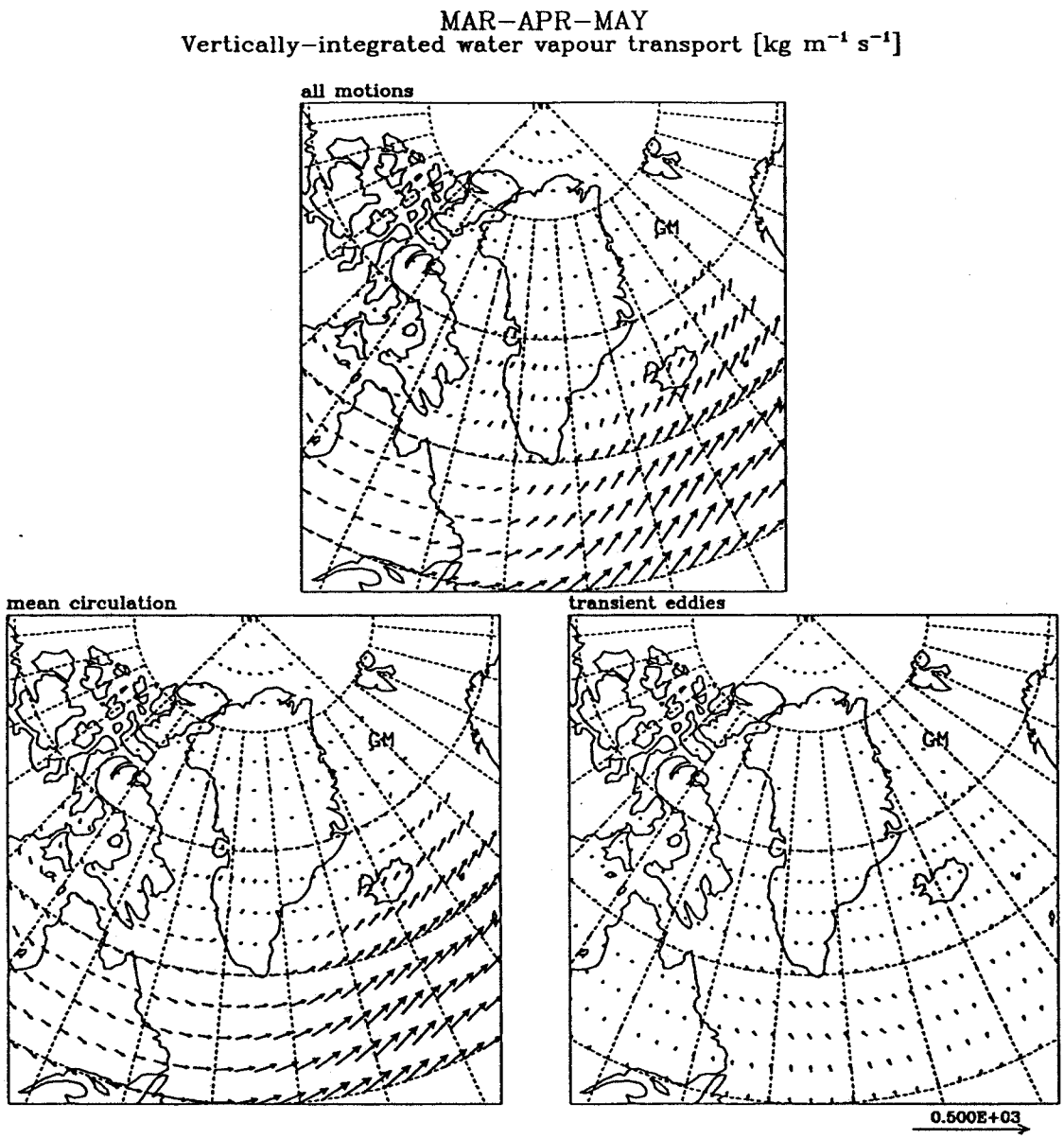


**Fig. 6.2b**: Same as Fig. 6.2a, but for spring.

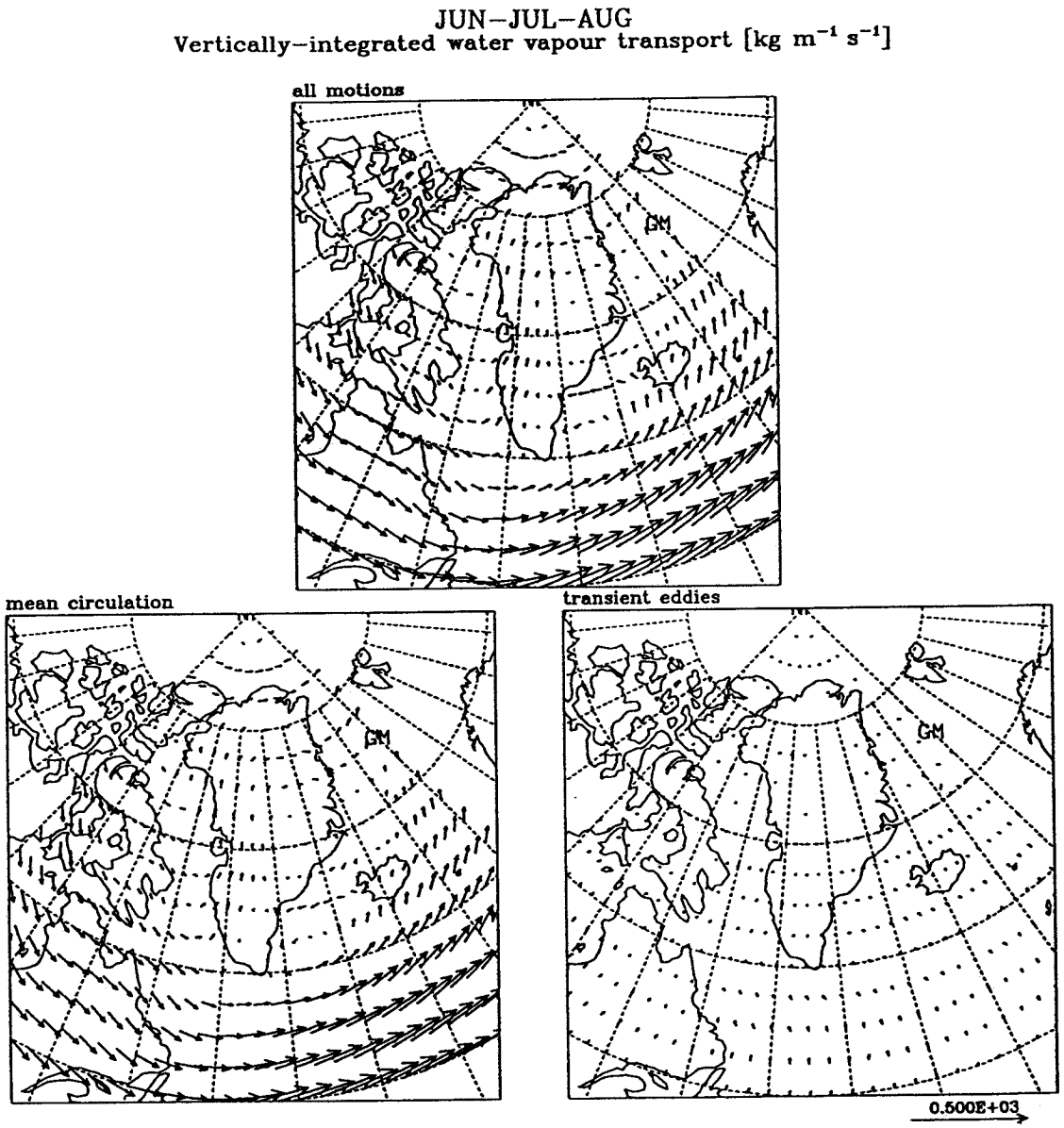


**Fig. 6.2c:** Same as Fig. 6.2a, but for summer.

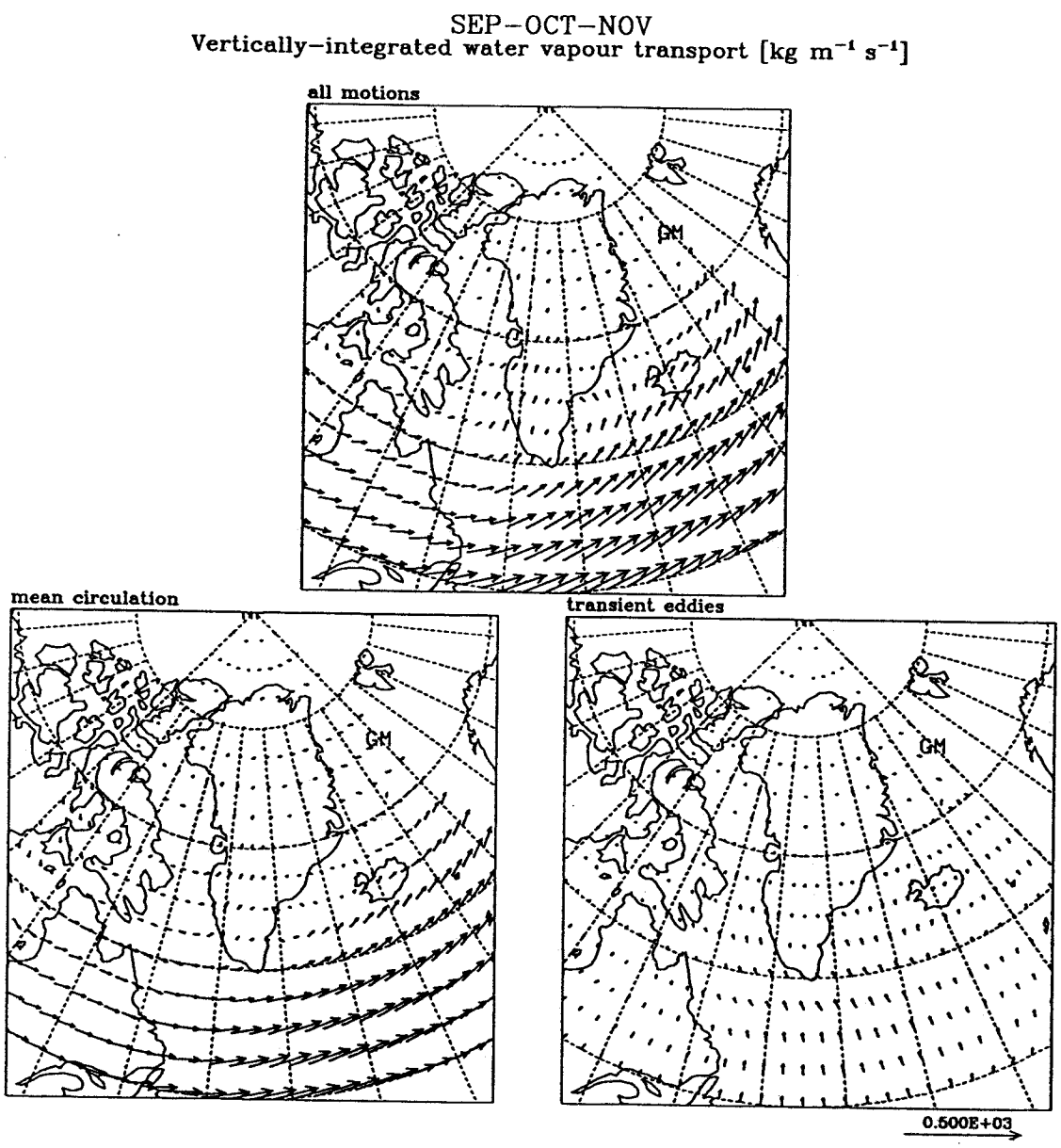


**Fig. 6.2d:** Same as Fig. 6.2a, but for autumn.

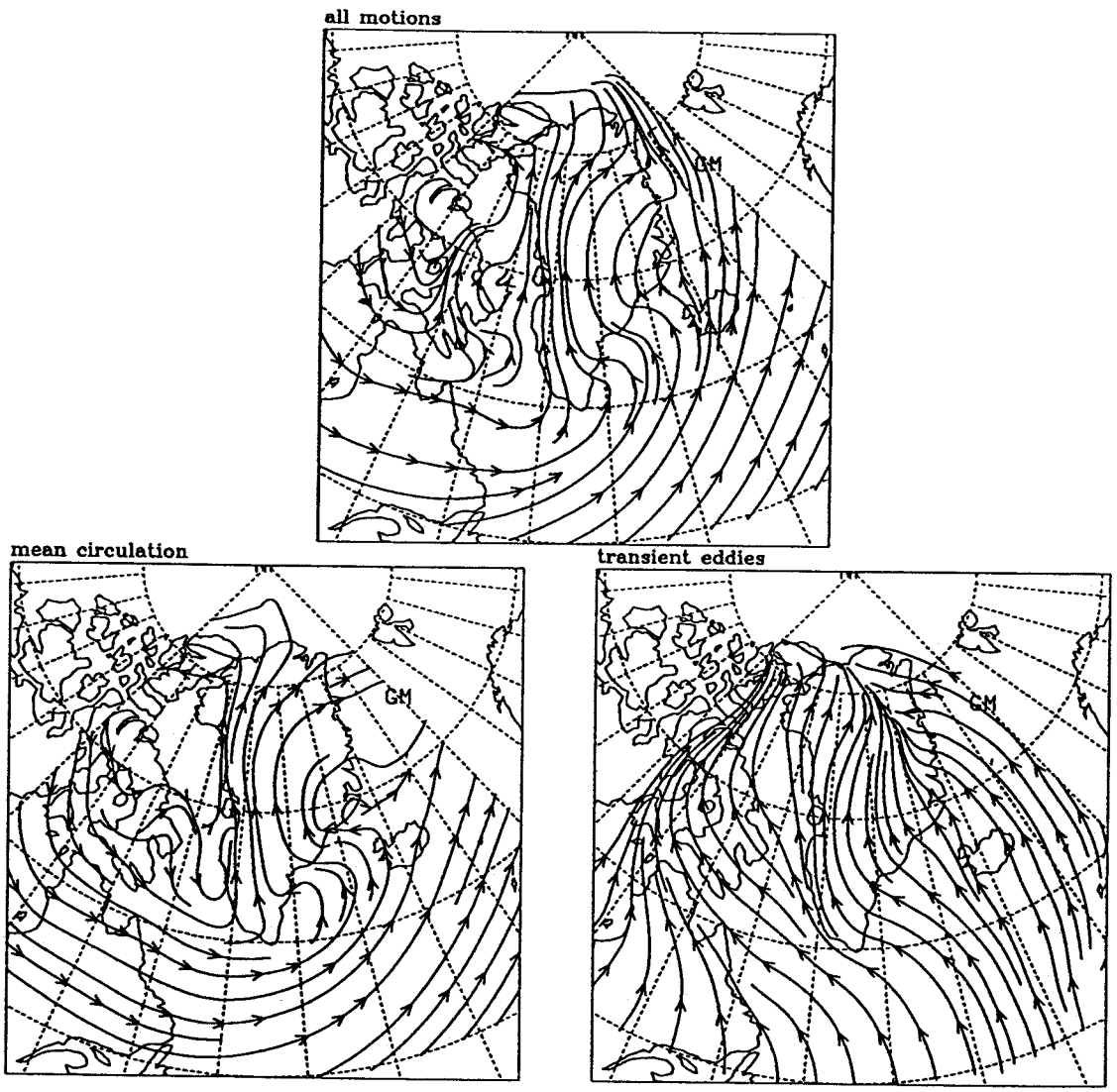


**Fig. 6.3a**: Streamlines of the vertically-averaged water vapour flux in winter.

MAR–APR–MAY
Streamlines of the vertically–integrated water vapour transport

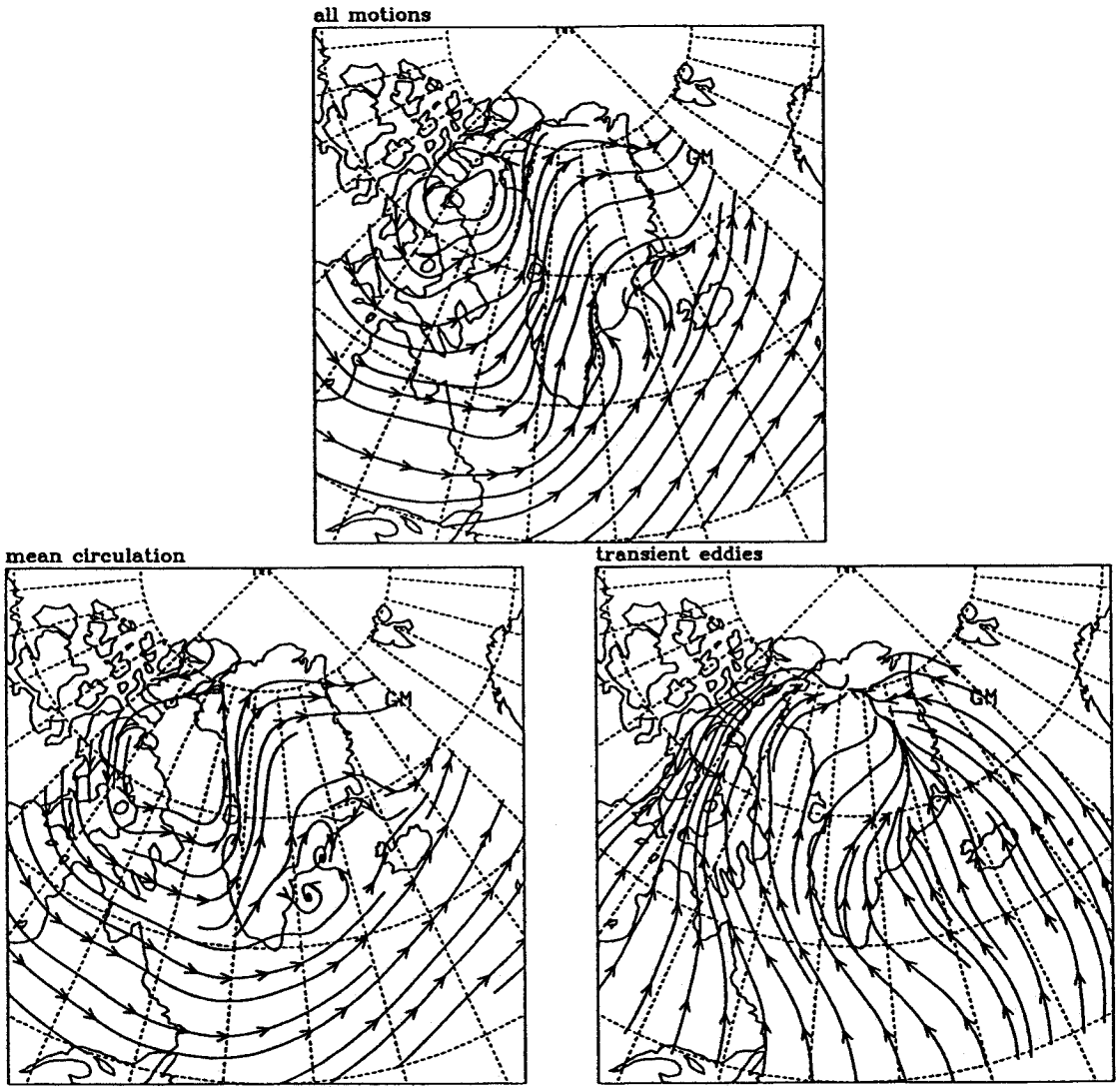


**Fig. 6.3b:** Same as Fig. 6.3a, but for spring.

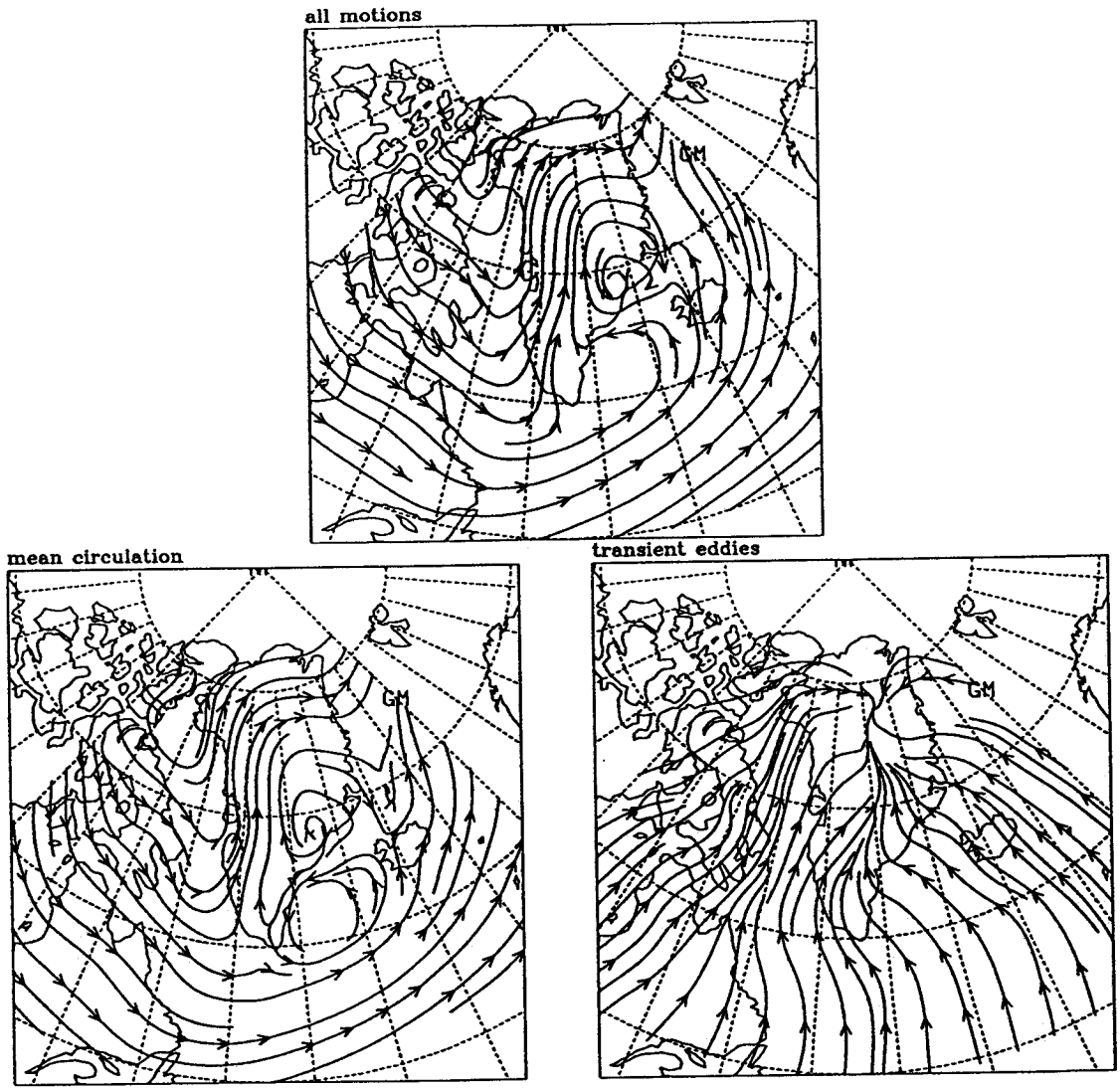


**Fig. 6.3c**: Same as Fig. 6.3a, but for summer.

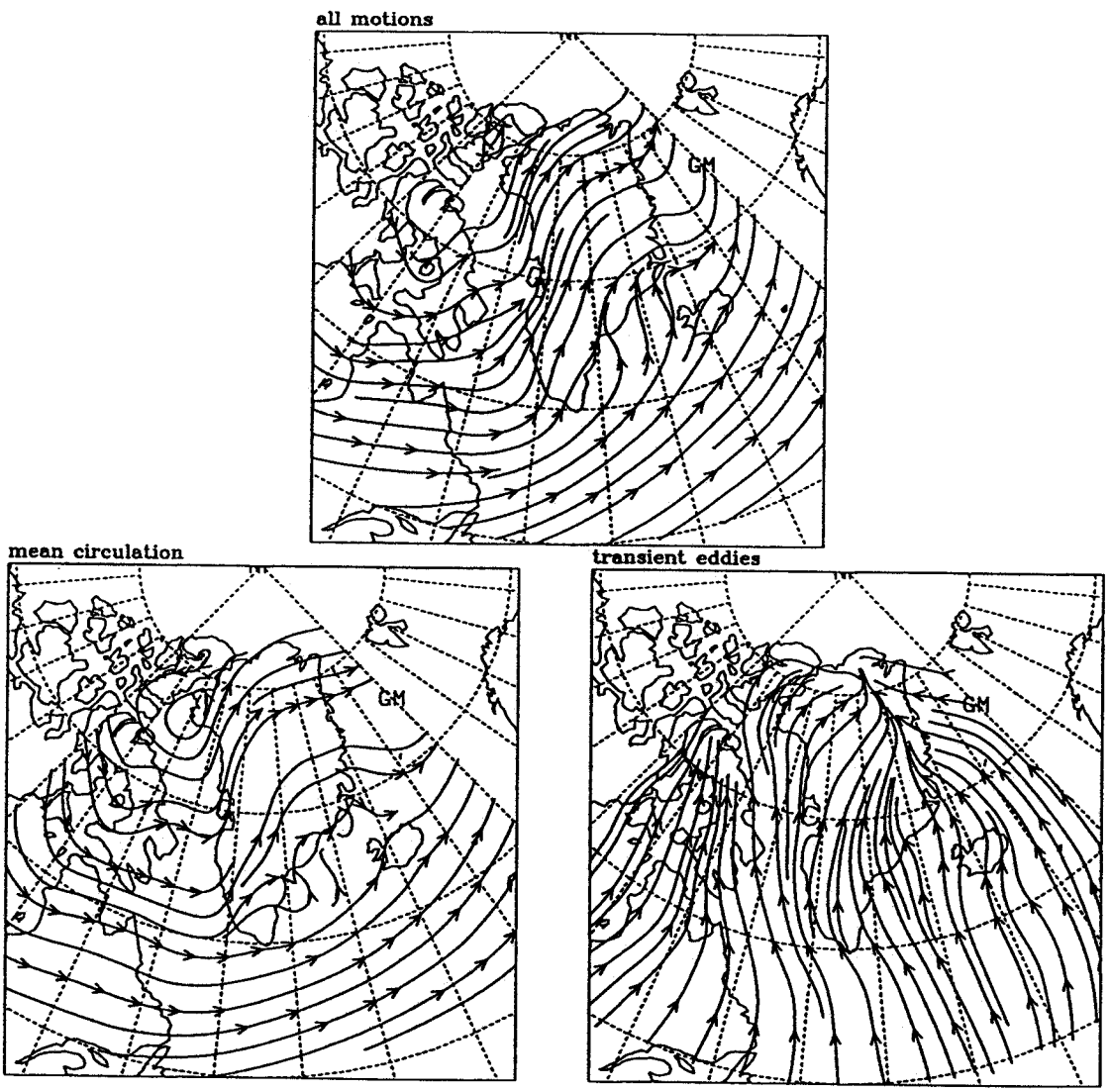


**Fig. 6.3d:** Same as Fig. 6.3a, but for autumn.

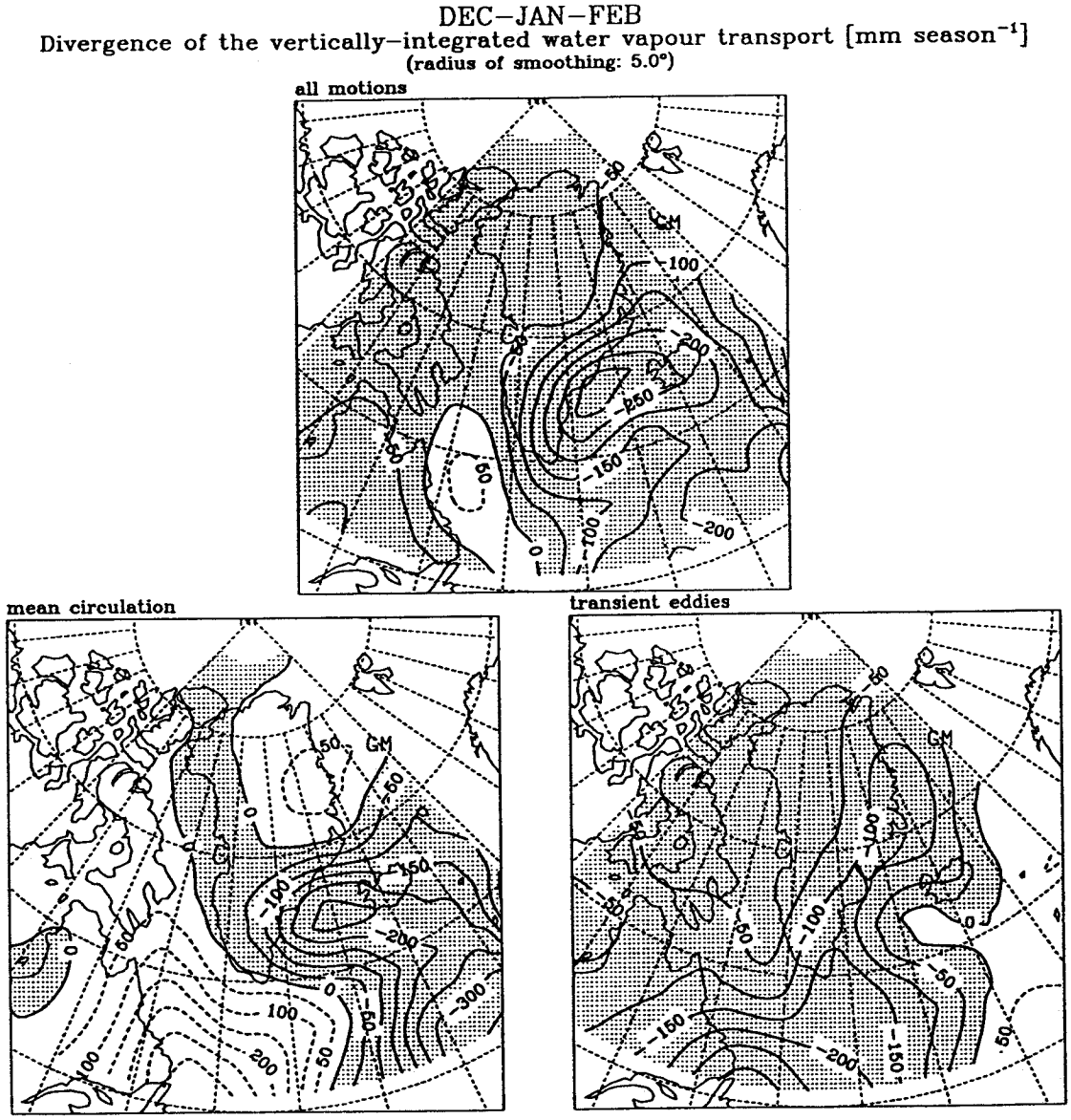


**Fig. 6.4a**: Geographical distribution of the moisture flux divergence [mm season$^{-1}$]. Winter.

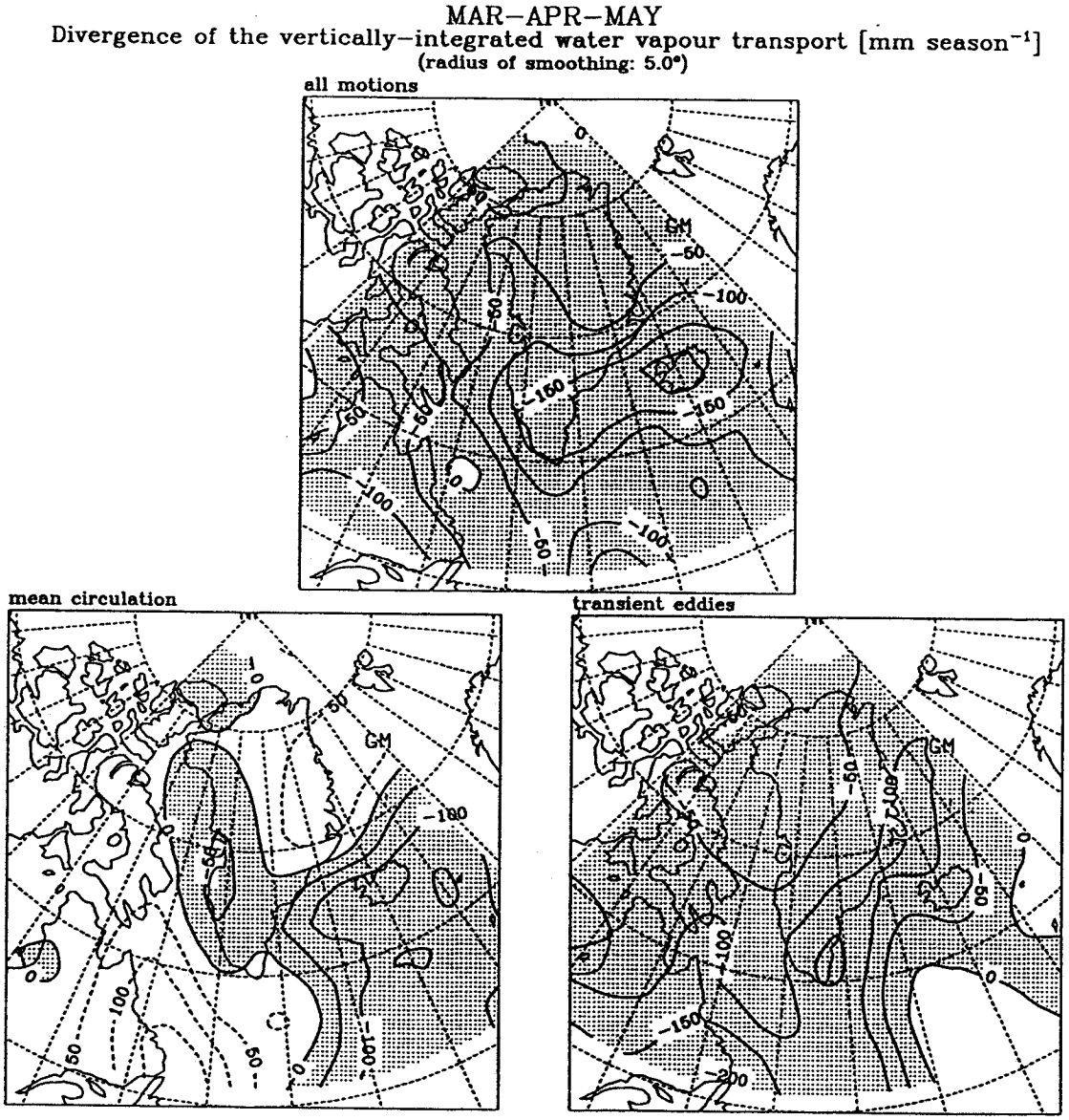


**Fig. 6.4b:** Same as Fig. 6.4a, but for spring.

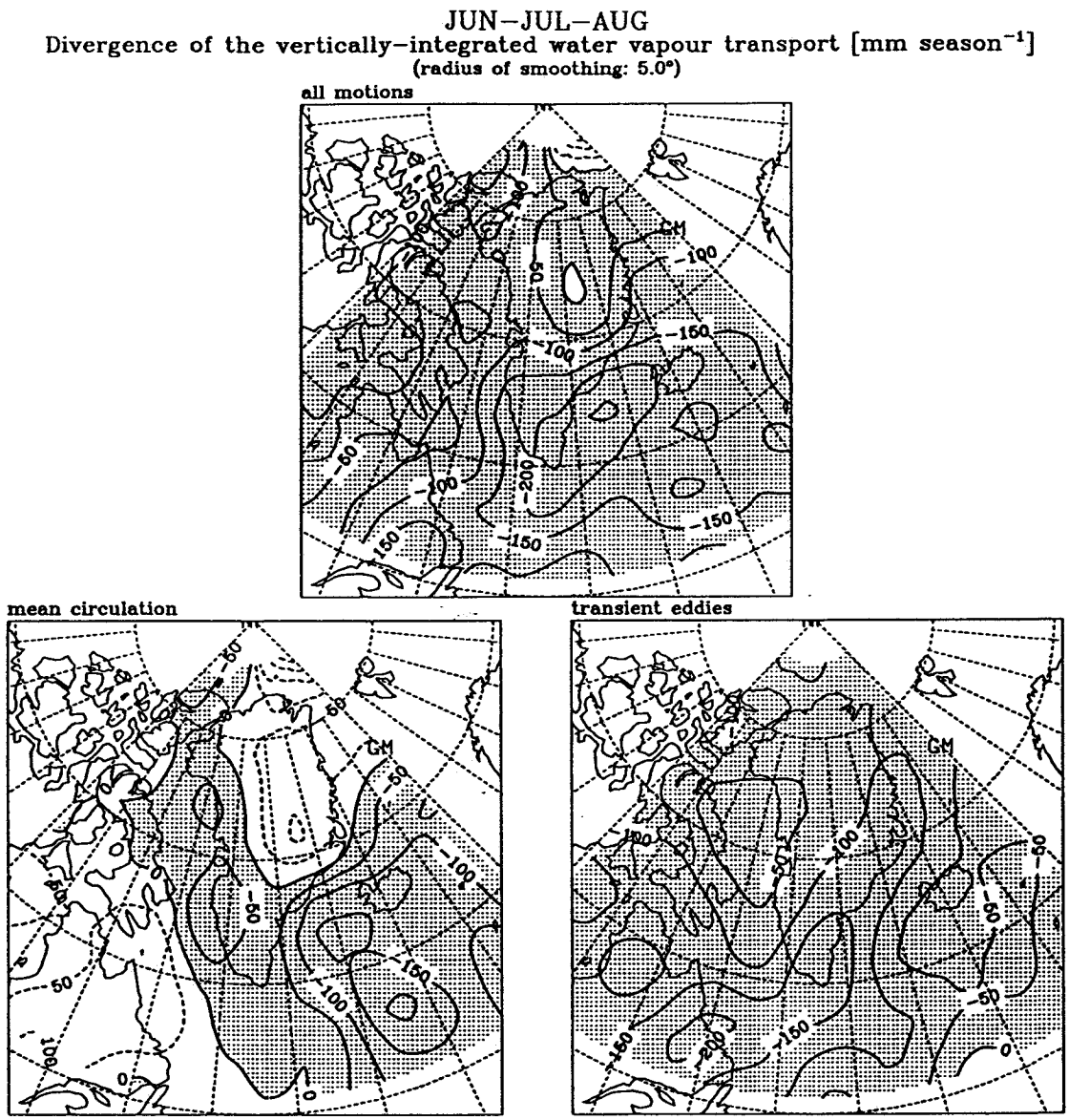


**Fig. 6.4c**: Same as Fig. 6.4a, but for summer.

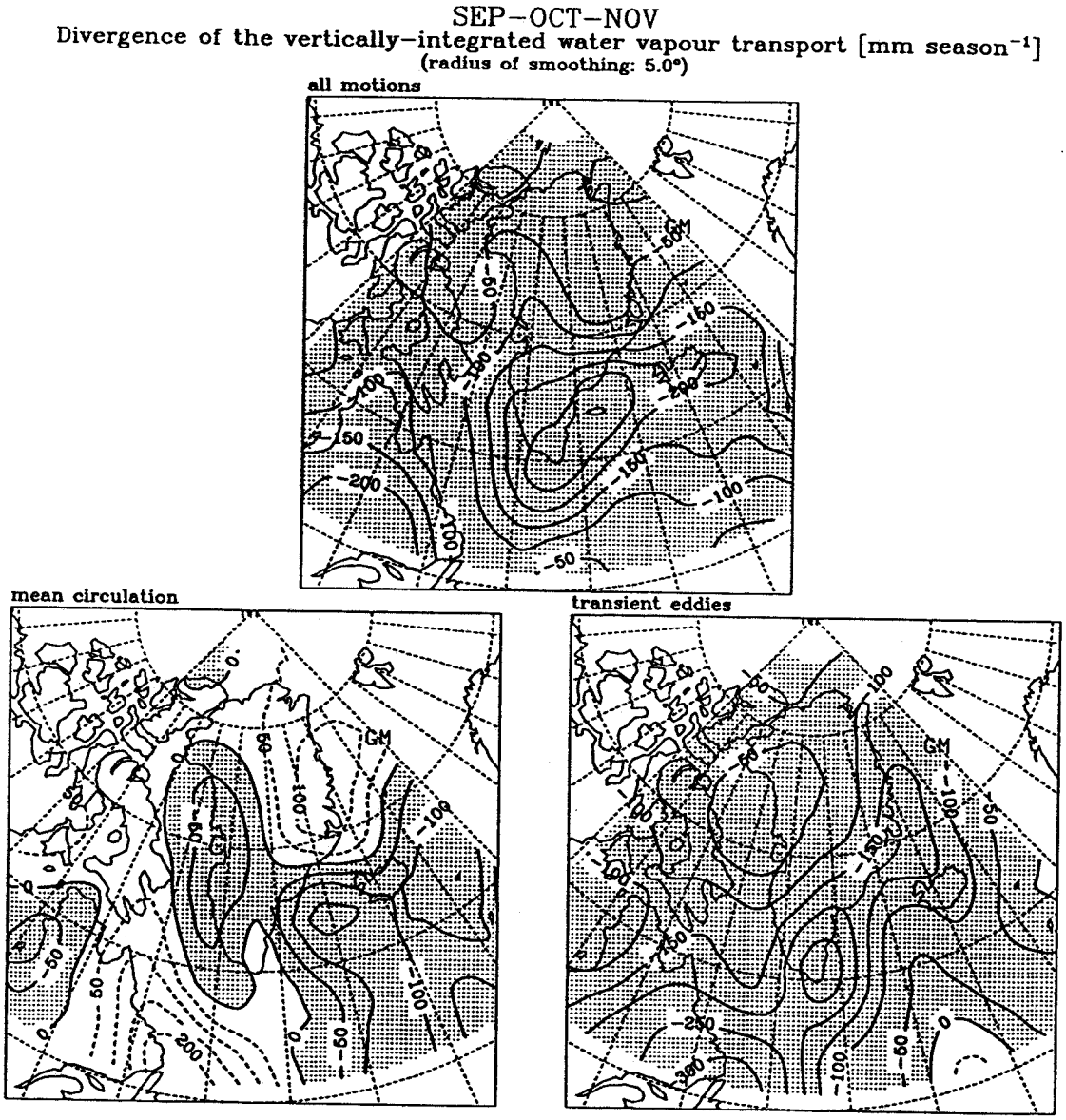


**Fig. 6.4d**: Same as Fig. 6.4a, but for autumn.

The magnitude of the moisture flux achieved by the mean circulation decreases northward and westward (Figs. 6.2a-d), in conjunction with the distribution of the (total) moisture content of the atmosphere (Figs. 6.1a-d) and with increasing distance from the belt of the strongest westerlies in the North Atlantic (expressed by the strong hypsometric gradients on the 700 hPa geopotential height map). It is highest in summer, when the holding capacity for water vapour of the atmosphere is highest and the precipitable water is about double as large as in winter (cf. Fig 6.1c and 6.1a). For all seasons, the transport achieved by the mean circulation is stronger than the water vapour flux by the eddies (Figs. 6.2a-d). The transient eddy flux of moisture has a dominant meridional (southerly) component and it is roughly down the gradient of the total moisture content. The same characteristics are observed in general in mid- to high latitudes, and in particular along the major storm tracks (Peixoto and Oort, 1983. Alestalo and Holopainen, 1980). A careful examination of the maps shows, in summer, a shift in the direction of the eddy flux in the eastern portion of study area. Whereas in winter the flux is directed from the North Atlantic toward the Canadian Arctic Archipelago, it points in summer from northern Canada (Hudson Bay and Labrador, here) toward Baffin Bay and the western coast of Greenland. This shift is related to the reversal of the temperature contrast between the land and ocean, as noted by Alestalo and Holopainen (1980) and Peixoto and Oort (1983), but also with the increase of the total water vapour content over Hudson Bay and Labrador (Fig. 6.1c). Moreover, the eddy flux north of about 80°N is a northerly one. This could be an indication of the (sub-)synoptic activity observed in the Polar Basin and particularly along its southern rim (Reed and Kunkel, 1960; Müller and Roskin-Sharlin, 1967; Bradley and Eischeid, 1985).

In contrast to what was noted for water vapour flux, the flux divergence contributions by the mean circulation and by the transient eddies are of the same order of magnitude in all seasons, although not similarly distributed (Figs. 6.4a-d). This is not surprising, since the moisture flow by the mean motion is essentially rotational (Salstein et al., 1980). A close inspection of the seasonal divergence maps reveals that, at the coast of Labrador and over the eastern North Atlantic, the areas of large convergence of the eddy flux are associated with areas of large divergence of the moisture flux by the mean circulation. The large divergence of the eddy flux at the east coast of Labrador is mainly associated with high-frequency transients, i.e., fluctuations with periods between 1 and 6 days (see next chapter). The partial cancellation between the divergence of the moisture flux by the mean circulation and the convergence of the eddy moisture flux (as well as the reversed combination) is even more striking in monthly maps (not shown). For the study area, the same kind of correspondence is

manifested also in the distribution of the divergence of the sensible heat flux, in particular at the 700 hPa level (cf. Figs. 20a and 20c in Lau, 1979).

Both the distributions of the moisture flux divergence due to the mean circulation and that of the flux due to the transient eddies exhibit large-scale patterns that are not dependent on season. The moisture flux due to the mean motion is usually divergent in the axis of the upper level trough and convergent further east, especially in relation to the Icelandic Low in winter. The area of divergence over Labrador and the western portion of the North Atlantic could be the result of the cold/dry air advection from the Polar Basin and northern Canada (Lau, 1979). The air is warmed and supplied with moisture as it moves westward. Over the North Atlantic, the lifting condensation level is low, the air conditionally unstable (or slightly stable), and the vertical motion is upward (Figs. 6.1a-d). These considerations are in agreement with the cloud distribution given by Vowinckel (1962) for latitudes north of 60°N.

The interaction of the mean flow with the topography creates a moisture flux convergence belt along the western coast of Greenland and a divergence area over northeastern Greenland, steadily associated with subsidence (see Figs. 6.1a-d). The former is modest in winter, when the flow is almost parallel to the topography and the moisture content low (Ohmura and Reeh, 1991). It is better developed in spring and summer, but best seen in autumn, when both the circulation and the temperature/moisture conditions in Baffin Bay are most favourable. It is in fact in this season that: the mean motion is strongly zonal over Baffin Island and Baffin Bay, impinging directly on the western slopes of the Greenland Ice Sheet (Fig. 6.2d); the stability is minimal; the upward motion is strong; the lifting condensation level is particularly low, lower by at least 200 m compared to the rest of the year (Fig 6.1d). The relative altitude of the lifting condensation level over Baffin Bay of approximately 400 m gives, when added to the 1400 m of the 850 hPa level, an absolute altitude of about 1800 m in autumn. The condensation level was estimated by Ohmura and Reeh (1991) at 2200 m in summer. In view of the various approximations, the agreement must be considered satisfactory.

With respect to the mean flow, as already noted by Ohmura and Reeh (1991), northeastern Greenland is permanently in the shadow of one of the main topographical barriers (depicted in their Fig. 5). If the divergence of the moisture flux by the mean circulation is assumed to represent the orographic component of the precipitation, the observed values between 50 and 100 mm season$^{-1}$ amount to a total of about 200 mm year$^{-1}$. In the absence of the transient eddies, this divergence would be

explained with an excess of evaporation over precipitation. Such a mechanism, however, is not plausible to this extent.

It is evident from Figs. 6.4a-d that the moisture flux achieved by the transient eddies is everywhere convergent, with the exception of the eastern North Atlantic in winter and partly in spring. The moisture flux divergence over the eastern North Atlantic has its counterpart in the divergence of the sensible heat flux at 700 hPa (Lau, 1979). As will be shown in Chapter 7, it is related to low-frequency fluctuations. The largest convergence of the moisture flux is observed at, or off the east coast of, Labrador, and in a belt stretching from there to southern Greenland and along the east coast of Greenland. These are known to be cyclogenetic areas (Whittacker and Horn, 1984). Along the east coast of Greenland, in addition, orographic lifting of air masses associated with the transient disturbances and a simultaneous breaking effect for onshore flows must be taken into account. This latter could probably explain why the belt of high convergence is always to the east of the zone of confluence displayed by the maps of the streamlines (compare Figs. 6.3a-d to Figs. 6.4a-d). If such a forcing could be demonstrated, then the observed higher convergence would be an evidence for the belt of higher precipitation postulated by Reeh (1989) and Ohmura and Reeh (1991) also along the eastern slopes of the Greenland Ice Sheet. Dynamically, the western and eastern slopes of the ice sheet act, therefore, on different components of the circulation.

In a statistical sense, the contribution of the transient eddies to the total, slightly positive moisture flux convergence in northeastern Greenland is illustrative of the synoptic nature of the precipitation in northeastern Greenland (Hamilton, 1958a and 1958b). In winter, moist air masses that produce precipitation are advected into northeastern Greenland when deep depressions are located in Denmark Strait. A more variagated synoptic activity characterized the summer season 1954 (Hamilton, 1958a), compared to the midwinter seasons. In summer 1954, frontal depressions from the southwest contributed partially to the precipitation at Nothice (78°04' N, 38°29' W), although the bulk of the precipitation was recorded under southeasterly flow conditions. Because precipitation is so minimal there, all events are significant for the total of a particular season.

For Greenland, the areal distribution of the total moisture flux convergence can be outlined as follows. In south-eastern Greenland, both the mean circulation and the transient eddies contribute to the total convergence to about the same extent. In western Greenland, the winter differs from the other seasons, in that the south-southeasterly moisture flux achieved by the mean circulation is only slightly convergent. The increase of the zonality of the mean motion and the establishment of more

advantageous thermal conditions in Davis Strait and Baffin Bay lead, during the course of the year, to the appearance of a moisture flux convergence belt of the mean motion along the west coast. The convergence of the transient eddy flux decreases northward and yields a similar northward depletion of the total convergence. An exception, however, is seen in summer, north of 75°N, when the northwest-northerly eddy moisture flux is responsible for a relative maximum of the convergence over Ellesmere Island of 100 to 150 mm season$^{-1}$. For comparison, the measured summer precipitation on Axel Heiberg Island (Müller and Roskin-Sharlin, 1967) for the summer 1961 averages up to about 150 to 200 mm. The precipitation maximum at Nord (81°36' N, 16°40' W) is also observed during the summer season, whereas the maximum usually occurs in winter at the east coast.

# 7. MOISTURE FLUX AND FLUX DIVERGENCE ACHIEVED BY THE TRANSIENT EDDIES

In the previous chapter, the transient eddy water vapour flux and flux divergence were discussed in relation to the flux and flux divergence achieved by the mean circulation. It was noted that the transient eddy flux is small compared to the moisture flux achieved by the mean circulation. But since this latter is highly rotational, the transient eddy contribution to the total moisture flux divergence field is at least as important as the contribution by the mean circulation. Moreover, it remains to determine how the transient eddy flux and flux divergence are concretized. This section, therefore, is an attempt to answer, among others, the following questions: what are the preferred modes of transfer in the frequency space, and how efficient is the transport of air masses that are characterized by moisture conditions departing from the average.

## 7.1 Time-spectral characteristics

Due to the limited spatial extent of the study area, only the time-spectral features of the transient eddy flux and flux divergence will be discussed in this section. However, the interpretation is partially based on a relaxed Taylor's hypothesis (Vinnichenko, 1970), which states that the time-spectra and the space-spectra are related through an appropriate velocity. Although the hypothesis is not proven, nor is it unanimously accepted (see for example Julian, 1971), it has been shown by Kao and Weddell (1970) and more distinctly by Blackmon (1976), that low-frequency transients are dominated by large-scale waves, whereas medium-frequency transients (i.e., with periods between 2 and 6 days) receive significant contributions from synoptic or shorter-scale waves.

In the present study, only three years are considered. As discussed by Hartmann (1974), a longer period would be suitable to yield more reliable statistics, since the statistical confidence increases with increasing number of realizations. To test the reliability of the present computations, the winter statistics at Ship C (53°N, 35°W) calculated with the 1989-1991 ECMWF analyses were compared with those computed by Hartmann (1974) on the basis of a 13-year record of rawinsonde data. For all meteorological parameters considered, that is the two horizontal wind components, the geopotential height, and the temperature and specific humidity, the characteristic features of the

spectra derived by Hartmann are reproduced by the present computations. The same holds for the cospectra of the meridional flux of zonal momentum, enthalpy, potential energy and moisture. Even more significant is the close agreement, for the same meridional fluxes, between the phase relations of the present investigation with those presented in Hartmann. This is so because the phase is statistically less robust than the cospectrum (Hartmann, 1973; Priestley, 1981). In sum, the comparison indicates that, at least at this particular location in the North Atlantic, which is subject to the frequent passage of synoptic disturbances, the statistics derived from the three-year analyses of the ECMWF are reliable and representative of the statistics inferred from a much longer data set.

Spectra of the meridional wind component, of the temperature and of the specific humidity, as well as cospectra of the meridional transport of temperature (enthalpy) and specific humidity (moisture) at Ship C based on the ECMWF analyses are shown in Fig. 7.1 for the standard pressure levels. The spectra clearly indicate that, below the tropopause (approximatively at 300 hPa), for all three parameters most of the variance falls at periods between 1 and 7 days. As noted by Hartmann (1974), travelling synoptic disturbances are the dominant elements of the atmospheric circulation at this location and it is therefore not surprising that, owing to their structure, they exert a strong control on the variability of these meteorological parameters. At 850 hPa, the spectrum of the temperature and of the specific humidity are very similar, except for a more conspicuous contribution in the range 1 to 2 days for the specific humidity. At this level, the two cospectra are also very similar. Noteworthy in both cospectra is the cut-off at about 8 days. It will be shown later that a sharp transition at 10 days is not limited in space to the North Atlantic, but appears consistently in the whole study area. The similarity between spectra of the temperature and specific humidity and between the cospectra of the corresponding meridional fluxes can be explained by the well-known fact that warmer air also means moister air. In this sense, it justifies the interpretation, later on, of some the regional features of the eddy moisture flux in terms of the eddy temperature flux.

The spectral contributions to the moisture flux in winter for the period intervals defined in Chapter 3 are shown in Fig. 7.2, while those for the summer season are displayed in Fig. 7.3.

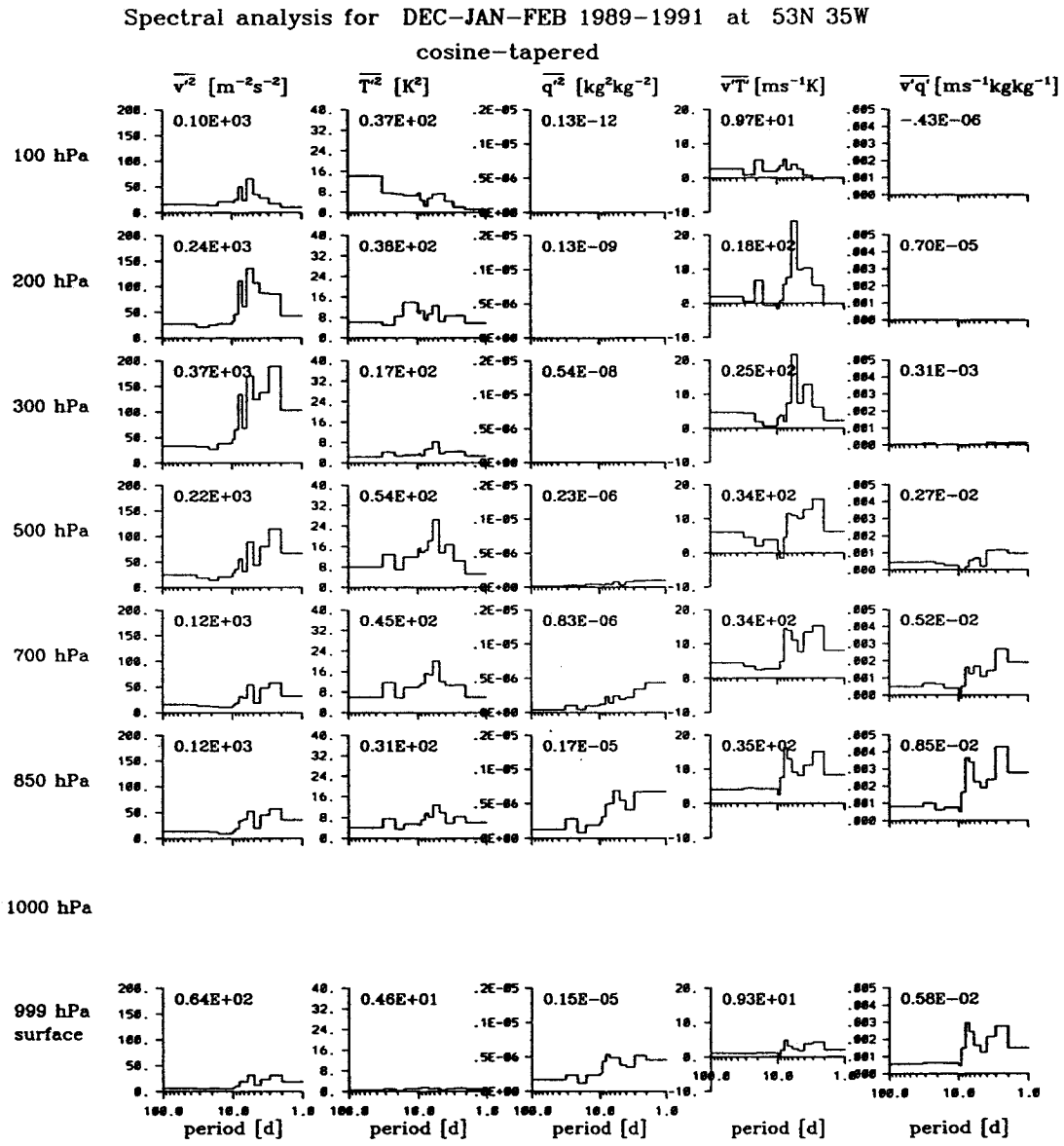


**Fig. 7.1** : From left to right: spectra of the meridional wind (v), of the temperature (T) and of the specific humidity (q), as well as cospectra of the meridional temperature and moisture fluxes. The units are given at the top of each column. Pressure levels to which the spectra and cospectra refer are shown on the left. The numbers at the top left corner of each diagram give the total variance (for the spectra) and covariance (for the cospectra). The abscissas are labeled in days. The scale is logarithmic. The ordinate is the power density multiplied by the frequency.

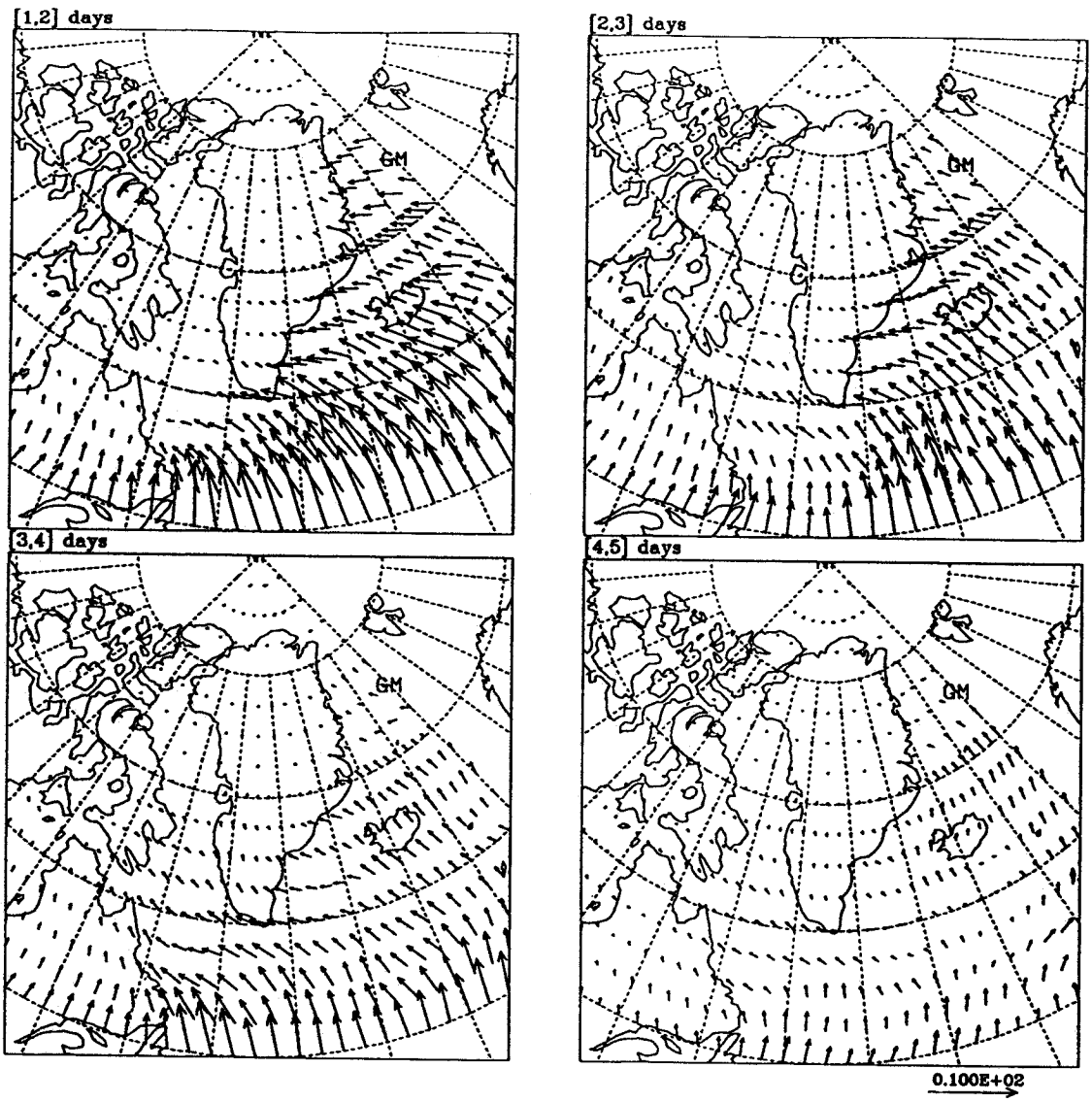


**Fig. 7.2:** Spectral contributions to the vertically-integrated eddy moisture flux in winter, for frequency intervals corresponding to: [1,2] days, [2,3], [3,4], [4,5], [5,6], [6,7], [7,8], [8,9], [9,10], [10,16], [16,21], [21,32], [32,90] days. The scale is shown in the lower right corner. Umits are [kg $m^{-1}$ $s^{-1}$]

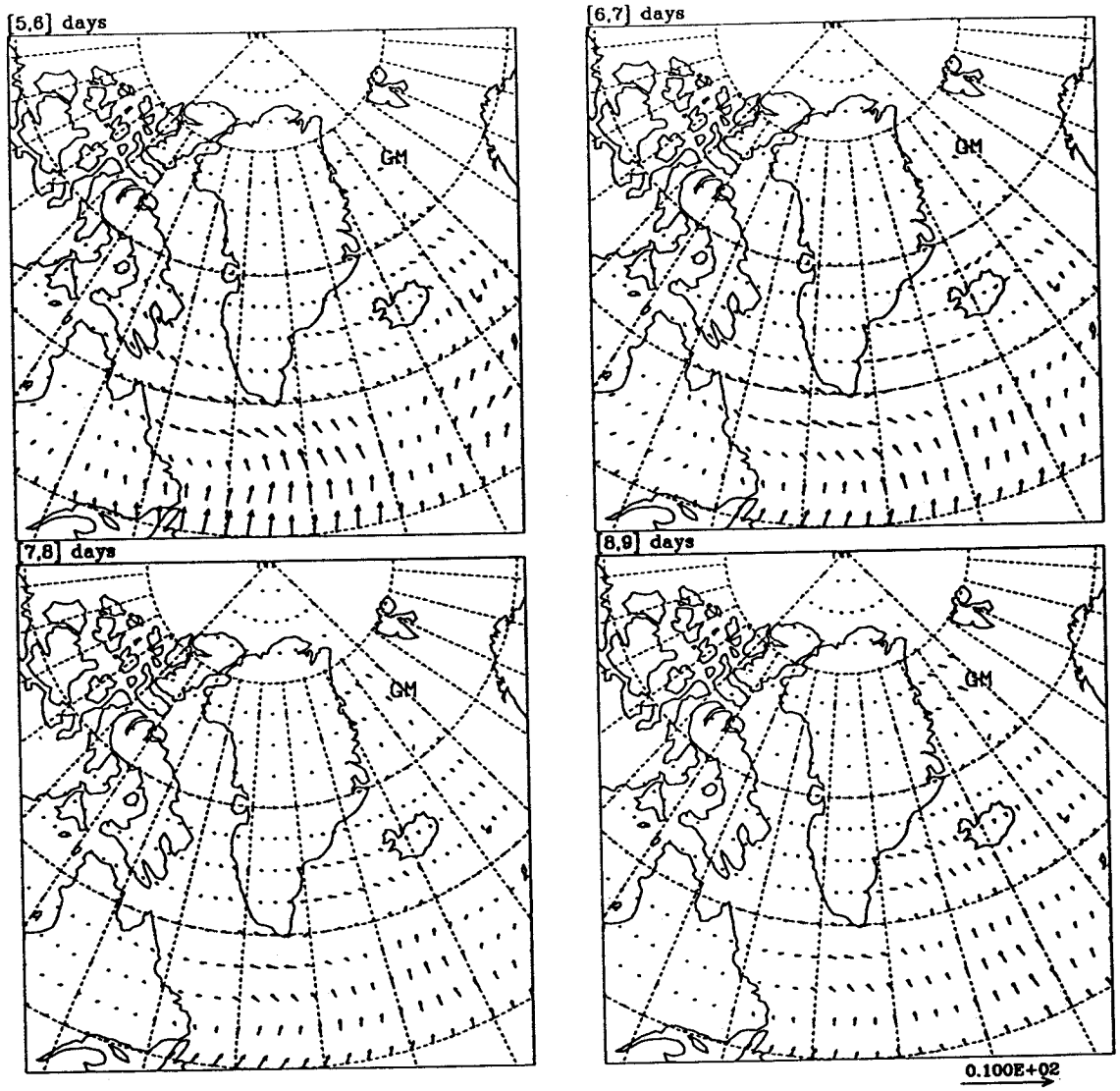


**Fig. 7.2:** (cont.)

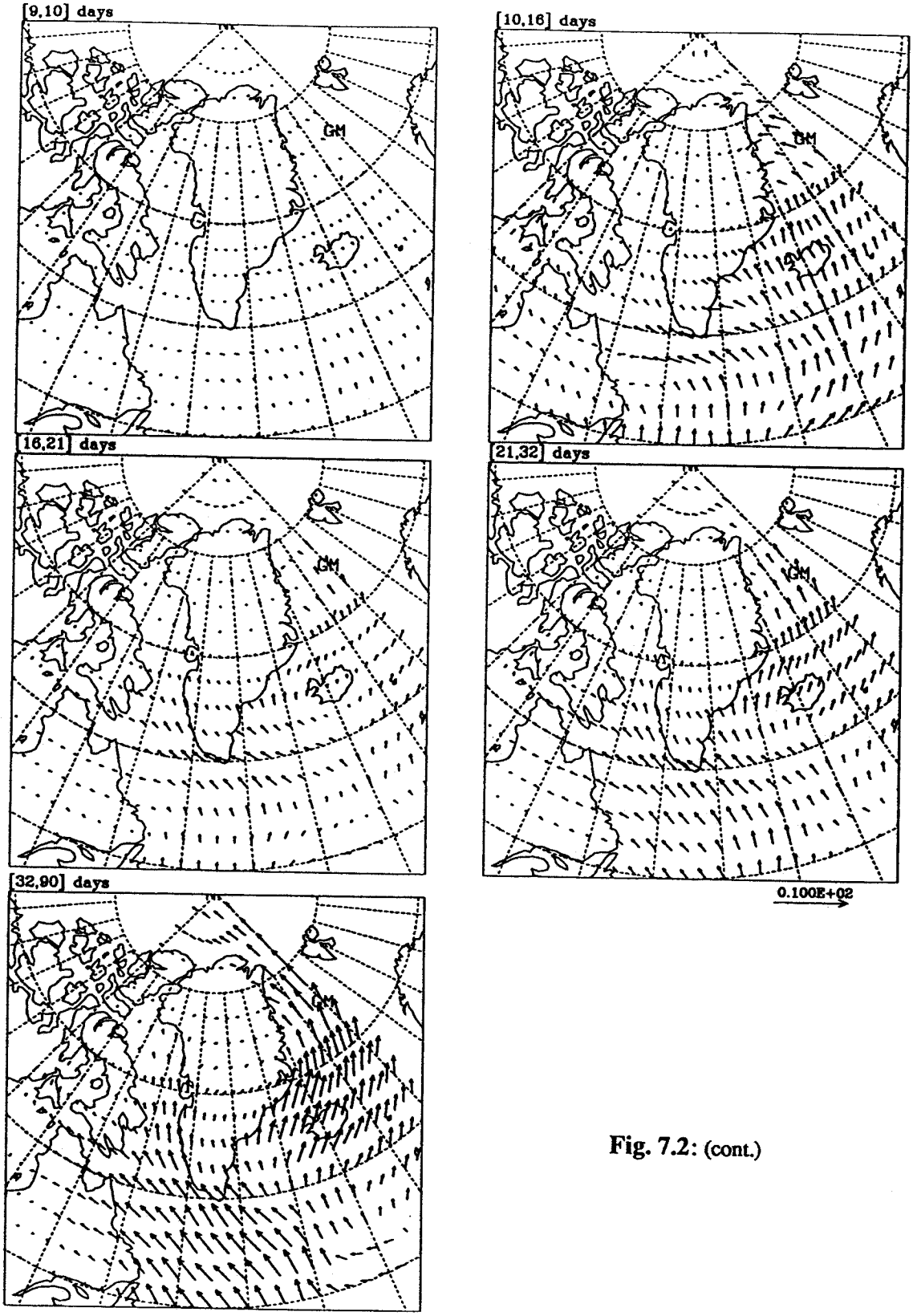
[9,10] days
GM
[10,16] days
GM
[16,21] days
GM
[21,32] days
GM
[32,90] days
GM
0.100E+02

**Fig. 7.2:** (cont.)

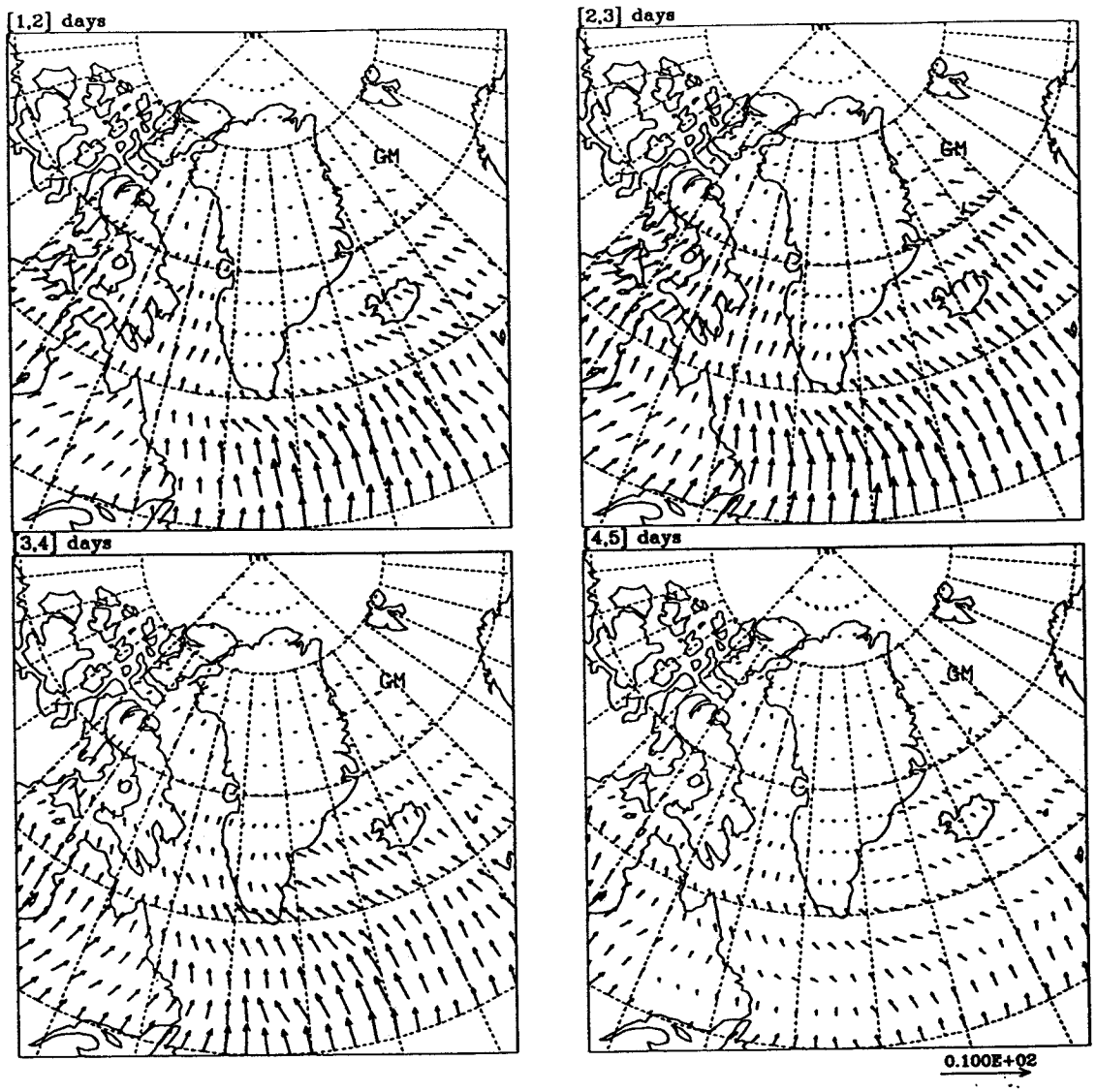


**Fig. 7.3**: Spectral contributions to the vertically-integrated eddy moisture flux in summer, for frequency intervals corresponding to: [1,2] days, [2,3], [3,4], [4,5], [5,6], [6,7], [7,8], [8,9], [9,10], [10,16], [16,21], [21,32], [32,90] days. The scale is shown in the lower right corner. Umits are [kg $m^{-1}$ $s^{-1}$]

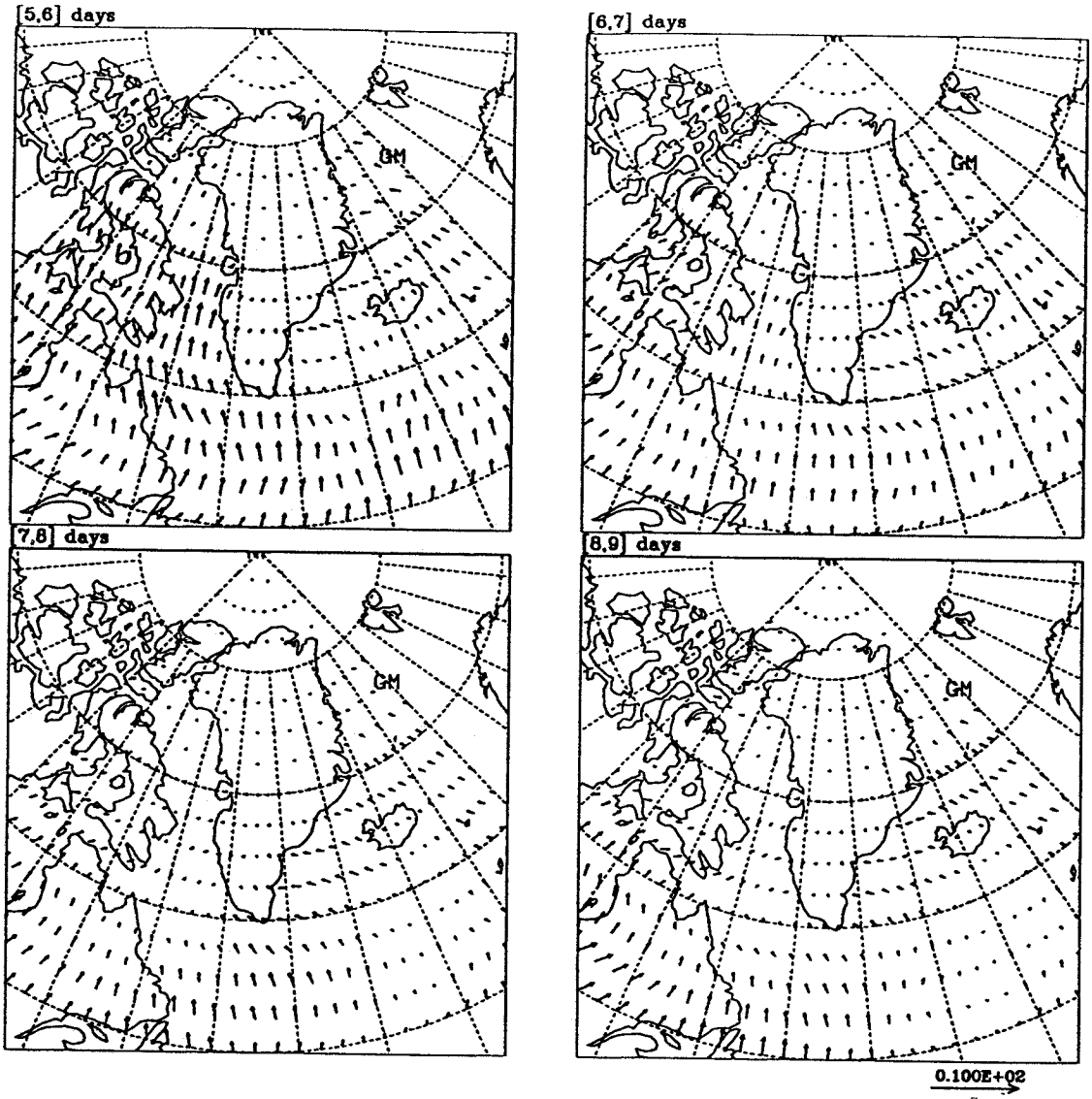


**Fig. 7.3:** (cont.)

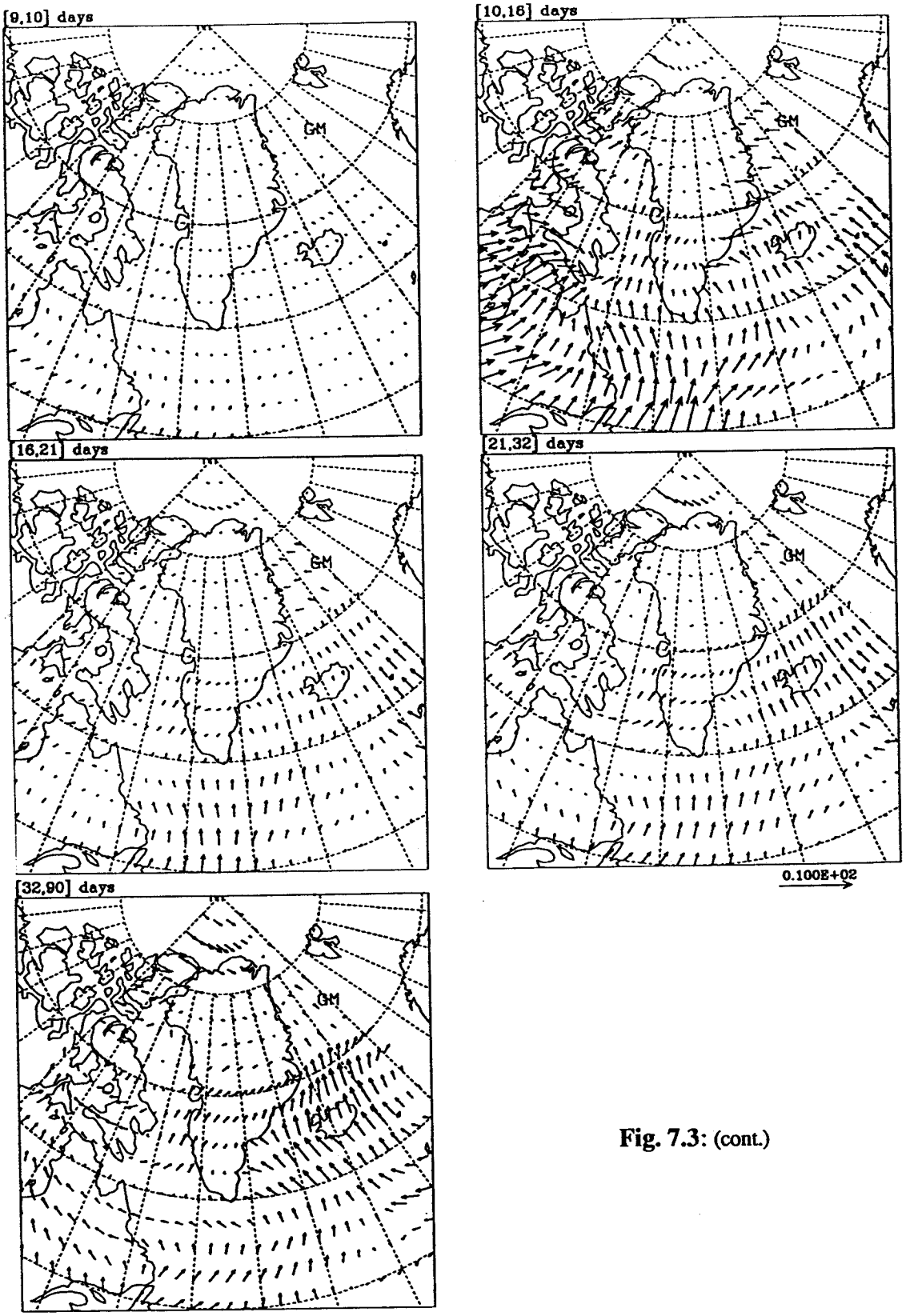
[9,10] days
GM
[10,16] days
GM
[16,21] days
GM
[21,32] days
GM
0.100E+02
[32,90] days
GM

**Fig. 7.3**: (cont.)

The eddy moisture flux in winter shows significant contributions mainly in two frequency ranges; the high-frequency end, corresponding to periods between 1 day and 6 days, and the low-frequency range, i.e., periods between 10 days and 90 days. Note that the high-frequency range as defined in the present study corresponds to the medium- or band-pass range of Blackmon (1976). The present definition is preferred, since no higher frequencies can be resolved with the given time resolution of 12 hours. The high-frequency range shows very large, vertically-integrated fluxes in the North Atlantic, in an area characterized by large high-frequency power in the geopotential variance (Blackmon, 1976). This high-frequency power in the geopotential variance results from the frequent eastward passage of synoptic disturbances. Taking low pressure centers at the surface as the characteristic signature of synoptic disturbances leads to an alternative definition of storm track (Whittacker and Horn, 1984). Thus, large contributions to the eddy moisture flux in the high-frequncy range may also be related to the presence of a major storm track in the North Atlantic (Whittacker and Horn, 1984). The flux is directed across the storm track and dominates, in magnitude, the pictures at these frequencies. At the other end of the spectrum, i.e., for periods longer than 10 days, large fluxes are confined mainly south of Greenland, in Davis Strait and around Iceland. The degree of order is very high and results graphically in flux arrows that are almost perfectly parallel and of almost equal length. This has of course an implication for the divergence (or convergence), which is in fact small in these areas (see Fig. 7.5). At low frequencies, small fluxes are observed in the eastern North Atlantic. In this area, and for the lowest frequency interval, i.e. periods in the range 32 days to 90 days, the flow is diffluent. Further north, the vectors outflank central-eastern and north-eastern Greenland. For a section across Denmark Strait, the flux is largest in the centre of the section. From there, the flux increases in magnitude as one proceeds northward. This will result in a dipolar distribution of the divergence (divergence in the south of Denmark Strait, convergence in the north; see Fig. 7.5).

The summer season is different in several ways (Fig. 7.3). Firstly, the flux is somewhat smaller than in winter. Secondly, there is an additional zone of high activity, both at high and medium-low frequencies, over north-eastern Canada, Hudson Bay and Baffin Island. A possible reason is seen in Fig. 3 of Whittacker and Horn (1984), which shows that the major storm track of the American-Atlantic sector still stretches from Hudson Bay eastward to the British Isles, but that a secondary track descends from Alaska toward Hudson Bay. In fact, this secondary track coincides with the Arctic frontal zone described by Reed and Kunkel (1960), which, in their analysis, is clearly separated from the polar front. Along this frontal zone, large high-frequency eddy activity is expected. The contributions from the interval 1 to 3 days is still important but, unlike

for the North Atlantic storm track, fluctuations with periods between 5 and 7 days are also significant in the Baffin Island/Davis Strait region. Large contributions to the eddy moisture flux in the relatively narrow frequency interval corresponding to periods between 10 and 16 days are limited to the southeastern portion of the study area, i.e., mainly to the Labrador peninsula.

A third characteristic of the summer season is the less clear spectral transition at the frequency corresponding to 6 days. This may be simply a secondary effect due to the less strong flux observed especially at higher frequencies. However, it is believed that it represents the broader interval of frequencies found in nature. On the other hand, the transition at the frequency corresponding to 10 days is at least as pronounced as in winter.

In summer, at frequencies corresponding to periods longer than 16 days, large contributions to the eddy moisture transport are seen south of Greenland and around Iceland (Fig.7.3). The overall distribution in the Iceland area is similar to that for the winter season, but the south-southeasterly flux from the North Atlantic is not able to penetrate into Davis Strait and further into Baffin Bay. In the Baffin Island region, the low-frequency contributions to eddy moisture flux shows a change in the direction with decreasing frequency. At the very low-frequency end, the flux is clearly diffluent (and divergent) over Baffin Bay. High systematicity of the water vapour transport in the low-frequency range characterizes the northernmost part of the study area. At the southern rim of the Polar Basin, the moisture flux contributions in the interval 10 to 90 days are directed southeastward, implying a transport of moisture out of the Polar Basin and toward the northern coast of Greenland. This is contrary to what was observed for the winter season (Fig. 7.2), when the southerly flow in the Greenland Sea follows the northeastern coast of Greenland and continues across the Polar Basin. This northerly component in summer does not reach further south than 80°N (Fig. 7.3), which may indicate the shallowness of the associated systems.

In winter, the spectral features of the moisture flux divergence (Fig. 7.5) are closely associated to those of the moisture flux (Fig. 7.2). In the frequency range corresponding to periods between 1 and 6 days, the moisture flux is convergent almost everywhere, with the largest convergence observed in relation to the North Atlantic storm track. A secondary zone of high convergence is observed at the east coast of Greenland, where the flux (Fig. 7.2) is perpendicular to the coast. For periods in the interval 6 to 10 days, the moisture flux divergence field is very weak, in particular in the interval between 8 and 10 days. For the low-frequency range, there is moisture flux convergence west of a line running approximately from Newfoundland northeastward towards Iceland and

Svalbard, whereas the water vapour flux is divergent over the eastern North Atlantic and the Norwegian Sea. A comparable distribution was found by Holopainen (1983) for the divergence of the eddy heat flux (his Fig. 8.8 for the 700 hPa level). He noted the importance of blocking episodes in influencing the behaviour of the transients over the eastern North Atlantic. It is certainly true that the high convergence observed along eastern Greenland, as well as the absence of a significant flux in the eastern North Atlantic (Fig. 7.2), is explainable by the northwestward shift of the cyclone path during blocking episodes. An illustrative example of the changes in the cyclones path following the establishment of a blocking high in the eastern North Atlantic is given in Fig. 12.8.9 of Petterssen (1956), reproduced here as Fig. 7.4. In addition, synoptic disturbances that have to travel along eastern Greenland are certainly favoured by the high baroclinicity there (see Fig. 2b of Whittacker and Horn, 1984). As was mentioned already in Chapter 6, the convergence may also be enhanced by orographic effects. If the moisture flux divergence distribution observed at low frequencies is really the consequence of blocking in the eastern North Atlantic, then it is not the direct result of low-frequency fluctuations but rather the result of high-frequency fluctuations modulated by the low-frequency variability.

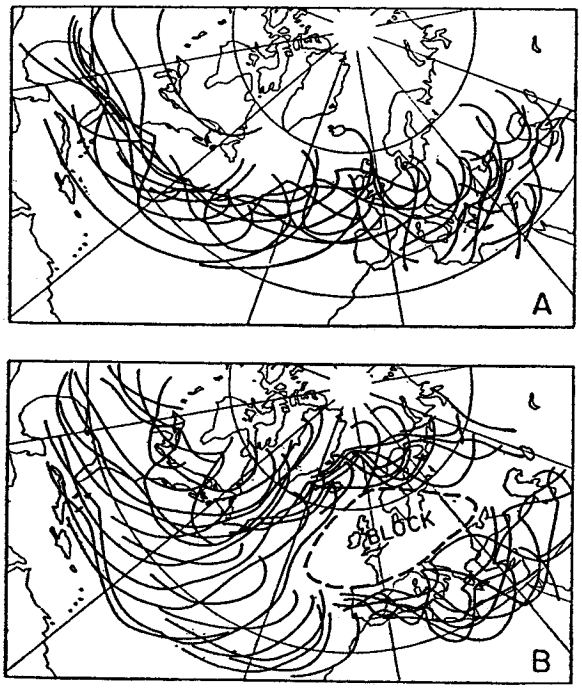


**Fig. 7.4:** Position of surface fronts during two 10-day periods: A, preceding the formation; B, following the establishment of a cutoff high on 18 February 1948 (after Petterssen, 1956).

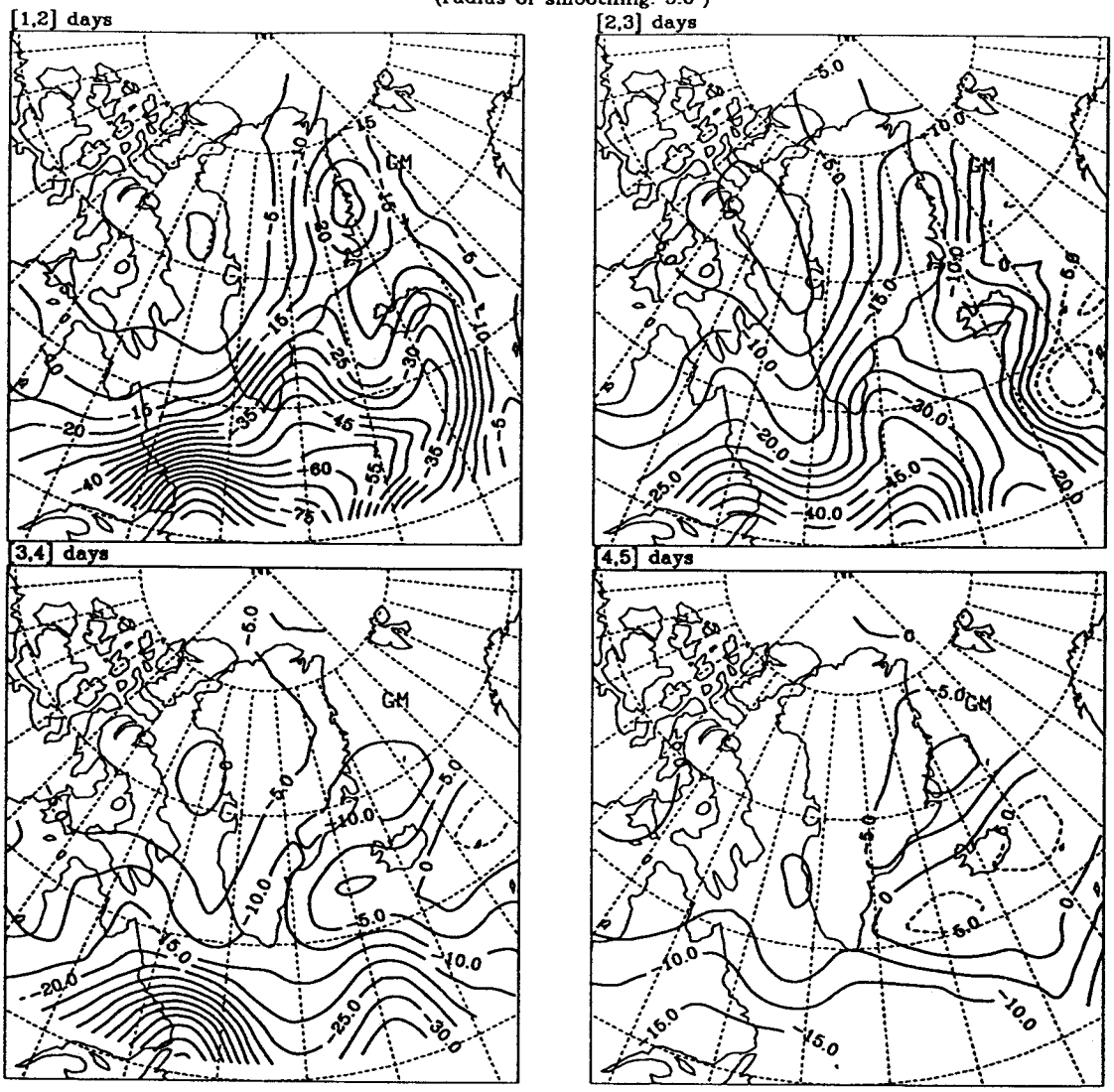


**Fig. 7.5**: Divergence of the spectral contributions to the vertically-integrated eddy moisture flux in winter, for frequency intervals corresponding to: [1,2] days, [2,3], [3,4], [4,5], [5,6], [6,7], [7,8], [8,9], [9,10], [10,16], [16,21], [21,32], [32,90] days. Units: [mm season$^{-1}$].

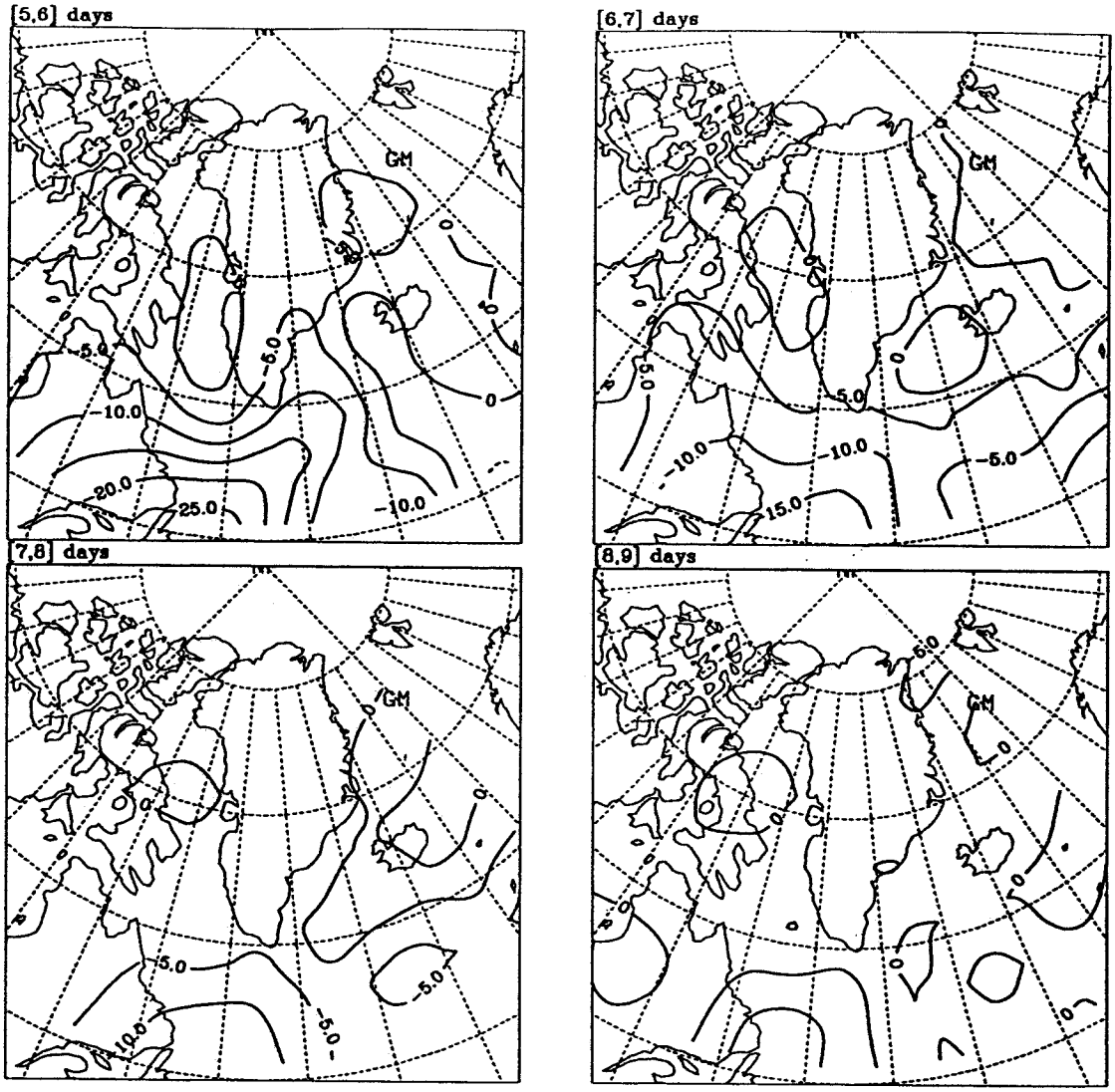


**Fig. 7.5**: (cont.)


**Fig. 7.5:** (cont.)

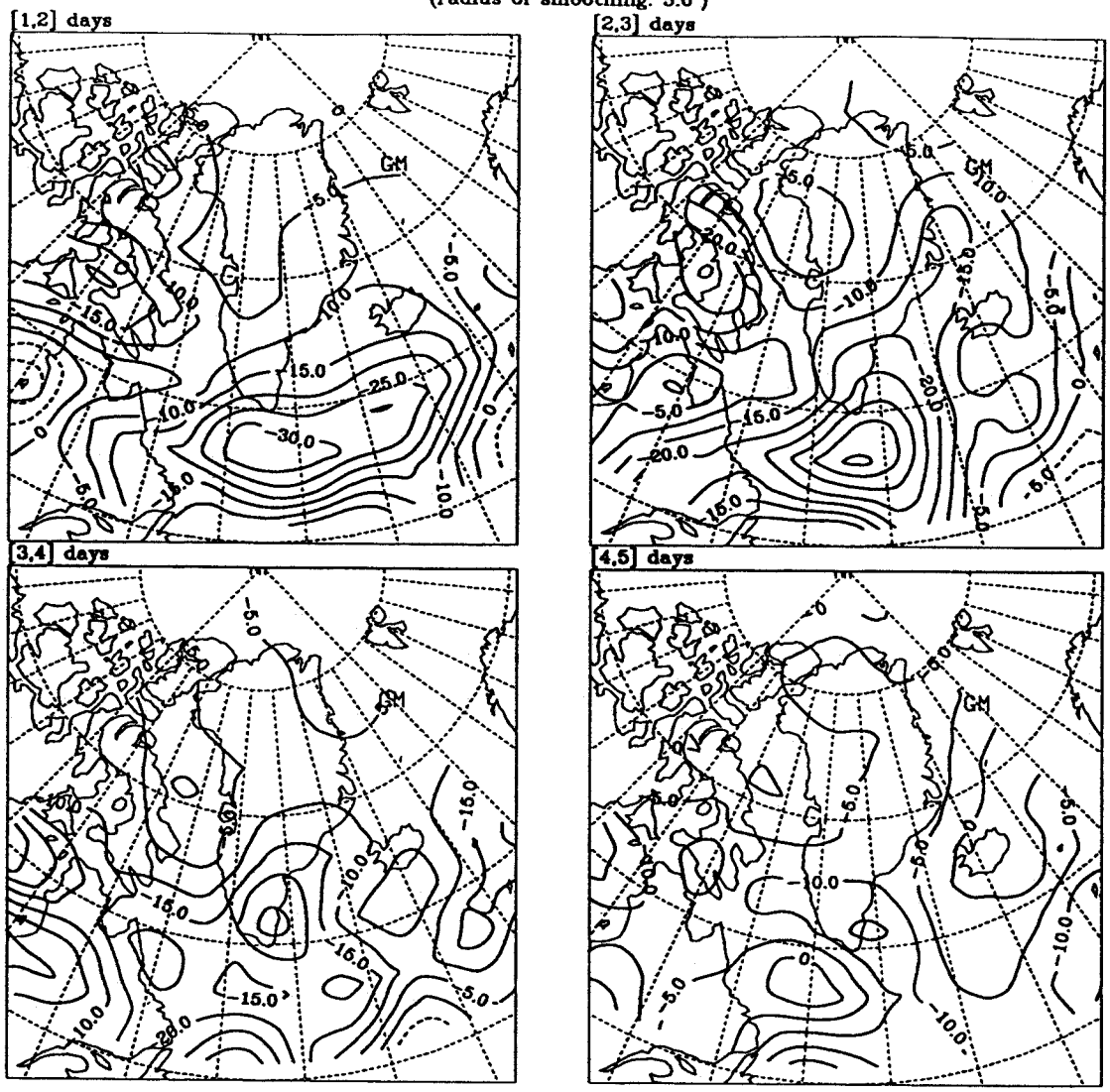


**Fig. 7.6**: Divergence of the spectral contributions to the vertically-integrated eddy moisture flux in summer, for frequency intervals corresponding to: [1,2] days, [2,3], [3,4], [4,5], [5,6], [6,7], [7,8], [8,9], [9,10], [10,16], [16,21], [21,32], [32,90] days. Units: [mm season$^{-1}$].

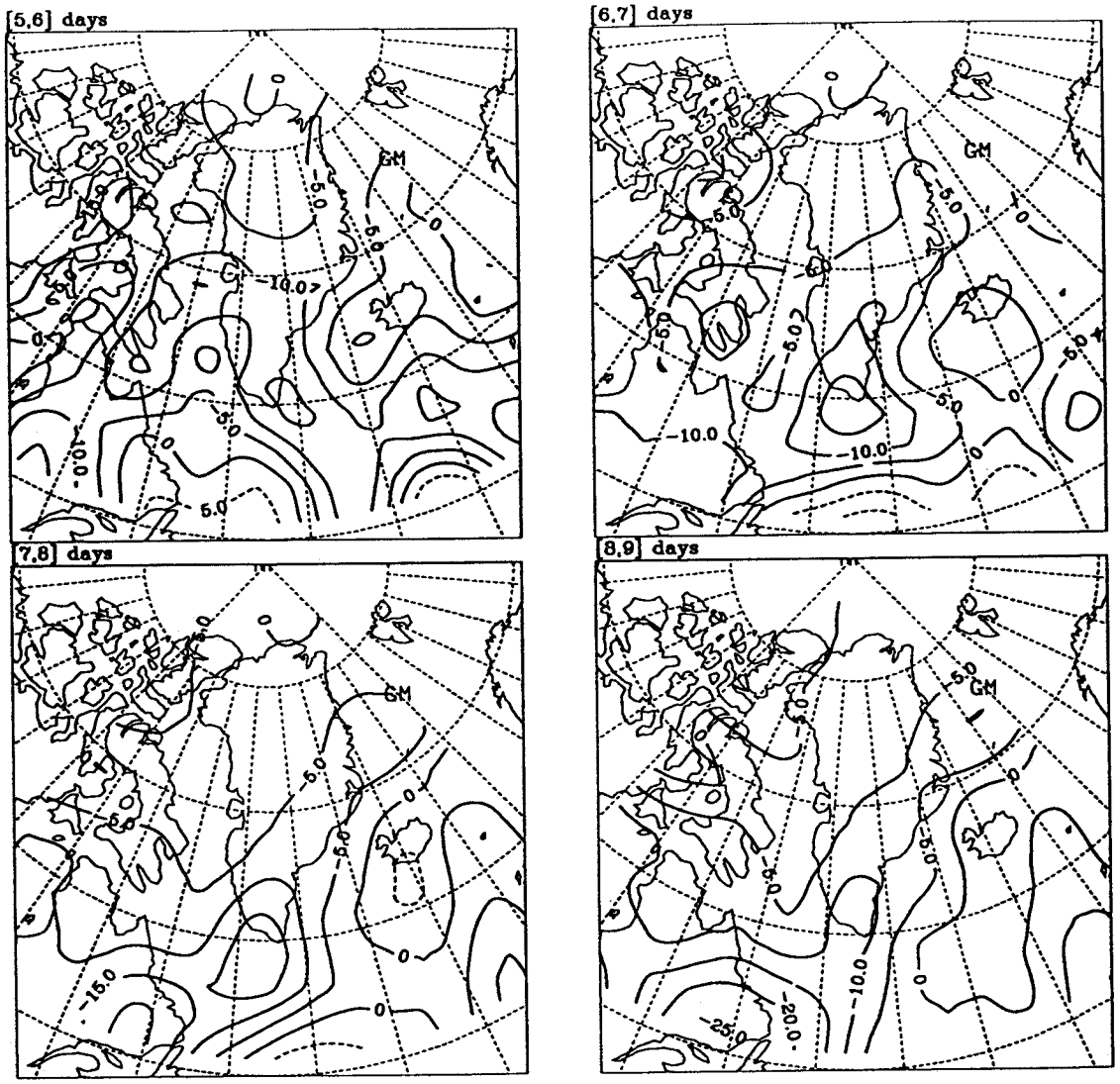
[5,6] days
GM
-5.0
-10.0
[6,7] days
GM
-5.0
-10.0
[7,8] days
GM
-5.0
-16.0
[8,9] days
GM
-5.0
-10.0
-20.0
-25.0

**Fig. 7.6**: (cont.)

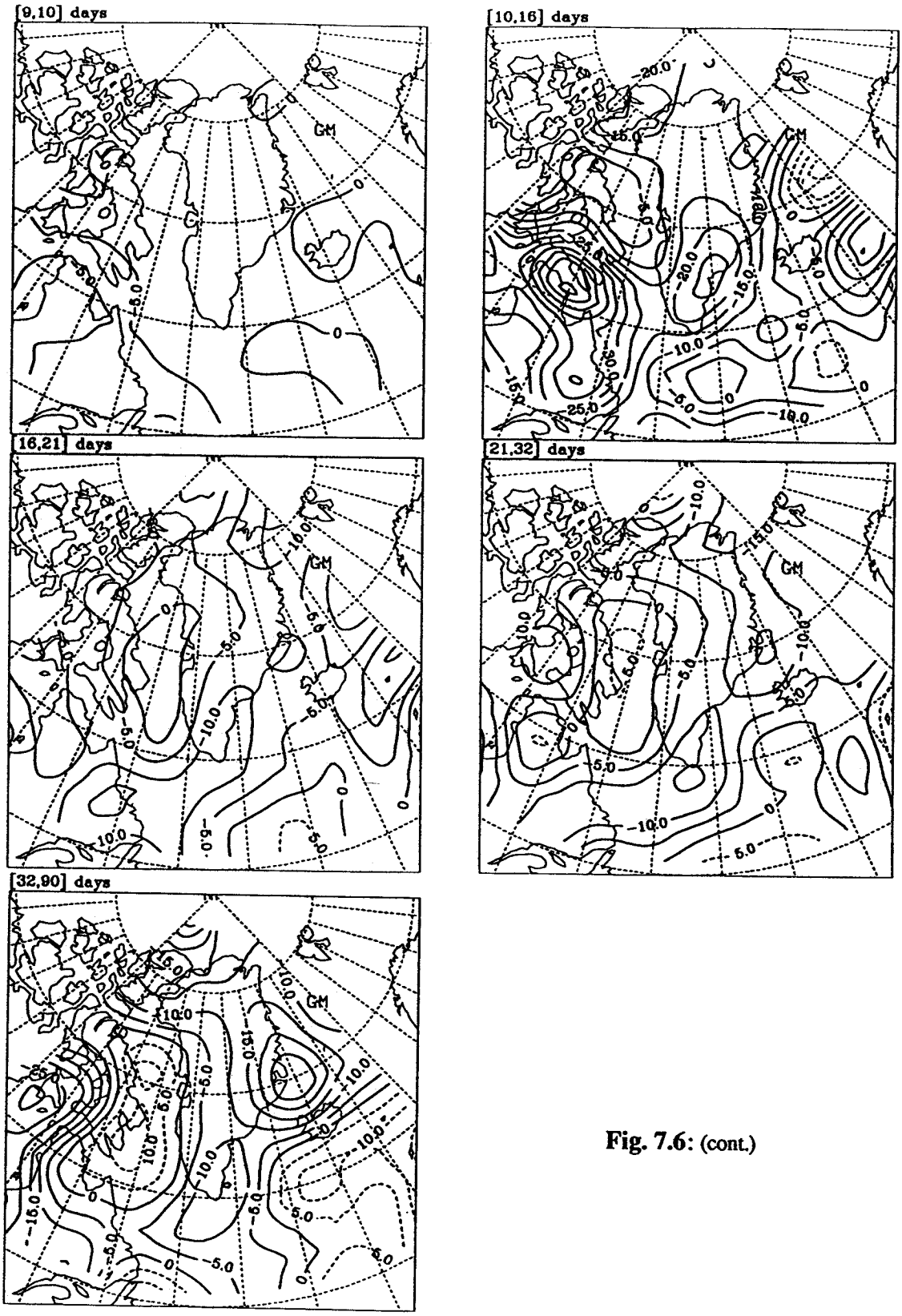


**Fig. 7.6:** (cont.)

In summer, the northward displacement of the storm track, as well as the appendix of the secondary track associated with the Arctic frontal zone, appears beautifully in the divergence distribution at high frequencies. The intensity of the convergence is about half that observed in winter. This is the consequence of, firstly, a general decrease in the cyclone frequency (compare Fig. 4a to Fig. 2a in Whittacker and Horn, 1984) and, secondly, a decrease of the intensity of the precipitation associated with a single low-pressure system (D. Grebner, pers. comm.). The monthly average daily precipitation can be computed using the monthly precipitation and the number of days with precipitation collected and published by Putnins (1970). A decrease of the average daily precipitation from winter to summer by about 30% is obtained for southern Greenland.

As was the case for the flux, the transition from the high-frequency range to the medium-frequency range, i.e., at a period of 6 days, is not as distinct in summer, with values of the convergence up to 10 to 20 mm season$^{-1}$ in the interval 7 days to 9 days. However, the transition is abrupt at 10 days. In the low-frequency range, the divergence zone in the eastern North Atlantic appears only at the lowest end of the spectrum, for periods longer than 32 days, and a second area of divergence is observed instead over Baffin Bay, that may be related to the persistence of high pressure systems in this area. Persistent anticyclones may prevent cyclones either from Davis Strait or from the western Canadian Arctic would to enter Baffin Bay.

For comparison with studies that use the time filters of Blackmon (1976), additional seasonal maps of the moisture flux divergence distribution for the intervals 1 days to 6 days, 6 days to 10 days, and 10 days to 90 days were prepared (Figs. 7.7 and 7.8). The divergence was calculated by summing up the contibutions from the single frequency intervals in each of the three ranges just defined. The maps are used to summarize the distribution in Greenland.

In winter, both the high-frequency and low-frequency transients contribute to the convergence mostly in eastern Greenland, the former with values decreasing from 75 mm season$^{-1}$ at the southern tip of Greenland to 25 mm season$^{-1}$ in northeastern Greenland, the latter by about 25 mm season$^{-1}$ all along the coast. In western Greenland, values never rise above 25 mm season$^{-1}$. At low frequencies, one can observe a dipolar structure with centre over Denmark Strait. This feature was mentioned in the discussion of the moisture flux. It is likely connected to a large export of moisture from the area south of Denmark Strait during blocking episodes.

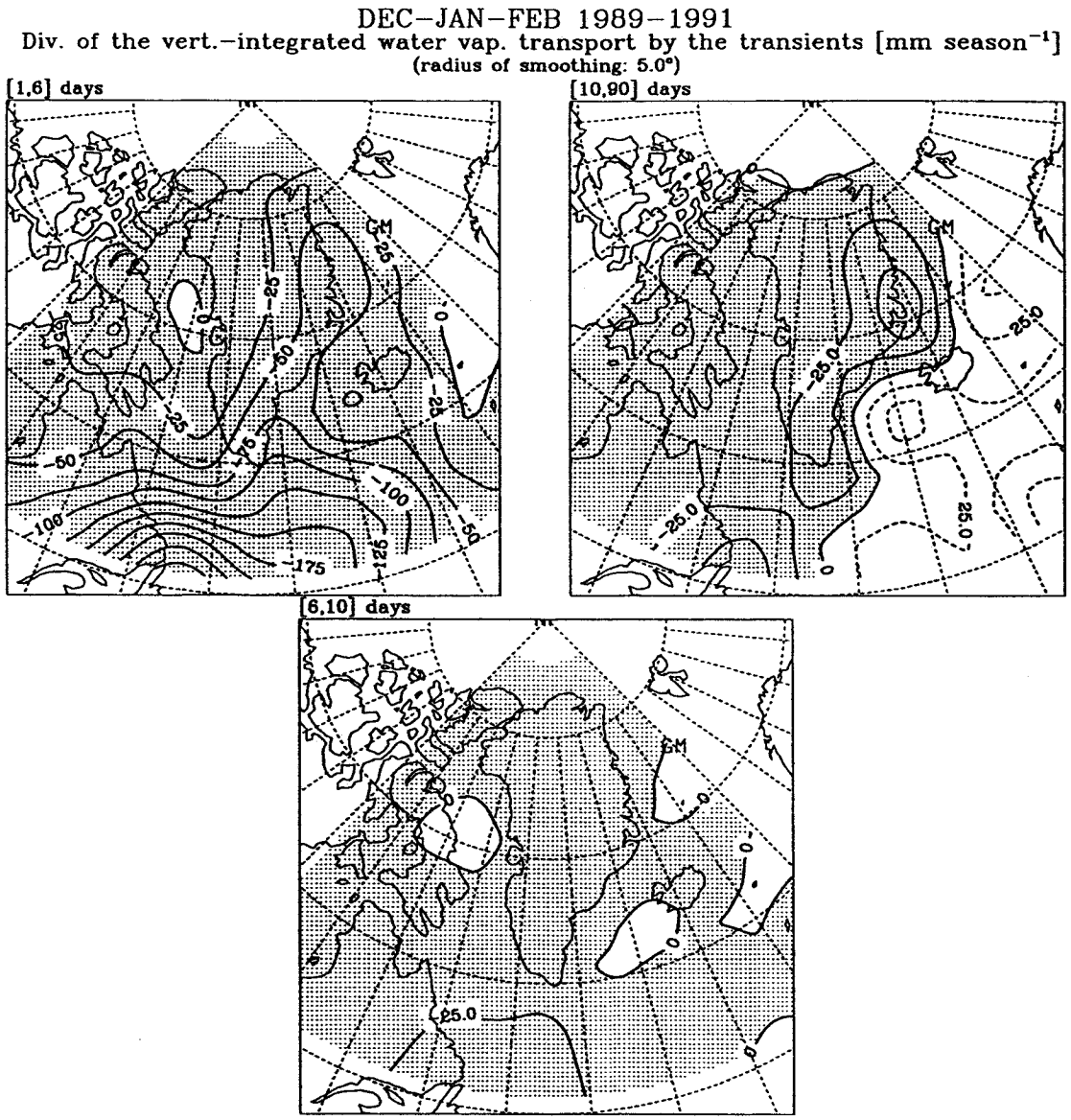


**Fig. 7.7**: Divergence of the spectral contributions to the eddy moisture flux in winter, for frequency intervals corresponding to [1,6] days (a), [6,10] days (b), and [10,90] days (c). Units are [mm season]$^{-1}$.

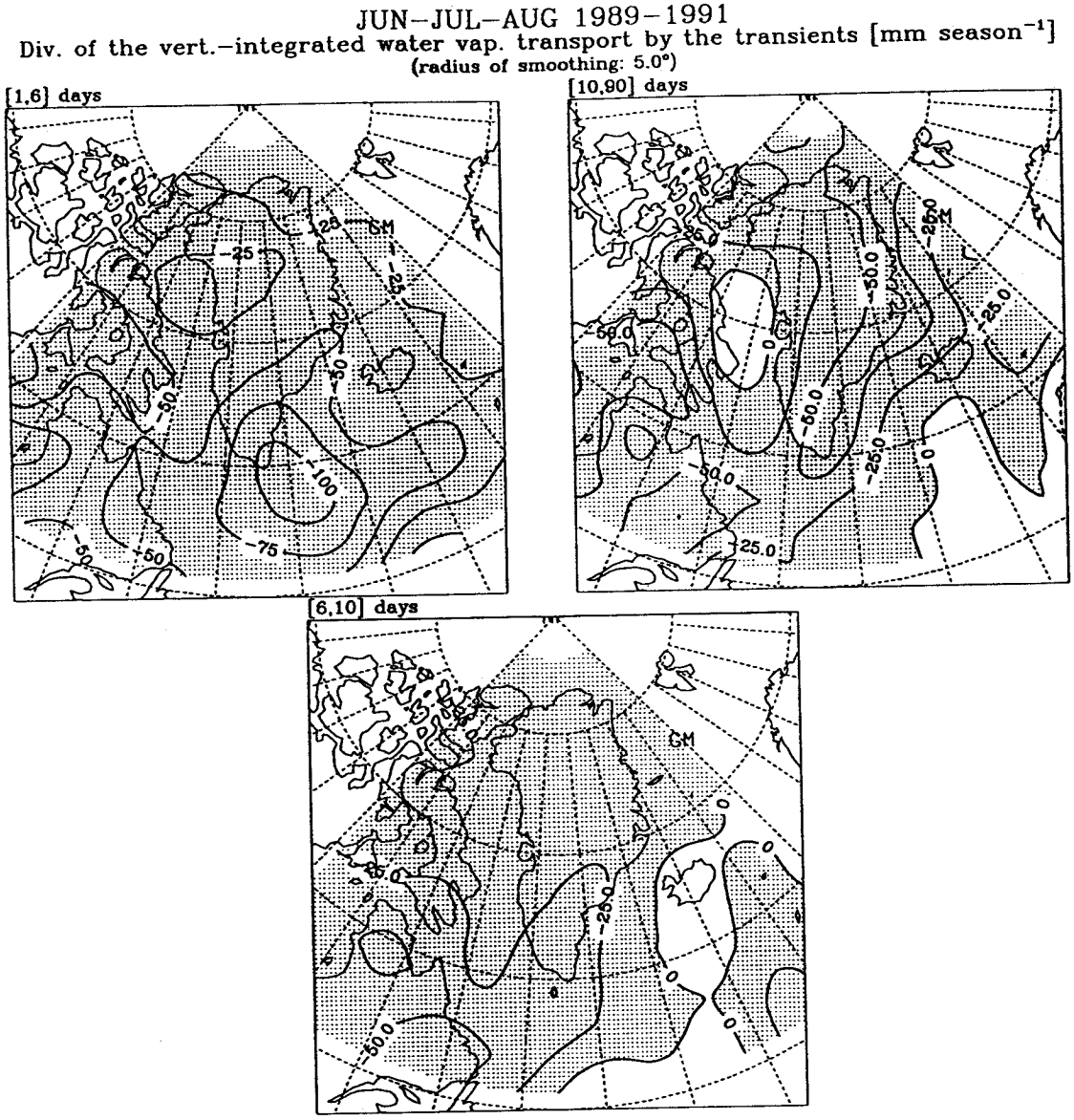


**Fig. 7.8**: Same as Fig. 7.7, but for summer.

In summer, the zonal gradients of the divergence by the high-frequency transients are not so large. This results in comparable meridional gradients along both the west and east coasts. The water vapour flux convergence varies between 100 mm season$^{-1}$ in the south to 25 mm season$^{-1}$ in the north. The contribution by the low-frequency transients, on the other hand, is more significant in eastern Greenland, with values that are about double as large as in winter, viz. 50 mm season$^{-1}$. Furthermore, the medium-frequency transients give a substantial contribution to the summer convergence, especially to the convergence over western Greenland.

## 7.2 Conditional sampling

An additional examination of the transient eddy flux and flux divergence is undertaken by conditionally resampling the transient eddy flux (see Chapter 2). In boundary layer studies, the technique is not new (see Rotach, 1991, and literature therein) and is used to break down the turbulent momentum and heat transfer statistically into events that may be of particular importance. In the present study it was applied to the transport of water vapour with some simplicistic preconceptions in mind. In particular the idea that the bulk of the transport is accomplished, in these latitudes, by travelling synoptic disturbances (see previous section) and that the structure of such disturbances corresponds to the classical description (Palmén and Newton, 1969). A very simplified view of developing synoptic disturbances is, in fact, that in which warm/moist air is advected northward east of the surface low, while cold/dry air is exported southward to lower latitudes in the rear of the system. From here the idea of separating the wet and dry spells. The additional condition upon the relative magnitude of the instantaneous event is an attempt to characterize the physical size of the systems. Consider a rotational system for which the cyclostrophic approximation holds (Holton, 1979). In this case, by assuming that the radial component of the pressure gradient is constant, the velocity becomes a function only of the radius of the system. For a zonal distribution of the moisture, the meridional transfer of moisture accomplished by the system is also only a function of the radius, i.e., of the size of the system. Large systems can realize (at the periphery) larger meridional velocities and therefore larger fluxes.

It is clear that the definition (2.6) through (2.9) presents some difficulties of interpretation. The definition of the relative size is a local one. Travelling disturbances are evolving systems, and their characteristics change as they move along their path. This means that a particular system may contribute to the wet (or dry) spells at some

locations but not at others down- or upstream. The definition is also local with regard to the vertical dimension. In practice however, the concentration of moisture in the lower troposphere should result in a vertical consistency of the analysis.

The flux for dry and wet spells at increasing relative size H is shown in Fig. 7.9 (winter season) and Fig. 7.10 (summer season). In winter, at the relative size H=0 (Fig. 7.9), dry and wet spells show a similar distribution. Because the dry spells are defined as those events for which the instantaneous departure of the specific humidity from its mean is negative, the moisture flux achieved by the dry spells has always the opposite direction as the wind deviation for these same events. Thus, the south-southeasterly flux by the dry spells observed in the North Atlantic implies in fact a southeastward transport of relatively (to the average) dry air. For H=0, the time fraction (not shown), which is simply the time integral of the indicator functions (2.7) and (2.9), shows that the dry spells occupy about 60% of the total time. This could mean that the dry spells are the sum of more frequent but slightly smaller single events than the wet spells. The symmetry between dry and wet spells breaks down with increasing relative size. Dry spells are naturally limited by the condition that the moisture cannot become negative, and it is therefore not surprising that the dry spells are important only at small relative sizes. At H=5, the dry spells are still significant (statistically) only in the eastern North Atlantic. In this sector, a southward transport of dry air is observed that is related to relatively large time fraction and directional constancy (not shown).

The decrease in the time fraction with increasing H is rapid for both dry and wet spells. At H=5, for example, it has already sunk to below 10% of the total time, while for larger H it is only of a few percentage points. Since for large H the average spells are effectively the sum of events of short duration, the very low time fraction is indicative of a large intermittency. The decrease in magnitude with increasing H of the wet spells is more rapid at the eastern end of the storm track than over Labrador, in Davis Strait and the Denmark Strait/Iceland area. The reason seems to be a smaller time fraction and a smaller directional constancy in the eastern North Atlantic (not shown).

At this point, it is also interesting to note that the behaviour of the wet spells for increasing H recalls the behaviour of the total (wet plus dry) eddy flux, in the low-frequency range, with decreasing frequency (see previous section). It appears, therefore, that in the eastern portion of the storm track, the bulk of the total eddy flux is caused by high-frequency transients and that the wet spells associated with these transients are of relatively small magnitude. On the other hand, large fluxes at low frequencies and large wet spells are rather found northward or northwestward of the main storm track and are supposed to be related to the north(west)ward shift of the track during blocking events.

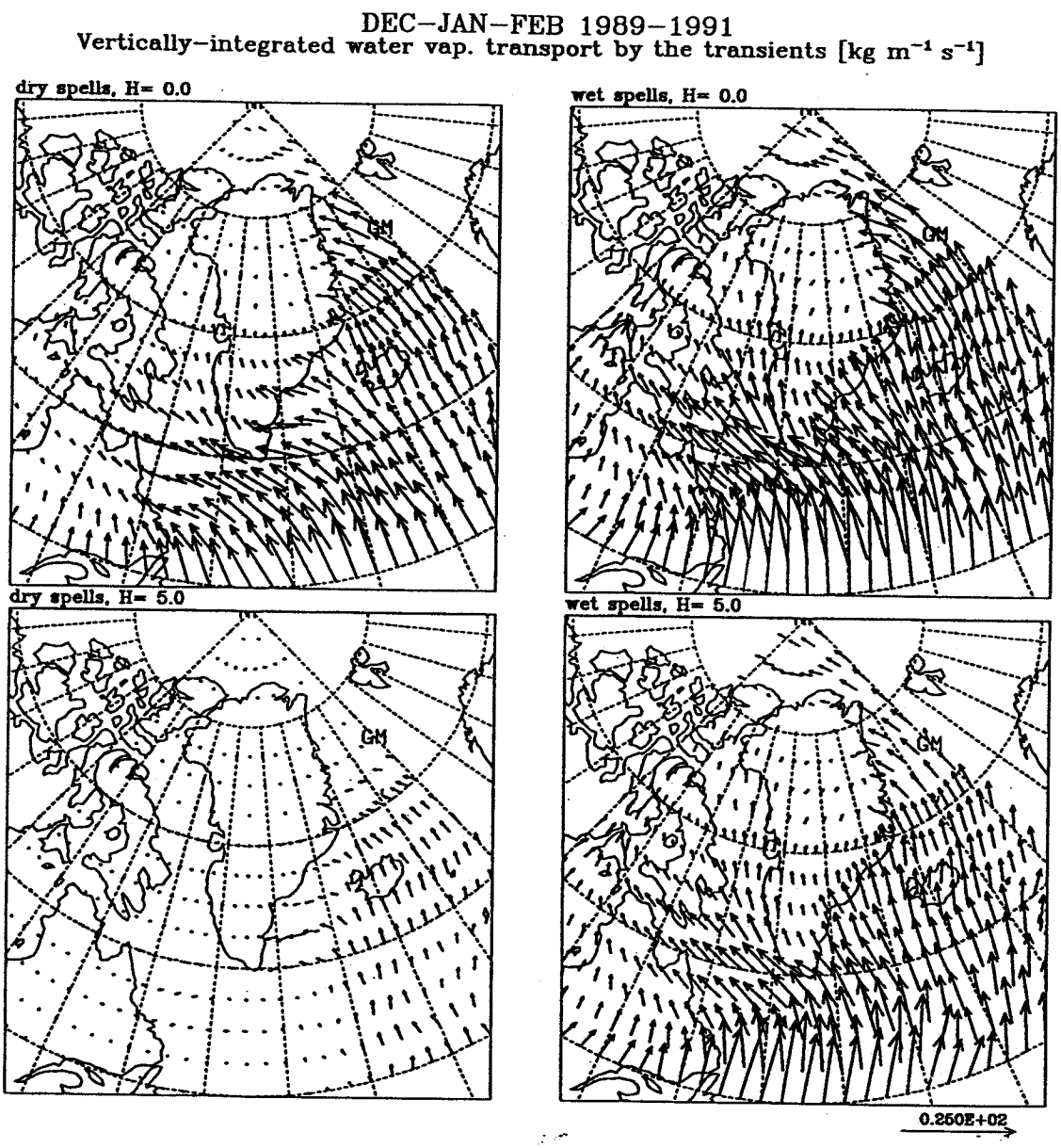


**Fig. 7.9**: Vertically-integrated water vapour transport by the transient eddies, separated into dry and wet spells (left and right column, respectively), and for increasing relative size H (top to bottom). Winter season. The scale is shown in the lower right corner. Units are [kg $m^{-1}$ $s^{-1}$].

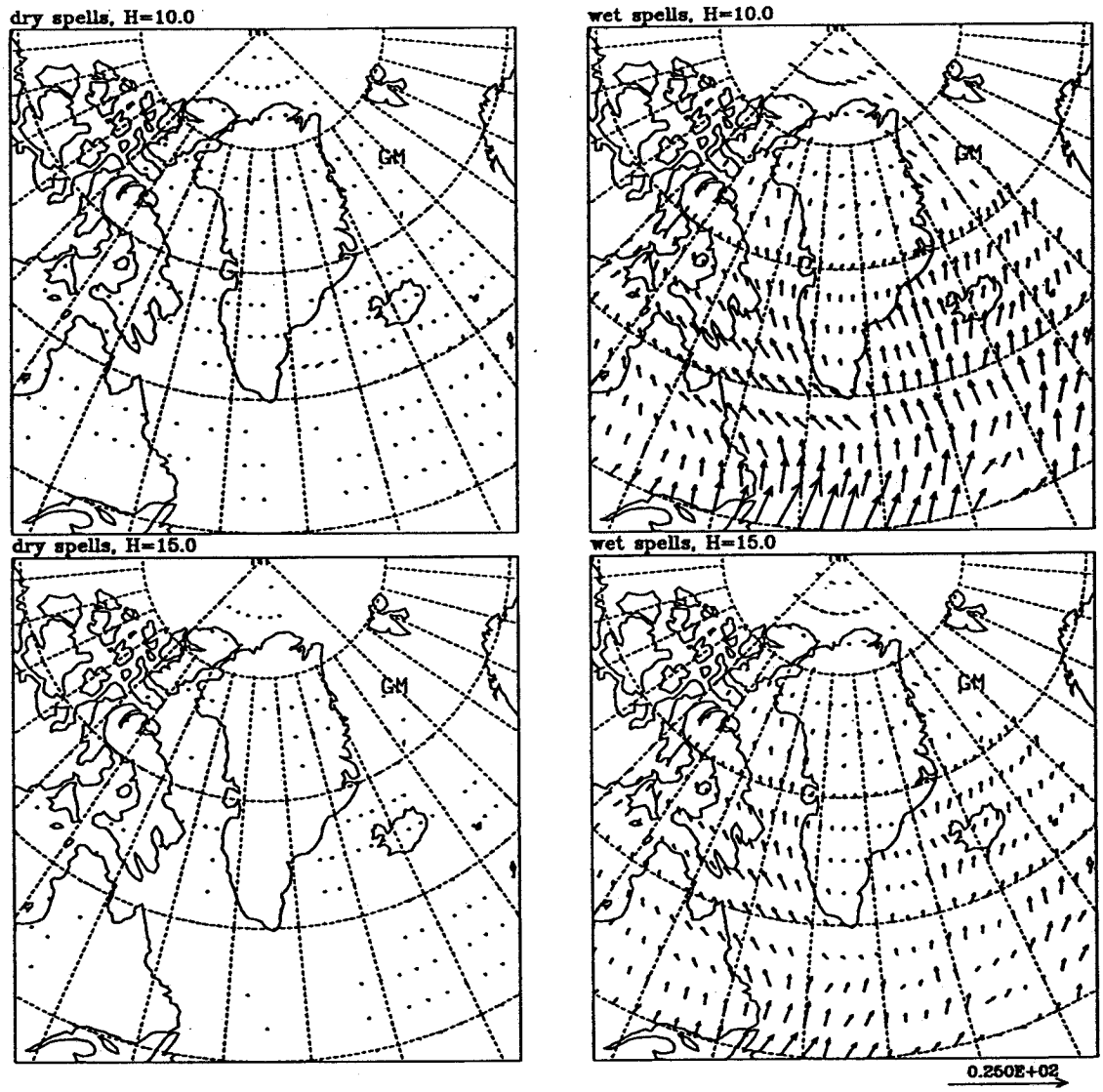
dry spells, H=10.0
wet spells, H=10.0
dry spells, H=15.0
wet spells, H=15.0
GM
0.250E+02

**Fig. 7.9:** (cont.)

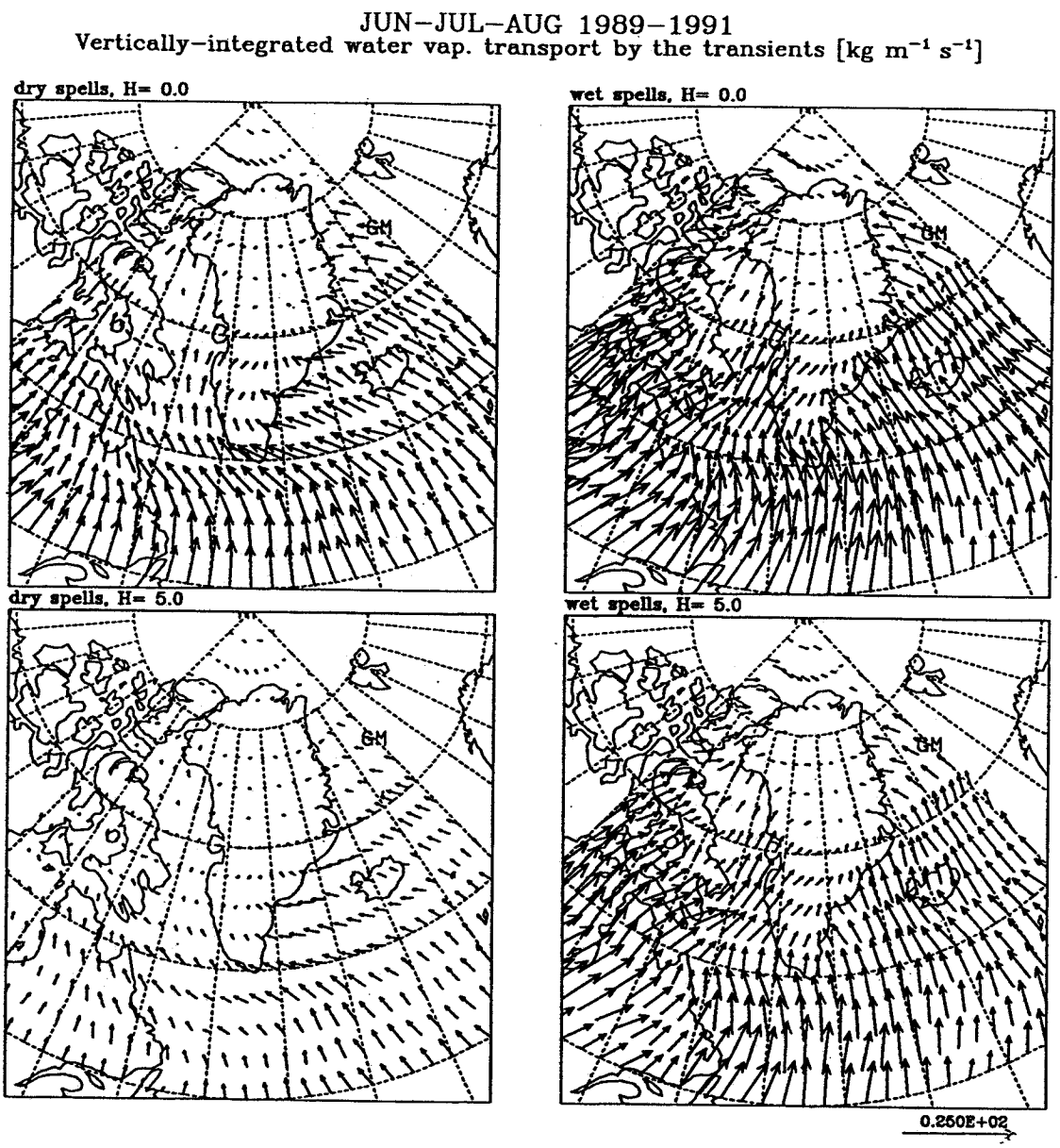


**Fig. 7.10**: Same as Fig. 7.9, but for summer.

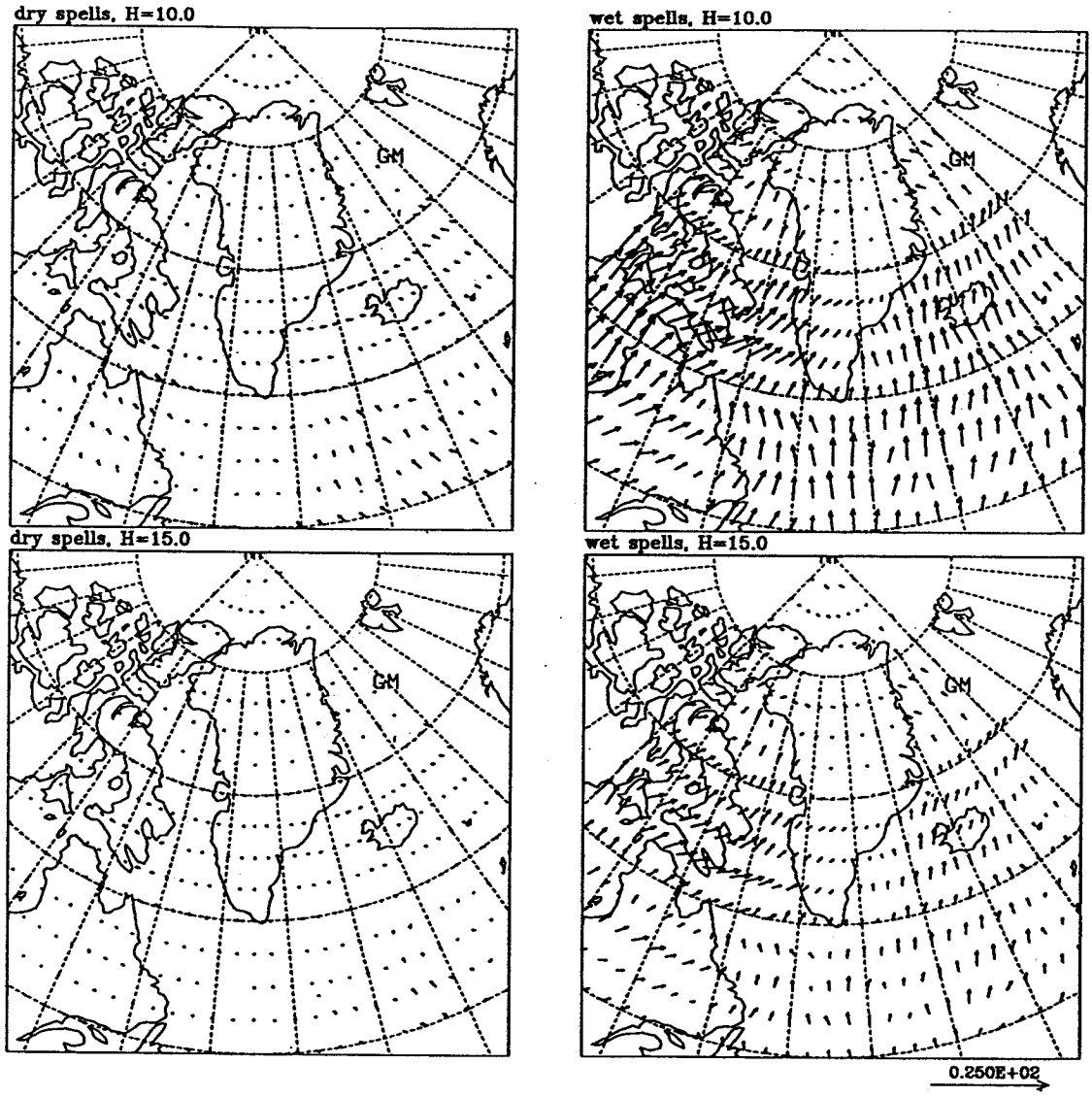
dry spells, H=10.0
wet spells, H=10.0
dry spells, H=15.0
wet spells, H=15.0
GM
0.250E+02

**Fig. 7.10**: (cont.)

In summer, the conditionally averaged dry spells are still significant at H=5. The reason is certainly the general increase in the average moisture content of the atmosphere, which allows larger negative departures. Also, at H=5 the time fraction is still around 15% of the total time (not shown). For the wet spells, the least decrease of magnitude with increasing relative size is seen in an area stretching from Foxe Bay eastward to the west coast of Greenland. This area is to the north of the Arctic frontal zone determined by Reed and Kunkel (1960). In relation to what was observed in the previous section, disturbances along the Arctic frontal zone show a distinctive behaviour from those along the main storm track.

The computation of the divergence of the conditionally sampled fluxes yields the following picture (Figs. 7.11 and 7.12). In winter, and for the longitudes west of 20°W, the contribution of the dry spells to the total eddy flux convergence, i.e., the contribution at H=0, is only half that of the wet spells. However, as a general rule, it can be stated that the net import of moisture into high latitudes is realized in a substantial way by a net export of drier air from high to lower latitudes. Over the eastern North Atlantic, both the wet and dry spells are divergent by the same amount. With increasing H, the contribution from the dry spells loses significance, whereas for the wet spells two areas of divergence appear. The first is seen in the eastern North Atlantic; the second centred at the southwest coast of Greenland. The second area corresponds to an area of large evaporation (Walmsley, 1966). The reason for the large divergence is seen in Fig. 7.9, which shows a consistent flux into Davis Strait over all sizes of H. Penetration of synoptic disturbances into Davis Strait and Baffin Bay is probably not very frequent in winter and seems to occur only when the disturbances are well developed. On their way to Baffin Bay, moisture is supplied to these disturbances by evaporation from the open sea surface along the southwestern coast of Greenland (Parkinson et al, 1977). It is certainly not necessary here to stress the importance of the West Greenland Current in mantaining favourable conditions along the western coast of Greenland.

In summer, the dry spells display divergence in Baffin Bay at H=0. For a larger H, this zone expands southward to include Davis Strait and the Labrador Sea. This area of divergence is coincident with the area of divergence observed at the low-frequency range in the previous section (Fig.7.6). If the latter is explained in terms of persisting anticyclones, then the former may be understood as arising from the import of dry air in the middle and upper troposphere and subsidence in the core of the anticyclone.

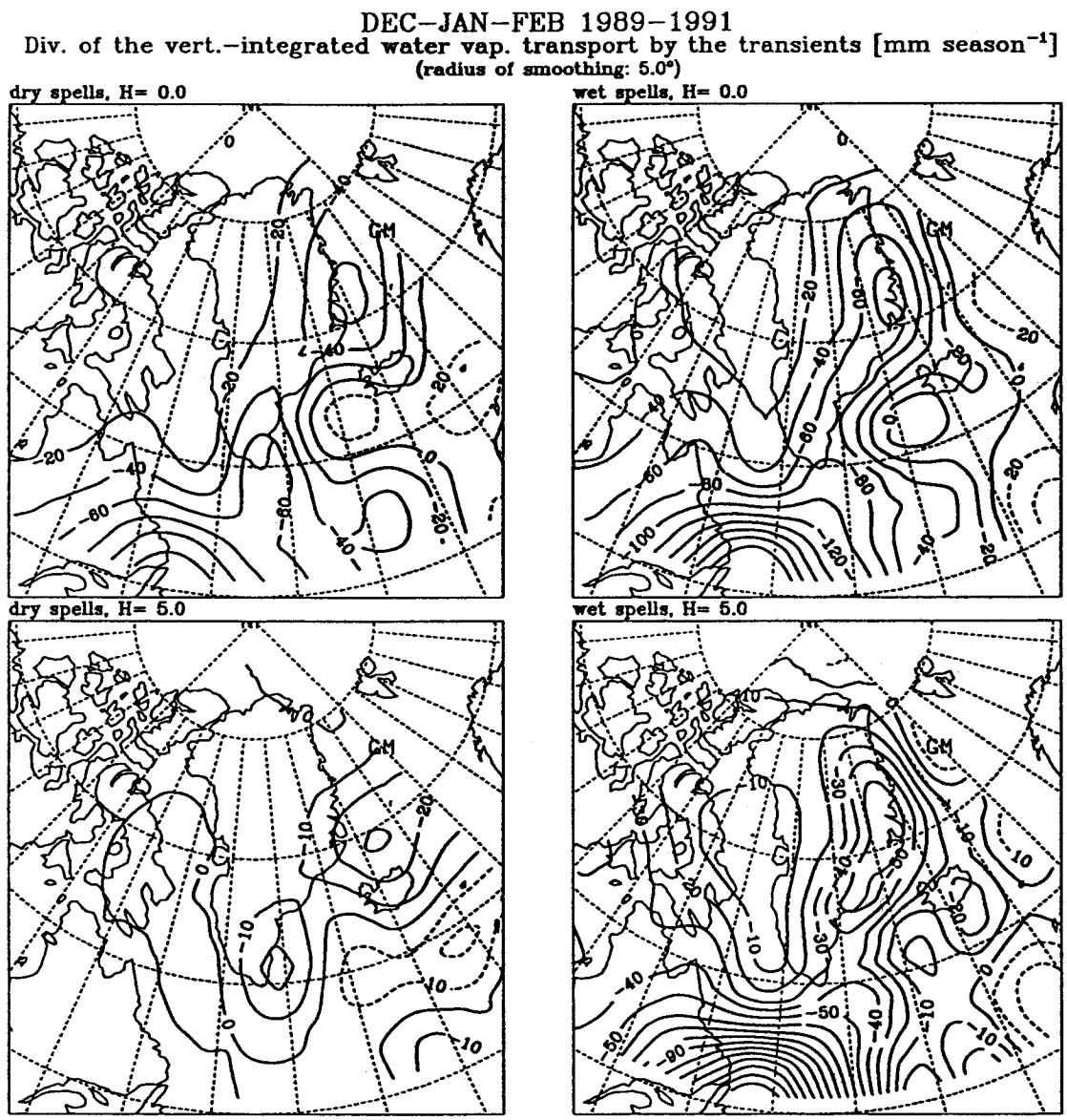


**Fig. 7.11**: Divergence of the vertically-integrated eddy flux, for dry and wet spells (left and right column, respectively), and for increasing relative size H (top to bottom). Winter season. Units are [mm season$^{-1}$]. Note that the interval is 20 mm season$^{-1}$ at H=0, 10 mm season$^{-1}$ at H=5 and H=10, and 5 mm season$^{-1}$ at H=15.

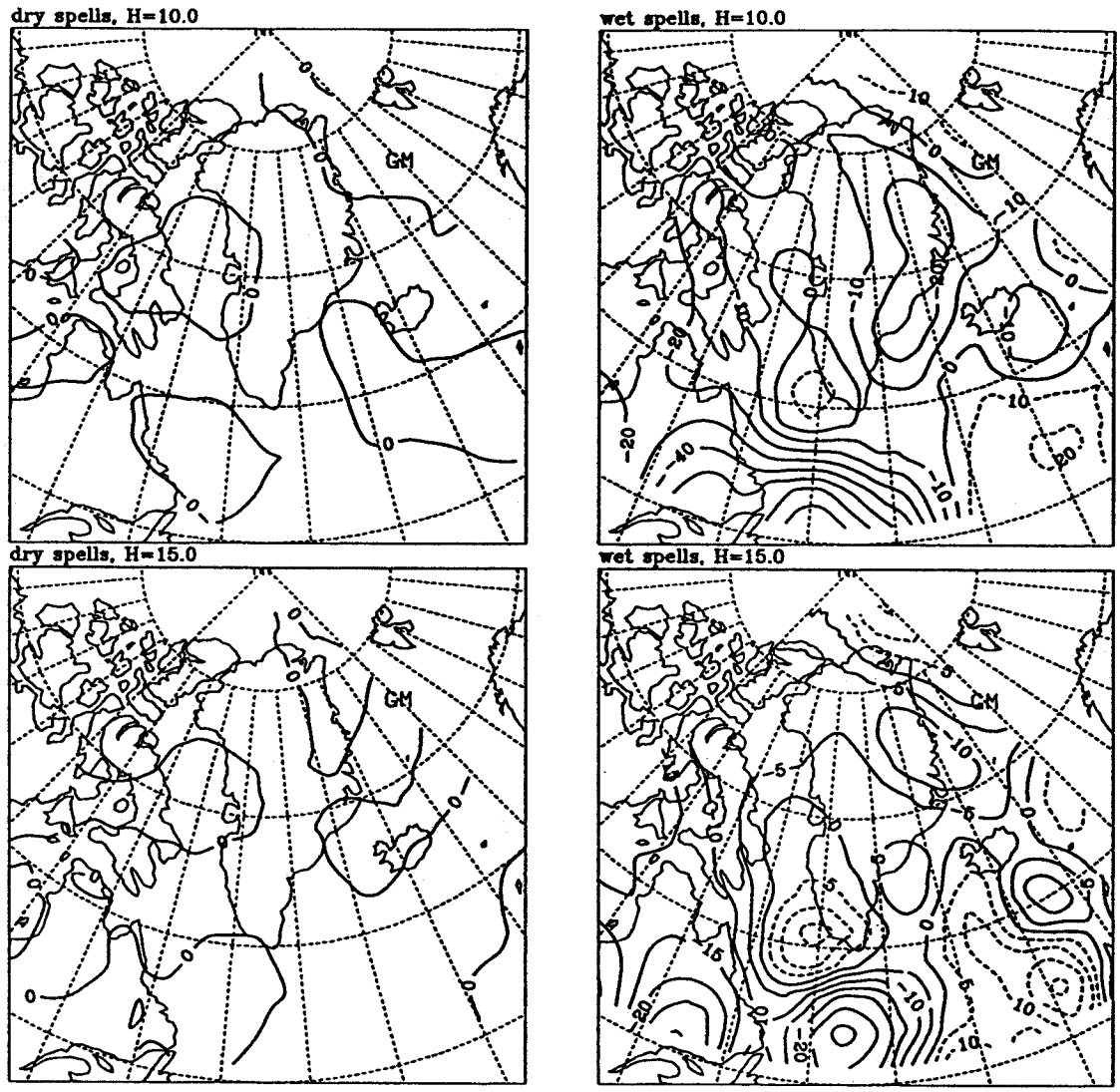
dry spells, H=10.0
wet spells, H=10.0
dry spells, H=15.0
wet spells, H=15.0
GM

**Fig. 7.11**: (cont.)

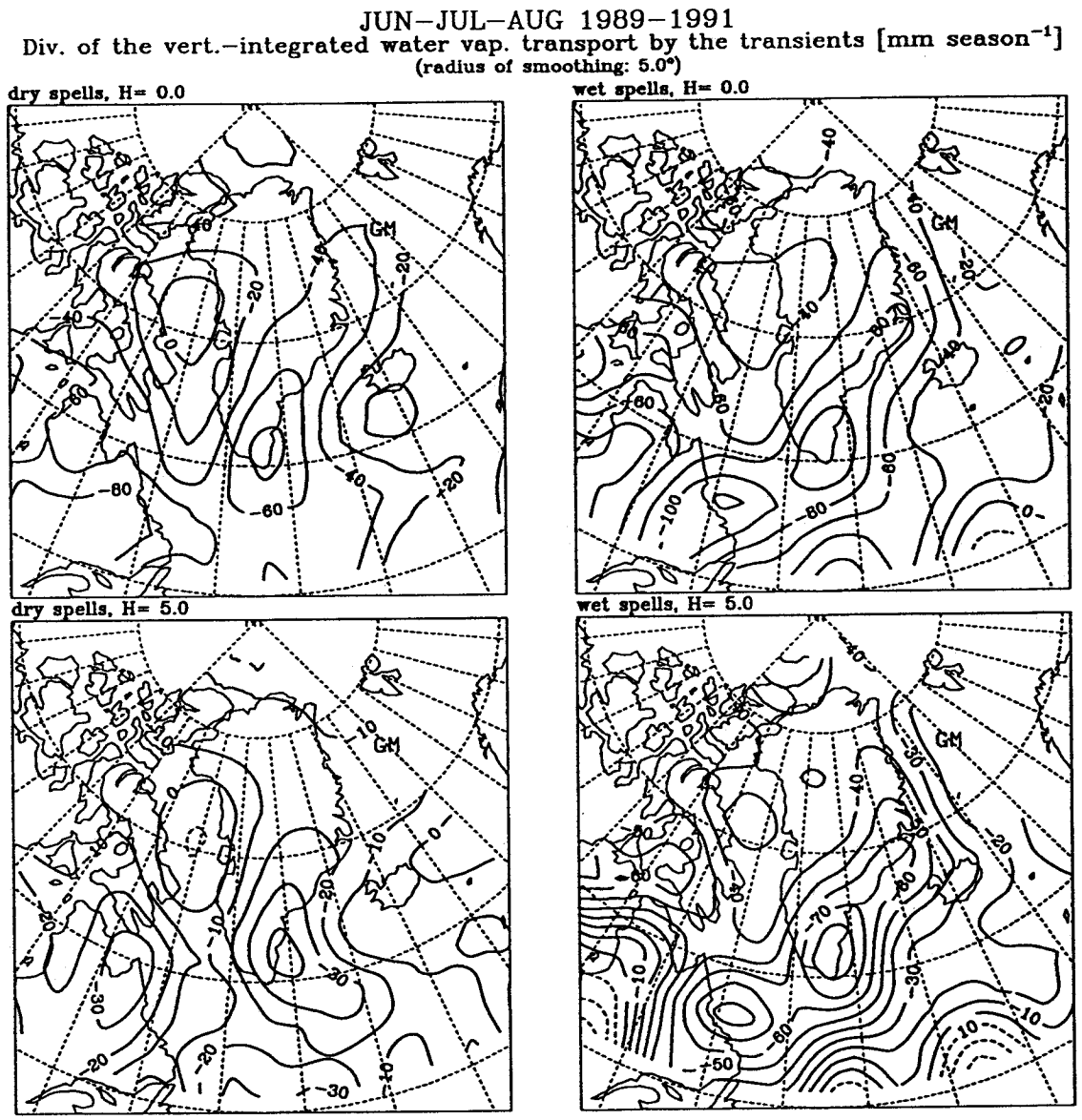


**Fig. 7.12**: Same as Fig 7.11, but for summer.

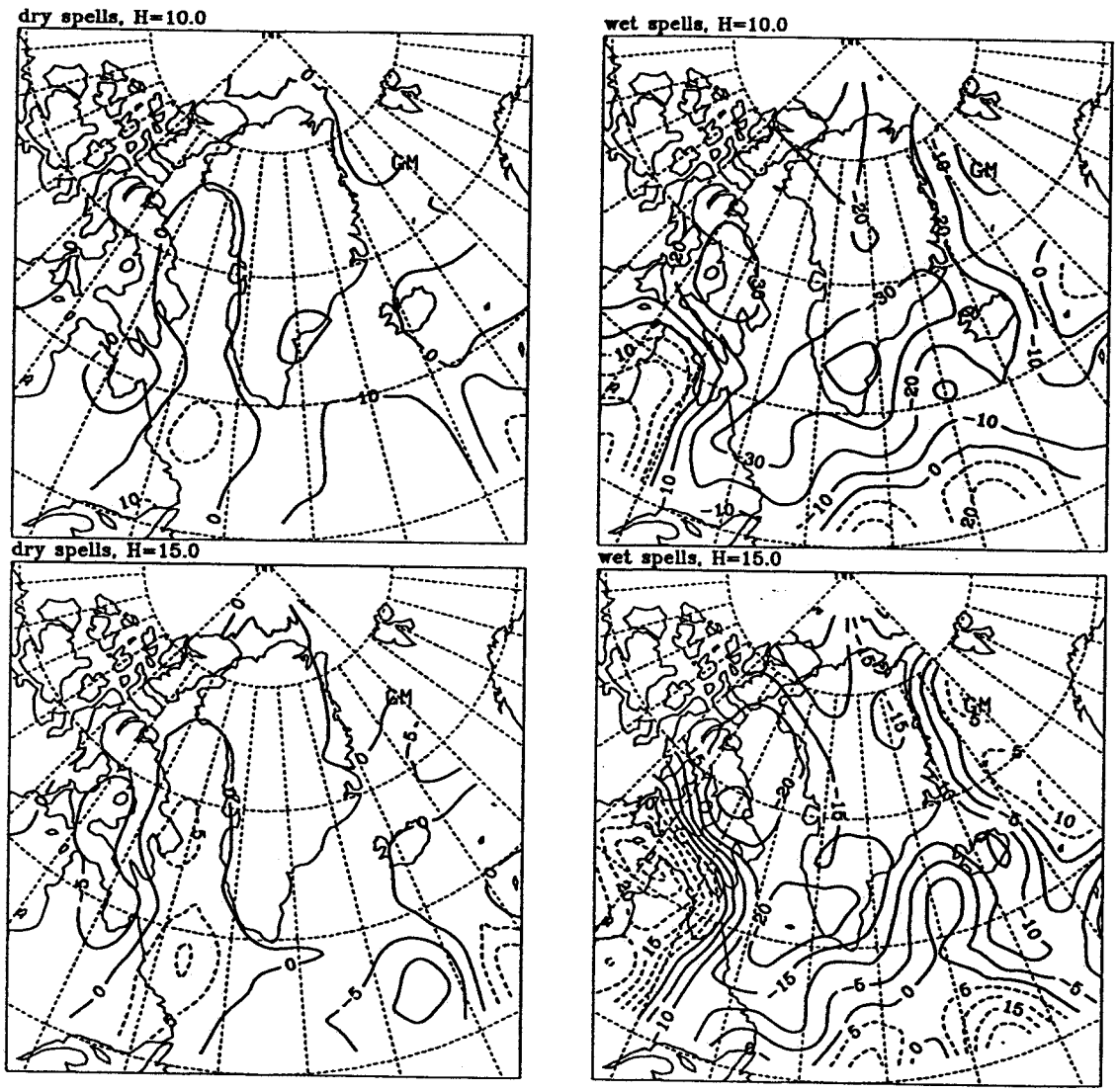
dry spells, H=10.0
wet spells, H=10.0
dry spells, H=15.0
wet spells, H=15.0
GM

**Fig. 7.12:** (cont.)

The divergence distribution for the wet spells at H=0 and H=5 looks very much the same as the distribution of the total divergence of the transient eddy moisture flux, although at H=5, and then at H=10, three centres of positive divergence develop: the first in the Hudson Bay/Labrador area; the second in the North Atlantic, at 50°N and 25°W; the third in the Norwegian and Greenland Sea. The divergence in the Hudson Bay/Labrador area increases in absolute with increasing relative size H. As was the case for the divergence core in winter at the southwest coast of Greenland, here also there is a concomitance of large divergence at large relative size and large evaporation. The parallelism may be fortuitous, but, by considering the maps of the flux (Figs. 7.9 and 7.10), it is seen that there is a systematic large northward flux by the wet spells just to the north of these areas. If it is assumed that such large wet spells arise as a consequence of very large moisture departures from the average (not proven in the present study), then a possible triggering mechanism can be suggested in which, for example, extremely large evaporation rates produce a surplus of moisture that is exported by travelling disturbances.

Seite Leer /
Blank leaf

# 8 SUMMARY AND CONCLUSIONS

In this work, the moisture flux, the flux divergence and the general atmospheric conditions have been investigated for the Greenland area using the uninitialized analyses produced routinely by the European Centre for Medium-Range Weather Forecasts (ECMWF) for the years 1989, 1990 and 1991.

In the first part of the thesis the limits of the analyses were discussed. It was shown that the artificial small scale fluctuations due to the discrete nature of the spatial grid can be efficiently eliminated from the moisture flux divergence by application of a simple spatial filter. A better alternative would be to perform the calculations in the spectral domain and on model levels and to interpolate only the results, if required.

At the ECMWF, the analyses are first derived on model levels and only interpolated to pressure levels in a second step. The interpolation introduces a mass imbalance in the archived wind field. It could be demonstrated by scale analysis and through the numerical implementation of a correction algorithm, that this mass imbalance affects the moisture flux divergence and the divergence distribution only marginally. The error that arises from the mass imbalance is of the same order as that caused by the choice of a sampling interval of 12 hours, compared to a sampling interval of 6 hours.

To verify the accuracy of the computations, the calculated annual moisture flux convergence was compared to independent estimates of the annual precipitation, supplemented for the North Atlantic with independent estimates of the annual evaporation. The comparison indicates that the large-scale features of the distribution of the difference between the evaporation and the precipitation are reproduced well by the present analysis. Quantitatively, the areally averaged moisture flux divergence for all of Greenland is very close to the areally averaged precipitation. For several coastal stations in the study area, the moisture flux convergence and measured precipitation agree well even on a monthly basis, a result that opens a concrete prospective for a discussion of the annual cycle of the precipitation based on the aerological method.

In the second part of the thesis, attention was focused on the seasonal characteristics of the moisture flux and flux divergence. The bulk of the moisture transport is accomplished by the mean circulation. The rotational character of the mean motion and its associated moisture flux explains why the contribution of the transient eddies to the

moisture flux divergence is of primary importance. The effect of the topography on the mean circulation is particularly evident in Greenland, with a strong moisture flux convergence along the western slopes and a large moisture flux divergence in northeastern Greenland. The eddy activity is concentrated along the major storm tracks and along the eastern coast of Greenland, which is known as an area of high baroclinicity. In eastern Greenland, the belt of strong convergence of the eddy flux is usually observed east of the confluence zone. The convergence could be partially enhanced by orographic lifting at the coast. In this sense, the role of the topography is twofold.

The spectral analysis of the eddy moisture flux and flux divergence has confirmed that, as for other fluxes in mid- to high latitudes, the most important contributions are those by the synoptic disturbances, with periods between two and six days, and those of the low-frequency eddies, with periods larger than ten days. However, the contribution of the low-frequency eddies should be understood rather as a low-frequency modulation of high-frequency transients. Medium-frequency disturbances are not at all important in winter, but make a substantial contribution to the moisture flux convergence in summer.

Resampling of the eddy flux, to account for the sign of the moisture deviation from the time average, has shown that a significant percentage of the total northward transport of moisture by the eddies is realized as a southward transport of dry air. This southward flux of dry air is the sum of many small instantaneous fluxes, whereas large and sporadic wet spells play an important role as carriers of moisture from the mid- to high latitudes. In particular, large wet spells seem responsible for the export of moisture from areas of large evaporation.

The present study has shown the potentiality of the ECMWF analyses for a statistical diagnosis of processes, in this case the moisture flux, but also for the description of the meteorological conditions in areas of difficult access. In this context, it is hoped that the present study makes a contribution to the statistical description of some climatic elements in the Greenland area. However, there are aspects of the atmospheric circulation and of the climate that cannot yet be investigated using the ECMWF analyses. In particular, a more consistent data set is required for the examination of the interannual variability.

## REFERENCES


Ambach, W., 1963: Untersuchungen zum Energieumsatz in der Ablationszone des Grönländischen Inlandeises. *Meddelelser om Grønland*, **174**. C.A. Reitzels Forlag, København. 311 pp.

Akima, H., 1978: A method of bivariate interpolation and smooth surface fitting for irregularly distributed data points. *ACM Transactions on Math. Software*, **4**, 148-159.

Alestalo, M., 1981: The energy budget of the earth-atmosphere system in Europe. *Tellus*, **33**, 360-371.

Alestalo, M. and E. Holopainen, 1980: Atmospheric energy fluxes over Europe. *Tellus*, **32**, 500-510.

Barry, R.G. and G.N. Kiladis, 1982: Climatic characteristics of Greenland. In: Radok, U. et al. (Eds.): *Climatic and Physical Characteristics of the Greenland Ice Sheet*. CIRES, University of Colorado, Boulder. 7-33.

Baumgartner, A. and E. Reichel, 1975: *Die Weltwasserbilanz*. R. Oldenburg Verlag, München. 179 pp.

Bengtsson, L. et al., 1982: FGGE 4-dimensional data assimilation at ECMWF. *Bull. Am. Met. Soc.*, **63**, 29-43.

Blackmon, M.L., 1976: A climatological spectral study of the 500 mb geopotential height of the Northern Hemisphere. *J. Atmos. Sci.*, **33**, 1607-1623.

Blackmon, M.L., J. Wallace, N.-C. Lau and S. Mullen, 1977: An observational study of the Northern Hemisphere wintertime circulation. *J. Atmos. Sci.*, **34**, 1040-1053.

Bradley, R.S. and J.K. Eischeid, 1985: Aspects of the precipitation climatology of the Canadian High Arctic. In: Bradley, R.S. (Ed.): *Glacial Geologic and Glacio-Climatic Studies in the Canadian High Arctic*. Contribution No. 49, Dept. of Geology & Geography, University of Massachussets at Amherst, 250-271.

Broccoli, A.J. and S. Manabe, 1992: The effects of orography on midlatitude Northern Hemisphere dry climates. *J. Climate*, **5**, 1181-1201.

Bronstein, I.N. and K.A. Semendjajew, 1985: *Taschenbuch der Mathematik*. Verlag Harri Deutsch, Thun, 840 pp.

Buck, A., 1981: New equations for computing vapor pressure and enhancement factor. *J. Applied Meteor.*, **20**, 1527-1532.

Church, J.E., 1941: Climate and evaporation in Alpine and Arctic zones. In: Hobbs, W.H. (Ed.): *Reports of the Greenland Expeditions of the University of Michigan. Part II: Meteorology, Physiography, and Botany. I: Meteorological Studies*. The University of Michigan Press, Ann Arbor. 7-45.

Dutton, J.A., 1976: *An Introduction to the Theory of Atmospheric Motion.* McGraw-Hill Company, New York, 617 pp.

Dorsey, H.G., 1945: Some meteorological aspects of the Greenland Ice Cap. *J. Met.*, 2, 135-142.

Ehrendorfer, M., M. Hantel and Y. Wang: A variational modification algorithm for three-dimensional mass flux non-divergence. Accepted for publication in *Quart. J. Roy. Met. Soc.*

European Centre for Medium-Range Weather Forecasts, 1992a: Research Manual 1. *ECMWF Data Assimilation.* 3rd Ed. ECMWF, Reading.

European Centre for Medium-Range Weather Forecasts, 1992b: *The Description of the ECMWF/WRCP Level III-A Global Atmospheric Data Archive.* Technical Attachment. ECMWF, Reading. 48 pp.

Forrer, J., 1992: *Prozesse in der stabilen Grenzschicht über dem Grönländischen Eisschild.* Diplomarbeit. Geogr. Inst. ETH, 52 pp.

Fortelius, C. and E. Holopainen, 1990: Comparison of energy source estimates derived from atmospheric circulation data with satellite measurements of net radiation. *J. Climate*, **3**, 646-660.

Greuell, W., 1992: Numerical Modeling of the Energy Balance and the Englacial Temperature at the ETH Camp, West Greenland. *Zürcher Geographische Schriften*, **51**, 81 pp.

Hamilton, R.A:, 1958a: The meteorology of North Greenland during the midsummer period. *Quart. J. Roy. Met. Soc.*, **84**, 142-158.

Hamilton, R.A:, 1958b: The meteorology of North Greenland during the midwinter period. *Quart. J. Roy. Met. Soc.*, **84**, 355-374.

Hare, F.K., 1968: The Arctic. *Quart. J. Roy. Met. Soc.*, **94**, 439-459.

Hartmann, D., 1974: Time spectral analysis of mid-latitude disturbances. *Mon. Wea. Rev.*, **102**, 348-362.

Held, I.M., 1983: Stationary and quasi-stationary eddies in the extratropical troposphere: theory. In: Hoskins, B. and R. Pearce: *Large-Scale Dynamical Processes in the Atmosphere.* Academic Press, London, 127-168.

Hoffmann, G. and J. Pelz, 1984: Näherungsgleichungen verschiedenen Genauigkeitsgrades für die pseudopotentielle Temperatur. *Beilage zur Berliner Wetterkarten*, **59/84**, SO 18/84. Meteorologisches Institut der Freien Universität Berlin. 6 pp.

Holopainen, E.O., 1983: Transient eddies in mid-latitudes: observations and interpretation. In: Hoskins., B. and R. Pearce (Eds.): *Large-Scale Processes in the Atmosphere.* Academic Press, London. 201-233.

Holton, J.R., 1979: *An Introduction to Dynamic Meteorology.* Academic Press, New York, 391 pp.

Hoskins, B.J. and P.J. Valdes, 1990: On the existence of storm-tracks. *J. Atmos. Sci.*, **47**, 1854-1864.

Hoskins et al., 1989: *Diagnostics of the Global Atmospheric Circulation Based on ECMWF Analyses 1979-1989.* World Climate Research Programme, WCRP 27, WMO/TD No. 326, World Met. Organization, 217 pp.

Hutchings, J.W., 1957: Water-vapour flux and flux-divergence over southern England: summer 1954. Hamilton, R.A:, 1958b: The meteorology of North Greenland during the midsummer period. *Quart. J. Roy. Met. Soc.*, **83**, 30-48.

Isemer, H.J. and L. Hasse, 1987: *The Bunker Climate Atlas of the North Atlantic Ocean. Vol. 2: Air-Sea Interactions.* Springer Verlag, Berlin, 252 pp.

Jaeger, L., 1976: *Monatskarten des Niederschlages für die ganze Erde.* Berichte des Deutschen Wetterdienstes, Nr. 139. Offenbach. 38 pp and 13 tables.

Jarraud, M., A.J. Simmons and M. Kanamitsu, 1988: Sensitivity of medium range weather forecasts to the use of an envelope orography. *Quart. J. Roy. Met. Soc.*, **114**, 989-1025.

Julian, P.R., 1971: Some aspects of variance spectra of synoptic scale tropospheric wind components in midlatitudes and in the tropics. *Mon. Wea. Rev.*, **99**, 954-965. *J. Atmos. Sci.*, **27**, 359-375.

Kaimal, J.C., 1988: T*he Atmospheric Boundary Layer - Its Structure and Measurement.* IITM Visiting Professorship Program. Lecture Notes. Indian Institute of Tropical Meteorology, Shivajinagar.

Kao, S.-K. and L.L. Weddell, 1970: The kinetic energy of the large-scale atmospheric motion in wavenumber-frequency space. I: Northern Hemisphere.

Keen, R., 1982: Statistical-dynamical model of accumulation on the Greenland Ice Sheet. In: Radok, U. et al. (Eds.): *Climatic and Physical Characteristics of the Greenland Ice Sheet.* CIRES, University of Colorado, Boulder. A1.1-A1.11.

Klinker, E., 1993: Aspects of Large Scale Modelling. In: Raschke, E. and D. Jacob (Eds.): *Energy and Water Cycles in the Climate System.* NATO ASI Series, Series I: Global Environmental Change, Vol. 5, 42-67.

Lau, N.-C., 1979: The structure and energetics of transient disturbances in the Northern Hemisphere wintertime circulation. *J. Atmos. Sci.*, **36**, 982-995.

Legates, D.R. and C.J. Willmott, 1990: Mean seasonal and spatial variability in gauge-corrected, global precipitation. *Int. J. Climatology*, **10**, 111-127.

Lindzen, R.S., 1991: *Dynamics in Atmospheric Physics*. Cambridge University Press, Cambridge, 310 pp.

Loewe, F., 1935: Klima des Grönländischen Inlandeises. In: Köppen, W. and R. Geiger (Eds.): *Handbuch der Klimatologie*. Band II, Teil K, III: Klima des Kanadischen Archipels und Grönlands. Berlin, Borntrarger, K67-K101.

Lynch, P., 1988: Deducing the wind from the vorticity and divergence. *Mon. Wea. Rev.*, **116**, 86-93.

Masuda, K., 1988: Meridional heat transport by the atmosphere and the ocean: analysis of FGGE data. *Tellus*, **40A**, 285-302.

Matsuyama, H., 1992: The water budget in the Amazon River Basin during the FGGE period. *J. Meteor. Soc. Japan*, **70**, 1071-1084.

Michaud, R. and J. Derome, 1991: On the mean meridional transport of energy in the atmosphere and oceans as derived from six years of ECMWF analyses. *Tellus*, **43A**, 1-14.

Müller, F. and N. Roskin-Sharlin, 1967: *A High Arctic Climate Study on Axel Heiberg Island, Canadian Arctic Archipelago - Summer 1961*. Part 1: General Meteorology. Axel Heiberg Island Research Reports, Meteorology No. 3, McGill University, Montreal. 82 pp.

Namias, J., 1958: Synoptic and climatological problems associated with the general circulation of the Arctic. *Trans. Am. Geophys. Union*, **39**, 40-51.

Newland, D.E, 1984: *An Introduction to Random Vibrations and Spectral Analysis*. Second Edition. Longman, New York, 377 pp.

Niederbäumer, G., 1992: *Katabatischer Wind über dem Grönländischen Eisschild*. Diplomarbeit. Geogr. Inst. ETH, 39 pp.

Numerical Algorithms Groups, 1990: *The NAG Fortran Library Manual, Mark 14*. NAG Ltd., Oxford.

Ohmura, A., 1982: Evaporation from the surface of the Arctic tundra on Axel Heiberg Island. *Water Resources Res.*, **18**, 291-300.

Ohmura, 1993: ETH Greenland Ice Sheet Programme: An Overview. Abstract in: Oerter, H. (Ed.): *Proceedings of the Workshop on Mass Balance and Related Topics of the Greenland Ice Sheet*. Bremerhaven, Germany, Nov. 30 - Dec. 2, 1992.

Ohmura, A. and N. Reeh, 1991: New precipitation and accumulation maps for Greenland. *J. Glac.*, **37**, 140-148.

Ohmura, A. et al., 1991: *ETH Greenland Expedition. Progress Report No. 2*. Dept. of Geography, Swiss Federal Inst. of Techn., Zurich, 108 pp.

Ohmura, A. et al., 1992: *ETH Greenland Expedition. Progress Report No. 2*. Dept. of Geography, Swiss Federal Inst. of Techn., Zurich, 94 pp.

Oort, A., 1983: *Global Atmospheric Circulation Statistics*, 1958-1973. NOAA Professional Paper 14. U.S. Dept. of Commerce, National Oceanic and Atmospheric Administration, Rockville, Md. 180pp., 47 microfiches.

Palmén, E., 1966: Computation of the evaporation over the Baltic Sea from the flux of water vapor in the atmosphere. Publication No. 62 of the International Association of Scientific Hydrology. International Union of Geodesy and Geophysics. 244-252.

Palmén, E., 1967: *Evaluation of Atmospheric Moisture Transport for Hydrological Purposes*. Reports on WMO/IHD Projects, Report No. 1. World Met. Organization, Geneva, 63 pp.

Palmén, E. and E.O. Holopainen, 1962: Divergence, vertical velocity and conversion between potential and kinetic energy in an extratropical disturbance. *Geophysica (Helsinki)*, **8**, 89-113.

Panofsky, H.A. and J.A. Dutton, 1984: *Atmospheric Turbulence*. John Wiley & Sons, New York, 397 pp.

Parish, T.R. and K.T. Waight III, 1987: The forcing of Antarctic katabatic winds. *Mon. Wea. Rev.*, **115**, 2214-2226.

Parkinson, C.L. et al., 1987: *Arctic Sea Ice, 1973-1976*. National Aeronautic and Space Administration, Scientific and Technical Information Branch. Washington D.C. 296 pp.

Paterson, W.S.B., 1980: *The Physics of Glaciers*. Second Edition. Pergamon Press, Oxford, 380 pp.

Peixoto, J.P., 1973: *Atmospheric Vapour Flux Computations for Hydrological Purposes*. Reports on WMO/IHD Projects, Report No. 20. World Met. Organization, Geneva, 83 pp.

Peixoto, J.P. and A.H. Oort, 1983: The atmospheric branch of the hydrological cycle and climate. In: Street-Perrot, A., M. Beran and R. Ratcliffe (Eds.): *Variations in the Global Water Budget*. Reidel, Dodrecht, 5-65.

Petterssen, S., 1956: *Weather analysis and forecasting*. Second Edition. Vol. I: Motion and Motion Systems. McGraw-Hill Book Company, New York, 428 pp.

Press, W.H. et al., 1986: *Numerical Recipes*. Cambridge University Press, New York, 818 pp.

Priestley, M.B., 1981: *Spectral Analysis and Time Series*. Vol. I and II. Series in Probability and Mathematical Statistics. Academic Press, London.

Putnins, P., 1970: The Climate of Greenland. In: Orvig, S. (Ed.): *Climates of the Polar Regions*. World Survey of Climatology, vol. 14. Elsevier, Amsterdam. 3-128.

Rasmusson, E.M., 1967: Atmospheric water vapor transport and the water balance of North America. Part I: Characteristics of the water vapor flux field. *Mon. Wea. Rev.*, 95, 7, 403-426.

Rasmusson, E.M., 1968: Atmospheric water vapor transport and the water balance of North America. Part II: Large-scale water balance investigations. *Mon. Wea. Rev.*, 96, **10**, 720-734.

Rasmusson, E.M., 1977: *Hydrological Application of Atmospheric Vapour-Flux Analyses*. Operational Hydrology, Report No. 11. World Met. Organization, Geneva, 50 pp.

Reed, R.J., 1959: *Arctic Circulation Studies*. Final Report, AF Contract 19(604)-3063, Dept. of Meteorology and Climatology, University of Washington. 57 pp.

Reed, R.J. and B.A. Kunkel, 1960: The Arctic circulation in summer. *J. Met.*, **17**, 489-506.

Reeh, N., 1989: Dynamic and climatic history of the Greenland Ice Sheet. In: R.J. Fulton (Ed.); *Quaternary Geology of Canada and Greenland*; Geological Survey of Canada, Geology of Canada no. 1, 795-822. (Also: Geological Society of America, The geology of North America, v. K-1).

Rossby, C.G., 1940: Planetary flow patterns in the atmosphere. *Quart. J. Roy. Met. Soc.*, **66**, suppl., 68-87.

Rotach, M., 1991: *Turbulence Within and Above an Urban Canopy*. Zürcher Geographische Schriften, 45, Geographisches Institut ETH, Zürich, 245 pp.

Rott, H. and F. Obleitner, 1992: The energy balance of dry tundra in West Greenland. *Arctic and Alpine Res.*, **24**, 352-362.

Salstein, D.A., R.D. Rosen and J.P.Peixoto, 1980: Hemispheric water vapor flux variability-Streamfunction and potential fields. In. Deepak, A., T.D. Wilkerson and L.H. Ruhnke (Eds.): *Atmospheric Water Vapor*. Academic Press, New York, 557-573.

Schaak, T., D. Johnson & R. Schneider, 1993: Regional characteristics of the atmospheric hydrological cycle. *Proc. Fourth Symp. on Global Change Studies*, 17-22 January, 1993, Anaheim, California. American Meterological Society, 361-366.

Sevruk, B., 1982: *Methods of Correction for Systematic Error in Point Precipitation Measurement for Operational Use*. Operational Hydrology, Report No. 21. World Met. Organization, Geneva, 91 pp.

Solomon, A. and K. Trenberth, 1993: Implications of global atmospheric spatial spectra for processing and displaying data. *J. Climate*, **6**, 531-545.

Tibaldi, S., 1986: Envelope orography and maintenance of the quasi-stationary circulation in the ECMWF global models. In: Saltzman, B., R. Benzi and A.C. Wiin-Nielsen (Eds.): *Anomalous Atmospheric Flows and Blocking*. Advances in Geophysics, Vol. **29**, Academic Press, Orlando, 339-374.

Trenberth, K.E., 1991: Climate diagnostics from global analyses: conservation of mass in ECMWF analyses. *J. Climate*, **4**, 707-722.

Vinnichenko, N.K., 1970: The kinetic energy spectrum in the free atmosphere-1 second to 5 years. *Tellus*, **22**, 158-166.

Vowinckel, E., 1962: *Cloud Amount and Type over the Arctic*. Publication in Meteorology No. 51, Scientific Report No. 4. Arctic Meteorology Research Group, McGill University, Montreal. 27 pp.

Wallace, J. M., 1983: The climatological mean stationary waves: observational evidence. In: Hoskins, B. and R. Pearce: *Large-Scale Dynamical Processes in the Atmosphere*. Academic Press, London, 27-53.

Wallace, J.M., S. Tibaldi and A.J. Simmons, 1983: Reduction of systematic forecast errors in the ECMWF model through the introduction of an envelope orography. *Quart. J. Roy. Met. Soc.*, **109**, 683-717.

Walmsley, J.L., 1966: *Ice Cover and Surface Heat Fluxes in Baffin Bay*. Publication in Meteorology No. 84. Arctic Meteorology Research Group, McGill University, Montreal. 94 pp.

Whittaker, L.M. and L.H. Horn, 1984: Northern Hemisphere extratropical cyclone activity for four mid-season months. *J. Climatology*, **4**, 297-310.

Wilson, C., 1967: *Introduction. Northern Hemisphere I.* Cold Regions Science and Engineering. Part I: Environment. Section A 3: Climatology. Cold Regions Science and Engineering Laboratory, Hanover, New Hampshire. 141 pp.

Seite Leer /
Blank leaf

## APPENDIX 1

### Substitution of $p_s(t)$ with $\overline{p_s}$ in time averaged vertical integrals

Define a variable $x = x(p,t)$, which is a continuous function of pressure and time. Its time averaged vertical integral is given by:

$$\overline{\frac{1}{g}\int_{p_t}^{p_s(t)} x(p,t)\,dp} = \frac{1}{\tau}\int_0^{\tau}\left\{\frac{1}{g}\int_{p_t}^{p_s(t)} x(p,t)\,dp\right\}dt\ , \tag{A1.1}$$

where an overbar denotes a time average, $\tau$ is the averaging time, $g$ is the acceleration due to gravity, $p_s(t)$ is the surface pressure and $p_t$ the lower limit of vertical integration, taken for example as the top of the atmosphere. $p_t$ is not a function of time. If the actual surface pressure at time t is less than the average surface pressure, it is assumed that:

$$x(p) = x(\overline{p_s}) \quad \text{if} \quad p_s(t) \le p < \overline{p_s}\ . \tag{A1.2}$$

Therefore, the rhs of (A1.1) can be expanded as follows:

$$\begin{aligned}\overline{\frac{1}{g}\int_{p_t}^{p_s(t)} x(p,t)\,dp} &= \frac{1}{\tau}\int_0^{\tau}\left\{\frac{1}{g}\left[\int_{p_t}^{\overline{p_s}} x(p,t)\,dp + \int_{\overline{p_s}}^{p_s(t)} x(p,t)\,dp\right]\right\}dt \\ &= \frac{1}{g}\int_{p_t}^{\overline{p_s}} \bar{x}(p)\,dp + \frac{1}{\tau}\int_0^{\tau}\left\{\frac{1}{g}\int_{\overline{p_s}}^{p_s(t)} x(p,t)\,dp\right\}dt\ .\end{aligned} \tag{A1.3}$$

Moreover, if for $p_s(t) > \overline{p_s}$, $\exists\,\varepsilon > 0$, $\varepsilon$ small enough, such that $\left|p_s(t) - \overline{p_s}\right| < \varepsilon$, then

$$x(p,t) \cong x_s(t) \ \text{ for } p \in \left[p_s, \overline{p_s}\right]\ . \tag{A1.4}$$

Whence:

$$\begin{aligned}\overline{\frac{1}{g}\int_{p_t}^{p_s(t)} x(p,t)\,dp} &\cong \frac{1}{g}\int_{p_t}^{\overline{p_s}} \bar{x}(p)\,dp + \frac{1}{g}\frac{1}{\tau}\int_0^{\tau} x_s(t)\cdot\left(p_s(t) - \overline{p_s}\right)dt \\ &\cong \frac{1}{g}\int_{p_t}^{\overline{p_s}} \bar{x}(p)\,dp + R\left(x_s(t), p_s(t), \overline{p_s}\right)\ ,\end{aligned} \tag{A1.5}$$

where $R\left(x_s(t), p_s(t), \overline{p_s}\right)$ is the residual. Provided that:

$$x_s(t) \ge 0\,,\ \forall t \ \text{ or } \ x_s(t) < 0\,,\ \forall t\ , \tag{A1.6}$$

the first Mean-Value Theorem of Integration (Dutton, 1976, p. 20; Bronstein and Semendjajew, 1985, p. 291) states that $\exists\,\xi$, $\xi \in [0,\tau]$ such that:

$$\begin{aligned} R\left(x_s(t), p_s(t), \overline{p_s}\right) &= \frac{1}{g}\frac{1}{\tau}\int_0^{\tau} x_s(t)\cdot\left(p_s(t)-\overline{p_s}\right)dt \\ &= \frac{1}{g}\left(p_s(\xi)-\overline{p_s}\right)\cdot\left(\frac{1}{\tau}\int_0^{\tau} x_s(t)\,dt\right) \\ &= \frac{1}{g}\left(p_s(\xi)-\overline{p_s}\right)\cdot\overline{x_s} \\ &= \frac{1}{g}p_s'(\xi)\cdot\overline{x_s}\ , \end{aligned} \tag{A1.7}$$

where a prime indicates the deviation from the time average. On the other hand, the first term on the rhs of (A1.5) is equal to:

$$\begin{aligned} \frac{1}{g}\int_{p_t}^{\overline{p_s}} \bar{x}(p)\,dp &= \frac{1}{g}\langle\overline{x}\rangle\cdot\left(\overline{p_s}-p_t\right) \\ &\cong \frac{1}{g}\langle\overline{x}\rangle\cdot\overline{p_s}\ , \end{aligned} \tag{A1.8}$$

where $\langle ... \rangle$ indicates a vertical average, and where $p_t$ is assumed to be negligibly small compared to $\overline{p_s}$. For $\langle\overline{x}\rangle \neq 0$, the ratio of the second to the first term in (A1.5), or the relative magnitude of the residual, is then given by:

$$\frac{R\left(x_s(t), p_s(t), \overline{p_s}\right)}{\frac{1}{g}\int_{p_t}^{\overline{p_s}} \bar{x}(p)\,dp} \cong \frac{\overline{x_s}}{\langle\overline{x}\rangle}\cdot\frac{p_s'(\xi)}{\overline{p_s}}\ . \tag{A1.9}$$

Under typical meteorological conditions, the day-to-day pressure change is of the order of 1 to 10 hPa. Setting $p_s' \approx 10^2$ to $10^3$ Pa, $\overline{p_s} \approx 10^5$ Pa yields:

$$\frac{\overline{x_s}}{\langle\overline{x}\rangle}\cdot\frac{p_s'(\xi)}{\overline{p_s}} \approx 10^{-3}\cdot\frac{\overline{x_s}}{\langle\overline{x}\rangle} \quad \text{to} \quad 10^{-2}\cdot\frac{\overline{x_s}}{\langle\overline{x}\rangle}\ . \tag{A1.10}$$

If $x$ is taken as the temperature or the specific humidity, $\overline{x_s}$ and $\langle\overline{x}\rangle$ are often of the same order of magnitude. Then, the relative magnitude of the residual that arises from the substitution of $p_s(t)$ with $\overline{p_s}$ is of the order of $10^{-3}$ or $10^{-2}$, which justifies the substitution.

If $x$ is one of the components of a vector quantity, (A1.6) is not always valid, i.e. $x_s(t)$ may change sign in the interval $[0,\tau]$. In this case, it is convenient to write $x_s(t)$ as:

$$x_s(t) = \left(\delta_L(t) + \delta_G(t)\right) \cdot x_s(t) \,, \tag{A1.8}$$

where:

$$\delta_L(t) = \begin{cases} 1 & if \quad x_s(t) < 0 \\ 0 & if \quad x_s(t) \geq 0 \end{cases}$$

$$\delta_G(t) = \begin{cases} 0 & if \quad x_s(t) < 0 \\ 1 & if \quad x_s(t) \geq 0 \end{cases} \,, \tag{A1.9}$$

and

$$\left(\delta_L(t) + \delta_G(t)\right) = 1 \quad , \quad \forall t \,. \tag{A1.10}$$

But then $\delta_L(t) \cdot x_s(t) < 0 \,, \forall t$ and $\delta_G(t) \cdot x_s(t) \geq 0 \,, \forall t$, which allows a derivation similar to (A1.7) for the two terms separately, whereby a partial or total cancellation can arise. In this case, however, it must be considered that $x$ may change sign also with changing $p$. In this case it is possible that $\langle \bar{x} \rangle = 0$ .

Seite Leer /
Blank leaf

## APPENDIX 2

### The saturation water vapour pressure

According to Buck (1981), the saturation vapour pressure over water can be expressed as follows:

$$e_s(T) = f \ a \ \exp\left\{\frac{\left(b - \frac{T_C}{d}\right)T_C}{T_C + c}\right\}, \qquad \text{(A2.1)}$$

where $e_s$ is the saturation vapour pressure in [hPa], $T_C$ the temperature in [°C], $a$=6.1121 hPa the saturation pressure at 0°C, and $b$=18.729, $c$=257.87 and $d$=227.3 are constants determined to yield the best agreement between (A2.1) and Wexler's (1976) formulation. $f$ is an enhancement factor introduced to account for the spherical shape of water droplets:

$$f = 1 + A + p\left[B + C\left(T_C + D + E\,p\right)^2\right], \qquad \text{A(2.2)}$$

where $T_C$ is again the temperature in [°C], $p$ is the pressure in [hPa], and $A$=4.1 · $10^{-4}$, $B$=3.48 · $10^{-6}$, $C$=7.4 · $10^{-10}$, $D$=30.6 and $E$=-3.8 · $10^{-2}$ are constants. Over the range of pressures and temperatures encountered in the atmosphere $f \in [\,1, 1.0070\,]$.

### The pseudo-equivalent potential temperature

The pseudo-equivalent potential temperature $\theta_e$ is calculated using the approximative formulation of Hoffmann and Pelz (1984):

$$\theta_e = T\left(\frac{1000}{p}\right)^{\kappa}(1 + 1.604\,\kappa\,x)\exp\left(\frac{Lx}{c_p\hat{T}}\right) + \delta\theta_e, \qquad \text{(A2.3)}$$

where $T$ is the temperature in [K], $\hat{T}$ the temperature at the lifting condensation level, $p$ the pressure in [hPa], $\kappa$ = 0.2681 the adiabatic coefficient, $x$ is the mixing ratio in [kg kg$^{-1}$], $L$ = 2 .5104 · $10^6$ [J kg$^{-1}$] the latent heat of condensation (assumed constant with T), $c_p$ = 1.00464 · $10^3$ [J kg$^{-1}$ K$^{-1}$] the specific heat of dry air at constant pressure, and $\delta\theta_e$ a correction factor given by:

$$\delta\theta_e = \begin{cases} \left\{ 0.0117\left[ \left(\hat{T} - 273.16\right) + 70 \right] \right\}^{8.8} & \text{for } (\hat{T} - 273.16) \geq -70 \\ 0 & \text{for } (\hat{T} - 273.16) < -70 \end{cases} . \qquad \text{(A2.4)}$$

The temperature $\hat{T}$ at the lifting condensation level is given by:

$$\hat{T} = T\left(\frac{\hat{p}}{p}\right)^{\kappa} , \qquad \text{(A2.5)}$$

where $T$ is the temperature at the parcel's level $p$ , and $\hat{p}$ is the pressure at the lifting condensation level. The determination of $\hat{p}$ is shown in the next section.

## Determination of the lifting condensation level (LCL)

An unsaturated air parcel will rise dry adiabatically until the lifting condensation level (*LCL*) is reached. During the dry-adiabatic expansion, both the potential temperature$\theta$ as well as the specific humidity $q$ are conserved, whereas the saturation vapour pressure $e_s$ is approached by the vapour pressure $e$ from below. Therefore, the *LCL* is the level where the vapour pressure $e$ becomes, for given $\theta$ and $q$, equal to the saturation vapour pressure $e_s$ , i.e.:

$$\hat{e}(\hat{p}, q) = \hat{e}_s(\hat{T}) = \hat{e}_s(\hat{p}, \theta) . \qquad \text{(A2.6)}$$

Here, $\hat{e}$ and $\hat{e}_s$ are the vapour pressure and the saturation vapour pressure at the *LCL*, respectively, $\hat{p}$ is the pressure at the *LCL*, and $\hat{T}$ is the temperature at the *LCL*. Clearly $\hat{q} = q$ and $\hat{\theta} = \theta$. In isobaric coordinates, $\hat{p}$ is the lifting condensation level. To proceed in the derivation, Buck's formula without enhancement factor is used to express the saturation vapour pressure. This yields:

$$\hat{p}\,\frac{q}{q + (1-q)\varepsilon} = a \exp\left\{ \frac{\left[ b - \frac{1}{d}\left( \theta\left(\frac{1000}{\hat{p}}\right)^{\kappa} - T_K \right) \right]\left( \theta\left(\frac{1000}{\hat{p}}\right)^{\kappa} - T_K \right)}{\left( \theta\left(\frac{1000}{\hat{p}}\right)^{\kappa} - T_K \right) + c} \right\} ,$$

(A2.7)

where $T_K$=273.16 is used to convert the absolute temperature to degrees centigrade, $\varepsilon$=0.622 is the ratio between the molecular mass of water and that of dry air, the constants $a$, $b$, $c$ and $d$ are the same constants as in (A2.1), and the vapour pressure $e$ as a function of pressure and specific humidity is derived by inverting the usual expression for the specific humidity. (A2.7) is a function only of (the pressure at) the lifting condensation level. With some manipulations, (A2.7) may be rewritten as:

$$F(\hat{p}) = A_1\,\hat{p}^{2\kappa} + A_2\,\hat{p}^{\kappa}\ln\hat{p} + A_3\,\hat{p}^{\kappa} + A_4\ln\hat{p} + A_5\,, \qquad \text{(A2.8)}$$

where the following abbreviations have been adopted:

$$\begin{aligned}
A_1 &= \frac{\gamma^2}{d} \\
A_2 &= \gamma \\
A_3 &= \gamma\left[\ln\left(\frac{\alpha}{a}\right) - b - 2\frac{T_K}{d}\right] \\
A_4 &= c - T_K \\
A_5 &= (c - T_K)\ln\left(\frac{\alpha}{a}\right) + \left(b + \frac{T_K}{d}\right)T_K \\
\gamma &= \frac{\theta}{1000^{\kappa}} \\
\alpha &= \frac{q}{q + (1-q)\varepsilon}\,.
\end{aligned} \qquad \text{(A2.9)}$$

The *LCL* in isobaric coordinates is the root of the nonlinear equation (A2.8), and can be found by iteration (a working routine is RTSAFE in Press et. al., 1986, p.258). Three special cases should be distinguished in advance (here *RH* is the relative humidity):

*RH*=100% : The air is already saturated. The parcel is at or above the condensation level. For numerical reasons, it is useful to somewhat relax the condition, e.g., *RH*>95%.

*RH*=0% : The air parcel will never saturate. The *LCL* can be set, for example, at the top of the atmosphere.

*RH*>0% : but F(50 hPa)=0. Under some conditions, it is possible that the air parcel reaches saturation only at very high (in altitude) levels. For numerical reasons, it is preferable to avoid such cases and to set the *LCL* directly at the top of the atmosphere, for instance.

Seite Leer /
Blank leaf

**Curriculum Vitae**

Nome : Calanca, Pierluigi

Data di nascita : 14. Juni 1963

Attinenza : Leontica, Ticino

Formazione :

| | |
|---|---|
| 1969-1974 | Scuola Elementare, Biasca, Ticino. |
| 1974-1979 | Ginnasio Cantonale, Biasca, Ticino. |
| 1979-1982 | Liceo Cantonale, Bellinzona, Ticino. Maturità Tipo C. |
| 1982-1987 | Studio della geografia al Politecnico Federale di Zurigo. Diploma in Scienze Naturali ottenuto con un lavoro dal titolo 'Verdunstung auf Hochgebirgsgletscher, Tianshan, China'. |
| 1986 | Partecipazione alla spedizione dell'Istituto di Geografia nello Tianshan, Cina. |
| Dal 1987 | Collaboratore scientifico e assistente al medesimo istituto. |
| Dall'autunno 1990: | Preparazione della tesi di dottorato dal titolo 'The Atmospheric Water Vapour Budget over Greenland'. |

Esperienze di lavoro : Dal 1983 diversi incarichi di supplenza nelle scuole medie del Canton Ticino. Materie di insegnamento: matematica e scienze naturali